Report No. CTI-UCD-2-94

The Deep Patch Technique for Landslide Repair

Bassam M. Helwany
Colorado Transportation Institute
4201 East Arkansas Avenue
Denver, CO 80222

Final Report
October, 1994

in cooperation with the
rtment of Transportation
ighway Administration

Technical Report Documentation Page

1. Report No.	2. Government Accession No.	3. Recipient's Catalog No.
CTI-UCD-2-94		

4. Title and Subtitle	5. Report Date
The Deep Patch Technique for Landslide Repair	October, 1994
	6. Performing Organization Code

7. Author(s)	8. Performing Organization Rpt.No.
Dr. M. Bassam Helwany	

9. Performing Organization Name and Address	10. Work Unit No. (TRAIS)
Colorado Transportation Institute 4201 East Arkansas Avenue Denver, CO 80222	11. Contract or Grant No. 93-482

12. Sponsoring Agency Name and Address	13. Type of Rpt. and Period Covered
Colorado Department of Transportation 4201 East Arkansas Avenue Denver, CO 80222	Final Report 14. Sponsoring Agency Code 270.01

15. Supplementary Notes

Prepared in Cooperation with the U.S. Department of Transportation and the U.S. Forest Service

16. Abstract

This report describes the laboratory testing of the "USFS deep patch" technique and a CTI modification of this technique for repairing landslides with geosynthetic reinforcement. The technique involves replacing sections of roadway lost due to landslides on top of a geosynthetically-reinforced embankment. The CTI modification involves replacing the reinforced slope with a geosynthetically-reinforced retaining wall with a truncated base. Both techniques rely on the cantilevering ability of the reinforced mass to limit the load on the foundation with a high slide potential.

The testing was done in a plane-strain device, (8 feet high, 16 feet long, and 3 feet wide) with a floor that can be lowered down to simulate the loss of support due to additional sliding of the foundation. Both road base fill and shredded tire fill were tested.

The tests with road base showed that (1) both the USFS and CTI repair reduced effectively the adverse effects of local landsliding on the highway pavement by preventing crack propagation; (2) the USFS repair increased the stability of the repaired slope, which was in progressive failure, by reducing the stresses exerted on it; and (3) the CTI repair produced substantially greater stresses on its foundation due to the truncated base of the reinforced mass. These higher stress of the CTI method will probably aggravate the stability of the slope which was in the state of progressive failure before repair. The CTI method, however, provides a wider base for pavement reconstruction. Tests with shredded tires found that excessive deformation makes them unsuitable for either repair technique.

17. Key Words	18. Distribution Statement
geosynthetic, landslide reinforcement, shredded tires	No Restriction

19.Security Classif. (report)	20.Security Classif. (page)	21. No. of Pages	22. Price
None	None	118	

PREFACE

This Research Project was sponsored by the Colorado Transportation Institute (CTI). Professor Jonathan Wu from the University of Colorado at Denver was the Principal Investigator. Mr. Robert Barrett, a physical science researcher / scientist III from the Colorado Department of Transportation (CDOT) and the geotechnical research manager of CTI, was the General Manager of this project. Mr. John B. Gilmore, the chief geologist of CDOT, Mr. Shan-Tai Yeh, a senior geotechnical engineer at CDOT, and Dr. Trevor Wang, a bridge design engineer at CDOT have all been involved in making this project successful.

TABLE OF CONTENTS

List of Tables

List of Figures

CHAPTER 1

INTRODUCTION

The United States Forest Service (USFS) is currently using a new method for landslide repair named "the USFS deep patch technique". The USFS deep patch technique involves the removal of the top portion (5-6 feet-high) of the small-scale sliding slope under a highway pavement and rebuilding that portion with the use of horizontal layers of geosynthetic inclusions.

The USFS deep patch technique is illustrated in Figure 1.1. Figure 1.1(a) depicts a cross-section of a typical highway in a mountain region. Part of the natural slope, which consists of inherently strong soil, is cut to allow for the highway. The loose soil from the cut is used to fill, without compaction, the lower part of the slope to form an extension to the existing foundation.

Due to the seasonal increase of pore water pressure in the soil combined with soil creep and other factors, the fill part of the highway foundation may develop a local landslide causing undesirable settlement in the highway pavement as shown

in Figure 1.1(a). The upper portion of the local landslide is removed and rebuilt, as shown in Figure 1.1(b), utilizing horizontal layers of geosynthetic reinforcement.

This study was aimed at investigating the effectiveness of the USFS deep patch technique in (1) reducing the adverse effects of local landslides on highway pavement and (2) increasing the stability of the repaired slope by reducing applied normal stresses exerted on top. The investigation was accomplished by devising a large-scale apparatus, as shown in Figure 1.1(c), in which the USFS deep patch technique can be closely simulated. Two large-scale deep patch tests were conducted. The first test, termed "the USFS unreinforced test", used a compacted backfill without geosynthetic reinforcement, whereas the second test, termed "the USFS reinforced test", used the same soil for backfill as the USFS unreinforced test along with five equally-spaced horizontal layers of geosynthetic reinforcement.

Another deep patch technique, evolved from the USFS deep patch technique, was also investigated. This technique, named the CTI (Colorado Transportation Institute) deep patch technique, was suggested by Professor Zhenghuan Liao from Chongqing University (P.R. of China). In the CTI deep patch technique the top portion (5-6 feet-high) of the small-scale sliding slope under a highway pavement is removed and then rebuilt in the form of a geosynthetic-reinforced soil "retaining

wall" with a reversed angle as shown in Figure 1.2.

There are two advantages of using the CTI deep patch technique. The first advantage is the tolerance of the CTI deep patch to any subsequent settlement of the repaired slope. If there is a tendency of further settlement in the repaired slope, the geosynthetic-reinforced portion of the CTI deep patch will separate from the repaired slope causing no distress in the highway pavement. The second advantage of using the CTI deep patch technique is its ability to widen the highway of an average of 4 feet as shown in Figure 1.2. Two CTI deep patch tests were conducted using two different backfill materials. Road base class 1 backfill was used in the first CTI deep patch test. On the other hand, shredded tire backfill, which weighs approximately 1/3 of the road base backfill, was used in the second CTI deep patch test.

CHAPTER 2

THE UNITED STATES FOREST SERVICE DEEP PATCH TECHNIQUE

2.1 THE DEEP PATCH TEST APPARATUS

A plane strain apparatus, within which the deep patch tests were conducted, was devised and constructed. The state of plane strain, as defined in engineering mechanics, is the state which occurs in structures that are not free to expand in the direction perpendicular to the plane of the applied loads. If the applied loads lie in the x-z plane (x is horizontal and z is vertical), then the displacement in the y-direction is zero.

The apparatus, shown in Figures 1.1(c) and 2.1, measures 8 feet high, 16 feet deep and 3 feet wide. The apparatus has two side panels, one back panel, and a bottom panel. The bottom panel consists of two parts: a stationary 7 feet-long part and a moveable 9 feet-long part. The moveable part is held in place by four jacks at its four corners as shown in Figure 2.1. The front two jacks can be lowered simultaneously by the use of one crank shown in Figure 2.2. The back two

jacks can also be lowered simultaneously by the use of another crank shown in Figure 2.3. This arrangement allows the moveable panel to be lowered at the front and at the back simultaneously in a uniform motion. Moreover, this arrangement allows the moveable panel to be lowered at an angle. The moveable part can be vertically lowered in a uniform manner about 1 foot. Figure 2.4 shows the moveable panel at 1 foot drop.

The side panels were constructed with 0.5 inch-thick transparent plexiglass as shown in Figure 2.1. The back panel was made of a 0.75 inch-thick plywood. The bottom of the testing apparatus was a rough surface created by gluing coarse aggregate to its steel plate floor. The treated surface was covered with a 2 inch-thick layer of Ottawa sand before placing the first layer of geosynthetic sheet. The side and back panels were heavily reinforced with 0.2 inch thick, 4.0 inches by 2.0 inches rectangular steel tubing with center-to-center spacing of 2 feet horizontal and 2 feet vertical. After the backfill was emplaced, the moveable part of the bottom panel was gradually lowered to simulate progressive local landslide such as the one shown in Figure 1.1(a).

To insure plane strain condition for the deep patch backfill throughout the test, the following three measures were taken:

(a) The test apparatus was made very rigid. The lateral deformation of the side

walls will be negligible.

(b) The adhesion between the backfill and the side panel was minimized so that the shear stress induced on the side walls became negligible. This was accomplished by creating a lubrication layer between the side wall and backfill. The lubrication layer consists of a 0.02 mm thick latex membrane and a thin layer of silicone grease. This procedure has been used extensively by Tatsuoka at the University of Tokyo and Wu at the University of Colorado at Denver. The friction angle between the lubrication layer and plexiglass as determined by direct shear test is less than one (1) degree (Tatsuoka, et al., 1984).

(c) The backfill was very uniform across the width of the deep patch test so that there was practically no variations in terms of the geometry and the material along the width of the wall.

2.2 CONSTRUCTION AND LOADING SEQUENCE

- Road base (class 1) backfill was placed in 6 inch-thick lifts to construct a 1:1.25 slope. Each lift was uniformly compacted using a vibratory plate compactor, shown in Figure 2.5, in a consistent pattern. The relative compaction of the backfill soil was approximately 98%. Upon completing the placement of two layers

of soil (12 inches-thick), a sheet of geosynthetic reinforcement was placed horizontally.

- Upon reaching the full height of 6 feet, three 6 inch-thick layers of the same backfill material, without reinforcement, were placed and compacted on the top surface of the backfill as surcharge.
- Ten uniform drop increments of the moveable part of the bottom panel were performed at a rate of 1 inch/minute. A waiting period followed each increment to allow for taking measurements. Table 2.1 gives the magnitude and the duration (drop time + waiting period) of each increment.

Table 2.1 Magnitude and Duration of Drop Increments

Increment	Magnitude (inches)	Duration (minutes)
1	0.2	5
2	0.2	5
3	0.2	5
4	0.4	20
5	0.5	5
6	0.5	20
7	1.0	20
8	2.0	20
9	3.0	20
10	3.0	20

2.3 TEST MATERIALS

2.3.1 THE GEOSYNTHETIC REINFORCEMENT

The reinforcement used in the tests was a nonwoven heat-bonded polypropylene geotextile. Some of its index properties provided by the manufacturer are presented in Table 2.2.

Table 2.2 Some Properties of the Geosynthetic Reinforcement

Unit weight (ASTM D-3776)	1.93 N/m^2
Grab tensile (ASTM D-4632)	890 N
Elongation at break (ASTM D-4632)	60 %
Modulus at 10% elongation (ASTM D-4632)	4.45 KN
A.O.S.(ASTM D-4751)	0.101 mm
Permittivity (ASTM D-4491)	0.1/sec
Coefficient of permeability	1.99×10^{-4} cm/sec
Nominal thickness	0.508 mm

To evaluate the load-extension behavior of the geosynthetic reinforcement a uniaxial load-deformation apparatus was devised and constructed. The apparatus, schematically shown in Figure 2.6, consists of two steel clamps which can be rigidly attached to the jaws of a MTS-810 machine as shown in Figure 2.7. The clamps were set to accommodate a 30 cm (1 ft)-wide and 2.54 cm (1 inch)-long geotextile sample (the aspect ratio of 12 to suppress "necking" of the geotextile sample). To insure uniform straining, the geotextile sample was reinforced at its top and bottom

with a 0.6 cm (0.25 inch)-thick layer of high strength epoxy as shown in Figure 2.6.

To insure test accuracy and repeatability, the uniaxial load-deformation apparatus was designed and constructed carefully taking the following measures into consideration:

- The apparatus was made very rigid to avoid bending and rotation.
- The two clamps were precisely made parallel to each other, i.e., the initial distance between the clamps (equal to the length of the geotextile sample) can be preset, for example, to a uniform distance of 2.54 cm (1 inch).
- The geotextile sample was reinforced with a thick layer of high strength epoxy at its top and bottom. A precision-made steel mold, shown in Figures 2.8 and 2.9, was used for that purpose.

Numerous load-deformation tests were performed on identical geotextile samples under identical conditions. The repeatability of the test was excellent even under different loading conditions such as uniaxial tension under constant strain rate, creep, relaxation, and recovery (Helwany and Wu, 1994).

The uniaxial load-deformation behavior of the geotextile used in all deep patch tests, tested at a constant strain rate of 1% per minute, is shown in Figure 2.10.

The results shown in the Figure were obtained by testing a geotextile specimen of 30 cm (12 inches) in width and 2.54 cm (1 inch) in gage length. The test was performed without pressure confinement on the geotextile specimen. Previous tests of this geotextile have indicated that the load-extension behavior of the geotextile is not affected by confining pressure up to about 300 KPa (Wu, 1991).

2.3.2 THE GRAVELLY SAND

The soil used in the gravelly sand backfill test was a brown gravelly sand classified as A-1-B (Road Base class 1) with the grain size distribution curve shown in Figure 2.11 (C_u=15.7 and C_c=0.77). The specific gravity of the soil was 2.63. The optimum water content of the soil was 10.2% and the maximum dry density was 19.84 KN/m^3 (126.3 pcf).

The compaction curve of the backfill soil is shown in Figure 2.12. The in-situ water content of the backfill soil in all deep patch tests was approximately 8.5%. The corresponding dry density was approximately 19.8 KN/m^3 (126.0 pcf) with a relative compaction of approximately 99%.

Three CD triaxial compression tests were performed on the gravelly sand at three confining pressures: 103 KPa, 207 KPa and 310 KPa (15 psi, 30 psi and 45 psi). The gravelly sand was compacted to achieve a dry density of approximately

19.8 KN/m^3 (126.0 pcf) at 8.5% water content (similar to the in-situ condition in the deep patch tests). The results of the CD tests are shown in Figure 2.13.

2.4 INSTRUMENTATION

All tests were instrumented to measure their behavior during construction and upon dropping the moveable part of the bottom panel. A number of different instruments were used to monitor the performance of the tests. They were two-component load cell, high-elongation strain gage, lubricated latex grid and dial indicator. Figure 2.14 illustrates the location of instrumentation in the USFS deep patch tests. Instruments were read by a MEGADAC 2200C data acquistion system.

2.4.1 Two-Component Load Cell

Six two-component load cells capable of measuring normal and shear stresses at the same point were installed along the bottom panel to monitor the stresses exerted to it by the backfill. These load cells have been used successfully by Tatsuoka and his colleagues at the University of Tokyo (Huang and Tatsuoka, 1990) and by Wu (1992b). A unique feature of the load cell is that there is a very little coupling between the forces registered in the two orthogonal directions, i.e., there is very little coupling between the normal and shear stresses.

A schematic diagram of the load cell is shown in Figure 2.15(a). In the figure, the normal stress applied to the load cell will cause stress concentration at the top (and bottom) of the horizontal cavities. On the other hand, the shear stress applied to the load cell will cause stress concentration at the top (and bottom) of the vertical cavities. Four strain gages arranged in full bridge configuration are set in stress concentration regions resulting from the application of normal stress. Another four strain gages arranged in full bridge configuration are set in stress concentration regions resulting from the application of shear stress as shown in Figure 2.15(a). The method of wiring the full bridge configuration is shown in Figure 2.15(b). Figure 2.16 shows a fully-instrumented load cell.

The method of mounting the load cell on the bottom panel is shown in Figure 2.15(c). To insure realistic and accurate measurements of normal and shear stresses exerted to the bottom panel by the backfill, the exposed surface of the load cell has to be even with the inner surface of the bottom panel as shown in the figure. The load cell was secured inside a 1.25 cm (0.5 inch)-thick steel box, shown in Figures 2.17 and 2.18, which was placed inside the bottom panel as shown in Figure 2.15(c).

To calibrate the load cell for normal stress, the load cell was horizontally positioned on a flat rigid surface and a vertical dead weight was applied to its top

surface in small increments as shown in Figure 2.19. The calibration curve of normal stresses for load cells 1, 2, 3 and 4 is shown in Figure 2.20. It is noted from the figure that the response of the load cell to applied normal stresses is linear.

To calibrate the load cell for shear stress, the load cell was vertically positioned on a flat rigid surface and a vertical dead weight was applied in small increments in the shear direction (parallel to the top surface of the load cell), using a special frame shown in Figure 2.21. The calibration curve of shear stresses for load cells 1, 2, 3 and 4 is shown in Figure 2.22. It is noted from the figure that the response of the load cell to applied shear stresses is linear.

The load cells were further calibrated for normal stresses using a different method. In this method a 30 cm-thick layer of Ottawa sand confined inside a plexiglass cylinder was placed on top of the load cell. A dead weight was applied to the top of the Ottawa sand as shown in Figure 2.23. The normal stress calibration factor of the load cell obtained from this method was 10-20% less than the normal stress calibration factor of the load cell obtained from the previously described calibration method. This was attributed to soil arching. It is to be noted that the adhesion between Ottawa sand and the inner surface of the plexiglass cylinder was minimized so that the shear stress induced on the inner

surface of the cylinder became negligible. This was achieved by creating a lubrication layer between the inner surface and the sand similar to the one used earlier in the plane strain loading facility.

2.4.2 High Elongation Strain Gage

High elongation strain gages were mounted along the length of the geotextile sheets to measure tensile strains induced in the geosynthetic reinforcement. The mounting method suggested by Billiard and Wu (Billiard, 1989; Billiard and Wu, 1991) for strain gage on "extensible" materials was employed. In this method the strain gage is glued to the geotextile sheet only at the two extremities of the gage as shown in Figure 2.24.

The strain gages were covered with a protective mixture made of wax and petroleum jelly as shown in Figure 2.25. This was necessary to protect strain gages from soil moisture. This procedure has been successfully used by Helwany (1993) in a fully saturated clay.

The wax and petroleum jelly protective mixture was very flexible yet nearly impermeable. To evaluate this procedure, five strain gages were mounted on a 30.0 cm (12 inch) by 5.08 cm (2 inch) geotextile specimen and covered with the protective mixture. The specimen was then strained using the uniaxial tension test

apparatus (described previously). The gage factor calculated from the calibration curves was nearly identical to that calculated from the curves for strain gages without the protective mixture. Figure 2.26 illustrates the uniaxial tension test for strain gage calibration (without the protective mixture). The calibration curve of the strain gages (without the protective mixture) is shown in Figure 2.27.

The mounting procedure of a strain gage on the geotextile sheet involves gluing the two extremities of the strain gage to the geotextile using high strength epoxy (5-ton clear epoxy). The epoxy is left to cure for at least 8 hours, thereafter, a 0.6 cm (0.25 inch)-thick layer of the protective mixture is used to cover the strain gage and its terminal. Another 0.6 cm (0.25 inch)-thick layer of the protective mixture is used to cover the strain gage and its terminal from the opposite side of the geotextile to provide complete protection against the moisture seeping through the geotextile. For further environmental and mechanical protection a layer of Neoprene rubber was used on top of the protective mixture as shown in Figure 2.28. Figure 2.29 shows a geotextile layer instrumented with five strain gages being placed in the test apparatus.

2.4.3 Lubricated Latex Grid System

A lubricated latex grid system was established on the side wall to measure the

internal movement of the slope. The lubricated side-wall grid system has been used successfully by Wu (1992b) to measure the internal movement of the backfill in full-scale retaining walls such as the Denver Test Walls. The lubricated side-wall grid system consists of a 0.02 mm thick latex membrane and a thin layer of silicone grease. A grid, with a vertical spacing of 7.5 cm (3 inch) and horizontal spacing of 7.5 cm (3 inch), was sketched on the latex membrane as shown in Figure 2.30. The friction angle between the lubrication layer and plexiglass as determined by direct shear test is less than one (1) degree (Tatsuoka, et al., 1984), therefore, the deformation of the lubricated side-wall grid will reflect very closely the deformation of the backfill. Figure 2.31 illustrates the lubricated latex grid system of the USFS deep patch test at the end of construction.

2.4.4 Dial Indicator

Four dial indicators were used to measure the movement of the moveable part of the bottom panel.

2.5 RESULTS AND DISCUSSION OF RESULTS

The displacement of the slope, the bottom panel, and the top surface in the USFS unreinforced test, as measured by the lubricated latex grid, is shown in Figure 2.32. A near vertical crack emanating from a point on the slope nearly above the inner end of the moveable part of the bottom panel is shown in the figure. The crack started with the first drop of 0.2 inch and propagated throughout the test due to further drops of the moveable part of the bottom panel. The depth of the crack was approximately 70 inches and its width was approximately 12 inches due to the 11 inch drop in the moveable part of the bottom panel (see Figure 2.33).

In contrast, the deformation behavior of the backfill in the USFS reinforced test was much more favorable than the one in the USFS unreinforced test. Several small cracks, shown in Figure 2.34, were detected in the beginning of the USFS reinforced test, however, their propagation was very limited due to the soil reinforcement. The deepest crack measured about 10 inches (deep) due to the 11 inch drop in the moveable part of the bottom panel. A detailed comparison of crack propagation of the two tests for different drops of the moveable part of the bottom panel is shown in Figure 2.35

A comparison between the crack in the USFS unreinforced test and the largest

crack in the USFS reinforced test is shown in Figure 2.36. The crack in the unreinforced case was at least 8 times deeper than the one in the reinforced case.

The measured normal stress distribution in the USFS unreinforced test along the bottom panel is depicted in Figure 2.37. It is to be noted from the figure that the normal stress has substantially increased with the increase of drop of the moveable part of the bottom panel in load cell #5 (located at 70 inches from the back panel, close to the moveable part of the bottom panel). On the other hand, the normal stress in load cell #4 (located at 97 inches from the back panel) decreased with increasing the drop until the drop of 3 inches was reached. Thereafter, the normal stress in load cell #4 drastically increased with increasing the drop. This is may be attributed to the total separation of the backfill, due to the aforementioned vertical crack, into two soil masses located above the moveable and the stationary parts of the bottom panel.

The measured normal stress distribution in the USFS reinforced test along the bottom panel is depicted in Figure 2.38. A substantial reduction in normal stress is measured along the moveable part of the bottom panel as shown in the figure. The sudden increase in normal stress in load cell #4, noted in the USFS unreinforced test, is not encountered in the USFS reinforced test. Obviously, the geosynthetic reinforcement was able to absorb the tension crack which occurred

in the USFS unreinforced test preventing the total separation of the soil into two masses.

The measured strain distribution along the geosynthetic layers 1, 3 and 5 located at elevations 1, 3 and 5 feet are shown in Figures 2.39(a), 2.39(b), and 2.39(c), respectively. The maximum strain of approximately 4%, corresponding to 8 inches drop of the moveable part of the bottom panel, was observed nearly in the center of the geosynthetic layer 1. Unfortunately, the three central strain gages in this layer were lost after the 8 inch-drop due to excessive straining.

At 8 inch-drop, the maximum strain of approximately 2.4% was observed in the geosynthetic layer 3. Again, the strain gage located at 115 inches from the back panel was lost due to excessive straining when the drop exceeded 8 inches.

Relatively smaller strains were observed in the geosynthetic layer 5. The maximum strain of approximately 1.0% was measured in the strain gage located at 72.7 inch from the back panel.

2.6 SUMMARY AND CONCLUDING REMARKS

To investigate the effectiveness of the USFS deep patch technique for landslide repair, a large-scale laboratory test apparatus was devised and constructed. Two slopes, one unreinforced and one reinforced with geosynthetic inclusions, were

constructed inside the apparatus in plane strain condition. The moveable part of the bottom panel of the apparatus was gradually dropped to simulate progressive local landslide. The response of each slope to the drop was carefully monitored.

The tests results showed that the unreinforced slope suffered a severe distress throughout the test. A large vertical crack initiated in the beginning of the USFS unreinforced test and propagated throughout the test to the extent that the slope was virtually separated into two parts. On the other hand, the reinforced slope remained intact throughout the test with the exception of the few cracks initiated in the beginning of the test but were suppressed by the geosynthetic reinforcements.

The stresses exerted on the moveable part of the bottom panel in the USFS reinforced test were substantially smaller than those in the USFS unreinforced test. This reduction in stresses will enhance the stability of the slope which was in the state of progressive failure before the USFS deep patch repair.

This investigation showed that (1) the USFS deep patch repair reduced effectively the adverse effects of local landslides on highway pavement by preventing crack propagation, and (2) the USFS deep patch increased the stability of the repaired slope, which was in progressive failure, by reducing the stresses exerted to it.

CHAPTER 3

THE CTI DEEP PATCH TECHNIQUE

3.1 INTRODUCTION

A new deep patch technique, evolved from the USFS deep patch technique, is investigated in this Chapter. The new technique, named the CTI (Colorado Transportation Institute) deep patch technique, was suggested by Professor Zhenghuan Liao from Chongqing University (P.R. of China). In the CTI deep patch technique the top portion (5-6 feet-high) of the small-scale sliding slope under a highway pavement is removed and then rebuilt in the form of a geosynthetic-reinforced soil "retaining wall" with a reversed angle as shown in Figures 1.2 and 3.1.

There are two advantages of using the CTI deep patch technique. The first advantage is the tolerance of the geosynthetic-reinforced portion of the CTI deep patch to any subsequent settlement of the repaired slope. If there is a tendency of further settlement in the repaired slope, the geosynthetic-reinforced portion of

the CTI deep patch will separate from the repaired slope causing no distress in the highway pavement. The second advantage of using the CTI deep patch technique is its ability to widen the highway of an average of 4 feet as shown in Figure 1.2.

Two CTI deep patch tests were conducted using two different backfill materials. Road base class 1 backfill was used in the first CTI deep patch test (described in this Chapter). On the other hand, shredded tire backfill, which weighs approximately 1/3 of the road base backfill, was used in the second CTI deep patch test (described in Chapter 4).

3.2 CONSTRUCTION AND LOADING SEQUENCE

- Road base (class 1) backfill was used (without compaction) to construct a 4 ft-high berm on top of the 3 inch-thick sand layer (which was placed on top of the bottom panel) as shown in Figure 3.1. The front face of the berm has the slope of 1 (vertical): 1.25 (horizontal). The inner face of the berm has the slope of 2.25:1.
- A long sheet of geosynthetic reinforcement (long enough to wrap around the soil layer, i.e., the length of the sheet =2 x length of the soil layer + the height of the soil layer) was positioned on top of the 3 inch-thick sand layer. The excess

length of the sheet was positioned on top of the berm.

- Road base (class 1) backfill was placed on top of the geosynthetic reinforcement in 6 inch-thick lifts to construct the geosynthetic-reinforced portion of the CTI deep patch. Each lift was uniformly compacted using a vibratory plate compactor in a consistent pattern. The relative compaction of the backfill soil was approximately 98%. Upon completing the placement of two layers of soil (total thickness of 12 inches), the excess length of the geosynthetic reinforcement layer was wrapped around on top of the compacted soil.
- The above procedure was repeated until reaching the height of 4 feet. Thereafter, the geosynthetic-reinforced portion of the CTI deep patch was constructed vertically until the height of 7 feet was reached, as shown in Figures 3.1 and 3.2, using an L-shaped form made of plywood.
- Ten uniform drop increments of the moveable part of the bottom panel were performed at a rate of 1 inch/minute. A waiting period followed each increment to allow for taking measurements. Table 2.1 gives the magnitude and the duration (drop time + waiting period) of each increment.

3.3 TEST MATERIALS

3.3.1 THE GEOSYNTHETIC REINFORCEMENT

The reinforcement used in the tests was a nonwoven heat-bonded polypropylene geotextile. The reinforcement was described in Section 2.3.1.

3.3.2 THE GRAVELLY SAND

The soil used in this test was a brown gravelly sand classified as A-1-B (Road Base class 1). The soil was described in Section 2.3.2.

3.4 INSTRUMENTATION

The CTI deep patch tests were instrumented to measure their behavior during construction and upon dropping the moveable part of the bottom panel. A number of different instruments were used to monitor the performance of the tests. They were two-component load cell, high-elongation strain gage, lubricated latex grid and dial indicator. Figure 3.3 illustrates the location of instrumentation in the CTI deep patch tests. A detailed description of instrumentation was given in Section 2.4.

3.5 RESULTS AND DISCUSSION OF RESULTS

The displacement of the CTI deep patch and the bottom panel, as measured by the lubricated latex grid, is shown in Figure 3.4 . It is noted from the figure that the vertical part of the face of the CTI deep patch remains vertical (with very limited lateral displacement) throughout the test. The maximum settlements of 7 and 16 inches were measured at the top of the wall corresponding, respectively, to the 5 and 11 inches drop in the moveable part of the bottom panel. Figure 3.5 shows the CTI deep patch after removing the berm which followed the 11 inch drop of the moveable part of the bottom panel. A gab between the bottom of the structure and the moveable part of the bottom panel is to be noted in the figure.

A vertical crack emanating from a point on the top of the CTI deep patch near the back panel is shown in the Figure 3.4. The crack started with the first drop of 0.2 inch and propagated throughout the test due to further drops of the moveable part of the bottom panel. The depth of the crack was approximately 7 ft and its width was approximately 1 inch due to the 11 inch drop in the moveable part of the bottom panel.

The measured normal stress distribution in the CTI test along the bottom panel is depicted in Figure 3.6. It is to be noted from the figure that the normal stress has substantially increased with the increase of drop of the moveable part of the

bottom panel in load cell #2 (located at 70 inches from the back panel, close to the moveable part of the bottom panel). On the other hand, the normal stress in load cell #1 (located at 97 inches from the back panel) decreased (as expected) with increasing the drop of the moveable part of the bottom panel. The maximum stress of approximately 12.0 psi was measured after berm removal (following the 11 inch drop in the moveable part of the bottom panel).

It is to be noted that the initial stresses measured in the CTI deep patch test are higher than the initial stresses measured in the USFS unreinforced test (Figure 2.37). This is obviously due to the odd shape of the CTI deep patch.

The measured strain distribution along the geosynthetic layers 2, 4 and 6 located at elevations 2, 4 and 6 feet are shown in Figures 3.7(a), 3.7(b), and 3.7(c), respectively. The maximum strain of approximately 1.2%, corresponding to 11 inches drop of the moveable part of the bottom panel, was observed near the edge of geosynthetic layer 2. At 11 inch-drop, the maximum strain of approximately 0.7% was observed in geosynthetic layer 4, whereas the maximum strain of approximately 1% was observed in geosynthetic layer 6. A substantial increase in measured strains corresponding to the removal of the berm is noted in the figures. It is to be noted that the strains measured in the CTI deep patch test are smaller than those measured in the reinforced USFS deep patch test.

3.6 THE CTI DEEP PATCH TECHNIQUE IN SILVERTHORNE

The newly developed CTI deep patch technique was used to repair a landslide within the city of Silverthorne-Colorado in October, 1993. The cost of traditional repair for the landslide could have easily exceeded $100,000, whereas the estimated cost of the CTI deep patch technique was less than $15,000. This tremendous reduction in cost could result in repairs to many present and future landslides around Colorado that would go un-repaired or that would cost tremendous amount of money with traditional technologies of landslide repair.

Figure 3.8 illustrates the configuration of the CTI deep patch in the Silverthorne site. Six layers of compacted soil with geogrid reinforcement were used. The construction procedure is very similar to the one described in Section 3.2. The construction procedure, shown in Figure 3.9, involves making a 6 ft-deep cut in the existing highway. The cut width was about 10 ft which was well beyond the slip surface of the landslide. The geogrid reinforcement was then positioned on top of the existing soil and on top of the berm which was constructed beforehand. A 1 ft-thick layer of soil was placed and compacted and the geogrid reinforcement was wrapped around it. This was repeated until reaching the total height of 6 ft. Figures 3.10 and 3.11 show the CTI deep patch during construction in Silverthorne.

3.7 SUMMARY AND CONCLUDING REMARKS

To investigate the effectiveness of the CTI deep patch technique for landslide repair, a large-scale plane strain laboratory test was conducted. The moveable part of the bottom panel of the plane stain apparatus was gradually dropped to simulate progressive local landslide. The response of the CTI deep patch to the drop was carefully monitored.

The test results showed that the CTI deep patch remained intact throughout the test with the exception of the tolerable crack near the back panel which initiated in the beginning of the test and propagated throughout the test. However, the stresses exerted to the bottom panel in the CTI deep patch test were substantially greater than those in the USFS unreinforced test. This increase in normal stresses, due to the odd shape of the CTI deep patch, will probably aggravate the stability of the slope which was in the state of progressive failure before the CTI deep patch repair.

CHAPTER 4

THE CTI DEEP PATCH TECHNIQUE WITH SHREDDED TIRE AS BACKFILL

4.1 INTRODUCTION

Chapter 3 described the CTI deep patch technique which evolved from the USFS deep patch technique. In the CTI deep patch technique the top portion (5-6 feet-high) of the small-scale sliding slope under a highway pavement is removed and then rebuilt in the form of a geosynthetic-reinforced soil "retaining wall" with a reversed angle as shown in Figures 1.2 and 3.1.

Two CTI deep patch tests were conducted using two different backfill materials. Chapter 3 described, in detail, the first CTI test which involved the use of Road base class 1 as backfill. In this Chapter, the second CTI test with shredded tire as backfill is described. The unit weight of the "compacted" shredded tire backfill used in this test is approximately 1/3 of the unit weight of the road base backfill used in the first test.

4.2 CONSTRUCTION AND LOADING SEQUENCE

- Road base (class 1) backfill was used (without compaction) to construct a 4 ft-high berm on top of the 3 inch-thick sand layer (which was placed on top of the bottom panel) as shown in Figure 3.1. The front face of the berm has the slope of 1 (vertical): 1.25 (horizontal). The inner face of the berm has the slope of 1:2.25.
- A sheet of geosynthetic reinforcement (long enough to wrap around the backfill layer, i.e., the length of the sheet =2 x length of the backfill layer + the height of the backfill layer) was positioned on top of the 3 inch-thick sand layer. The excess length of the sheet was positioned on top of the berm.
- Shredded tire backfill was placed on top of the geosynthetic reinforcement in 12 inch-thick lifts to construct the geosynthetic-reinforced portion of the CTI deep patch as shown in Figure 3.1. Each lift was uniformly compacted by simply "stepping" on top in a reasonably consistent pattern. The unit weight of the shredded tire backfill was approximately 40 pcf. Upon completing the placement of a layer of shredded tire, the excess length of the geosynthetic reinforcement layer was wrapped around it.
- The above procedure was repeated until reaching the height of 4 feet. Thereafter, the geosynthetic-reinforced portion of the CTI deep patch was

constructed (vertically) with compacted road base as backfill. The height of the vertical portion, with road base backfill, was 3 feet.

- Ten uniform drop increments of the moveable part of the bottom panel were performed at a rate of 1 inch/minute. A waiting period followed each increment to allow for taking measurements. Table 2.1 gives the magnitude and the duration (drop time + waiting period) of each increment.

4.3 TEST MATERIALS

4.3.1 THE GEOSYNTHETIC REINFORCEMENT

The reinforcement used in the test was a nonwoven heat-bonded polypropylene geotextile. The reinforcement was described in Section 2.3.1.

4.3.2 THE SHREDDED TIRE

The backfill material used in this test was a coarse shredded tire, with its average grain size (chip length) of 4 to 6 inches.

A one-dimensional compression test was performed on the shredded tire prepared at 6.3 KN/m^3 (40 pcf) density. The one-dimensional compression test apparatus, shown in Figure 4.1, consisted of a 0.5 inch-thick, 20 inch-diameter and 20 inch-high steel cylinder. The steel cylinder had one close end (the bottom end) made

of a 0.5 inch-thick steel plate. The inner surface of the steel cylinder was lined with a thin layer of plexiglass. A lubrication layer made of a thin layer silicon grease and a latex membrane was used to minimize friction between the shredded tire and the lining plexiglass. After the shredded tire was placed in the cylinder, a circular 0.5 inch-thick steel cover (with a diameter slightly smaller than the diameter of the cylinder) was positioned on top. A vertical load was applied to the steel cover using an MTS-810 machine.

The load history of the one-dimensional compression test is shown in Figure 4.2. As shown in the figure, the load history consists of three stages. The first stage is a controlled load stage at a load rate of approximately 150 lb/minute which correspond to a stress rate of 0.6 psi/minute. The second stage is a constant load stage (creep), in which the applied load of 1500 lb (which correspond to a 6.3 psi stress) was kept constant for 300 minutes. The third stage is a unload stage at a unload rate of approximately 150 lb/minute (0.6 psi/minute).

The stress-strain behavior of the shredded tire under one-dimensional compression is shown in Figure 4.3. The stress-strain behavior of the shredded tire in the controlled load stage is nearly linear with a slight upward concavity. Assuming a linear behavior during loading, a constant Constrained Modulus of approximately 56.0 psi for shredded tire is estimated from the figure. Additional

modulus, such as Poisson's ratio, is needed to completely characterize the elastic behavior of this material.

During the constant load stage, a significant creep can be noted in Figure 4.3. The creep strain which occurred during the 300 minutes-period was approximately 15% of the total axial strain. Figures 4.4 and 4.5 show in arithmetic and semi-logarithmic planes, respectively, the creep behavior of shredded tire under a constant stress of 6.3 psi.

At the end of the unload stage, as shown in Figure 4.3, most of the axial strain was recovered. Only 2% to 3% axial strain of the 12.5% total axial strain (corresponding to 6.3 psi normal stress) was not recovered (plastic strain). Since the applied normal stress of 6.3 psi in the one-dimensional compression test is comparable to the maximum compaction stress normally used in the field, it is obvious from the figure that most of the strain will be recovered as the compaction factory is removed. Therefore, it can be concluded that the static compaction of shredded tire is ineffective.

4.4 INSTRUMENTATION

The CTI deep patch test with shredded tire was instrumented to measure its behavior during construction and upon dropping the moveable part of the bottom

panel. A number of different instruments were used to monitor the performance of the tests. They were two-component load cell, lubricated latex grid and dial indicator. A detailed description of instrumentation was given in Section 2.4.

4.5 RESULTS AND DISCUSSION OF RESULTS

The displacement of the CTI deep patch and the bottom panel, as measured by the lubricated latex grid, is shown in Figure 4.6. It is noted from the figure that the face of the CTI deep patch suffers excessive vertical and lateral displacements throughout the test. The maximum settlements of 8 and 18 inches were measured at the top of the wall corresponding, respectively, to the 5 and 11 inches drop in the moveable part of the bottom panel. Lateral displacements in excess of 12 inches were measured corresponding to the 11 inch drop of the moveable part of the bottom panel.

A vertical crack emanating from a point on the top of the CTI deep patch near the back panel is shown in the Figure 4.6. The crack started with the first drop of 0.2 inch and propagated throughout the test due to further drops of the moveable part of the bottom panel. The depth of the crack was approximately 7 ft and its width was approximately 7 inches due to the 11 inch drop in the moveable part of the bottom panel. It is noted from the figure that the whole structure seems

to be rotating clockwise with further drops in the moveable part of the bottom panel. This rotation did not cease even after the maximum drop of 11 inches was reached. The excessive movements and the large crack in the backfill render the CTI deep patch technique with shredded tire as backfill unapplicable.

4.6 SUMMARY AND CONCLUDING REMARKS

To investigate the effectiveness of the CTI deep patch technique (with shredded tire as backfill) for landslide repair, a large-scale plane strain laboratory test was conducted. The moveable part of the bottom panel of the plane stain apparatus was gradually dropped to simulate progressive local landslide. The response of the CTI deep patch to the drop was carefully monitored.

The test results showed that the CTI deep patch with shredded tire backfill suffered excessive movements throughout the test. A large crack near the back panel initiated in the beginning of the test and propagated throughout the test. The depth of the crack was approximately 7 ft and its width was approximately 7 inches due to the 11 inch drop in the moveable part of the bottom panel. The whole structure seems to be rotating clockwise with further drops in the moveable part of the bottom panel. This rotation did not cease even after the maximum drop of 11 inches was reached. The excessive movements and the large crack in the

backfill render the CTI deep patch technique with shredded tire as backfill unapplicable.

CHAPTER 5

SUMMARY AND CONCLUSIONS

5.1 SUMMARY

The USFS deep patch technique involves the removal of the top portion (5-6 feet-high) of the small-scale sliding slope under a highway pavement and rebuilding that portion with the use of horizontal layers of geosynthetic inclusions.

This study was aimed at investigating the effectiveness of the USFS deep patch technique in (1) reducing the adverse effects of local landslides on highway pavement and (2) increasing the stability of the repaired slope by reducing applied normal stresses exerted to its top. The investigation was accomplished by devising a large-scale apparatus in which the USFS deep patch technique can be closely simulated. Two USFS large-scale deep patch tests were conducted. The first test, termed "the USFS unreinforced test", used a compacted backfill without geosynthetic reinforcement, whereas the second test, termed "the USFS reinforced test", used the same soil for backfill as the USFS unreinforced test along with five

equally-spaced horizontal layers of geosynthetic reinforcement.

Another deep patch technique, evolved from the USFS deep patch technique, was also investigated. This technique, named the CTI (Colorado Transportation Institute) deep patch technique, was suggested by Professor Zhenghuan Liao from Chongqing University (P.R. of China). In the CTI deep patch technique the top portion (5-6 feet-high) of the small-scale sliding slope under a highway pavement is removed and then rebuilt in the form of a geosynthetic-reinforced soil "retaining wall" with a reversed angle.

There are two advantages of using the CTI deep patch technique. The first advantage is the tolerance of the CTI deep patch to any subsequent settlement of the repaired slope. If there is a tendency of further settlement in the repaired slope, the geosynthetic-reinforced portion of the CTI deep patch will separate from the repaired slope causing no distress in the highway pavement. The second advantage of using the CTI deep patch technique is its ability to widen the highway of an average of 4 feet.

Two CTI deep patch tests were conducted using two different backfill materials. Road base class 1 backfill was used in the first CTI deep patch test, and shredded tire backfill, which weighs approximately 1/3 of the road base backfill, was used in the second CTI deep patch test.

5.2 CONCLUSIONS

The USFS deep patch tests results showed that the unreinforced slope suffered a severe distress throughout the test. A large vertical crack initiated in the beginning of the USFS unreinforced test and propagated throughout the test to the extent that the slope was virtually separated into two parts. On the other hand, the reinforced slope remained intact throughout the test with the exception of the few cracks initiated in the beginning of the test but were suppressed by the geosynthetic reinforcements.

The stresses exerted on the moveable part of the bottom panel in the USFS reinforced test were substantially smaller than those in the USFS unreinforced test. This reduction in stresses will enhance the stability of the slope which was in the state of progressive failure before the USFS deep patch repair.

This USFS tests results showed that (1) the USFS deep patch repair reduced effectively the adverse effects of local landslides on highway pavement by preventing crack propagation, and (2) the USFS deep patch increased the stability of the repaired slope, which was in progressive failure, by reducing the stresses exerted to it.

The CTI deep patch test (with road base as backfill) results showed that the CTI deep patch remained intact throughout the test with the exception of the tolerable

crack near the back panel which initiated in the beginning of the test and propagated throughout the test. However, the stresses exerted to the bottom panel in the CTI deep patch test were substantially greater than those in the USFS unreinforced test. This increase in normal stresses, due to the odd shape of the CTI deep patch, will probably aggravate the stability of the slope which was in the state of progressive failure before the CTI deep patch repair.

The CTI deep patch test (with shredded tire as backfill) results showed that the CTI deep patch suffered excessive movements throughout the test. A large crack near the back panel initiated in the beginning of the test and propagated excessively throughout the test. The depth of the crack was approximately 7 ft and its width was approximately 7 inches due to the 11 inch drop in the moveable part of the bottom panel. The whole structure seems to be rotating clockwise with further drops in the moveable part of the bottom panel. This rotation did not cease even after the maximum drop of 11 inches was reached. The excessive movements and the large crack in the backfill render the CTI deep patch technique, with shredded tire as backfill, unapplicable.

REFERENCES

Billiard, J.W. 1989. Performance of a Large Scale Fabric Wall During Load Test. M.S. Thesis, University of Colorado at Denver.

Billiard, J. W. and Wu, J. T. H. (1991). "Load Test of A Large-Scale Geotextile-Reinforced Retaining Wall." Proceedings of Geosynthetics '91 Conference, Atlanta, Georgia, pp. 537-548

Helwany, M. B. (1993). "The Long-Term Behavior of Geosynthetic-Reinforced Soil Structures." Ph.D. Thesis, University of Colorado at Boulder.

Helwany, M. B. and Wu, J. T. H. (1994)."In-Confinement Creep Characteristics of Geotextiles." To be submitted to ASTM Geotechnical Testing Journal.

Huang, C. C. and Tatsuoka, F. (1990). " Bearing Capacity of Reinforced Horizontal Sandy Ground." Geotextiles and Geomembranes, Vol. 9, pp. 51-82.

Tatsuoka, F., Molenkamp, F., Torii, T. and Hino, T. (1984). "Behavior of Lubrication Layers of Platens in Element Tests." Soils and Foundations, vol.24, No.1, pp. 113-128.

Wu, J. T. H. (1991). "Measuring Inherent Load-Extension Properties of Geotextiles for Design of Geosynthetic-reinforced Structures." ASTM Geotechnical Testing Journal, Vol. 14, No. 2, June 1991, pp. 157-165.

Wu, J. T. H. (1992a). "Predicting Performance of the Denver Walls: General Report." Geosynthetic-Reinforced Soil Retaining Walls, Wu (editor), Balkema Publisher, pp. 3-20.

Wu, J. T. H. (1992b). "Construction and Instrumentation of the Denver Walls." Geosynthetic-Reinforced Soil Retaining Walls, Wu (editor), Balkema Publisher, pp. 21-30.

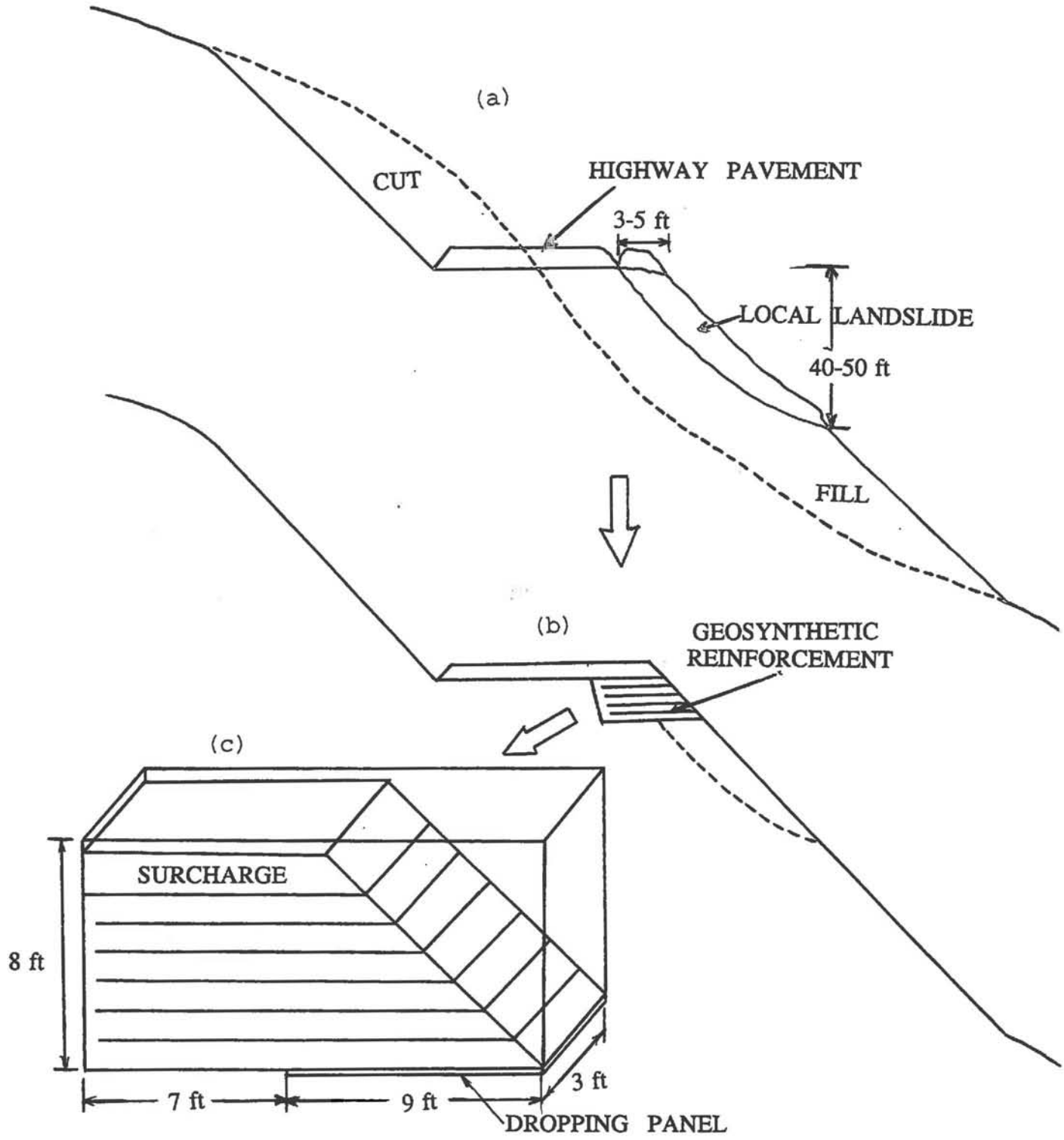

Figure 1.1 Schematic Diagram of the USFS Deep Patch Technique

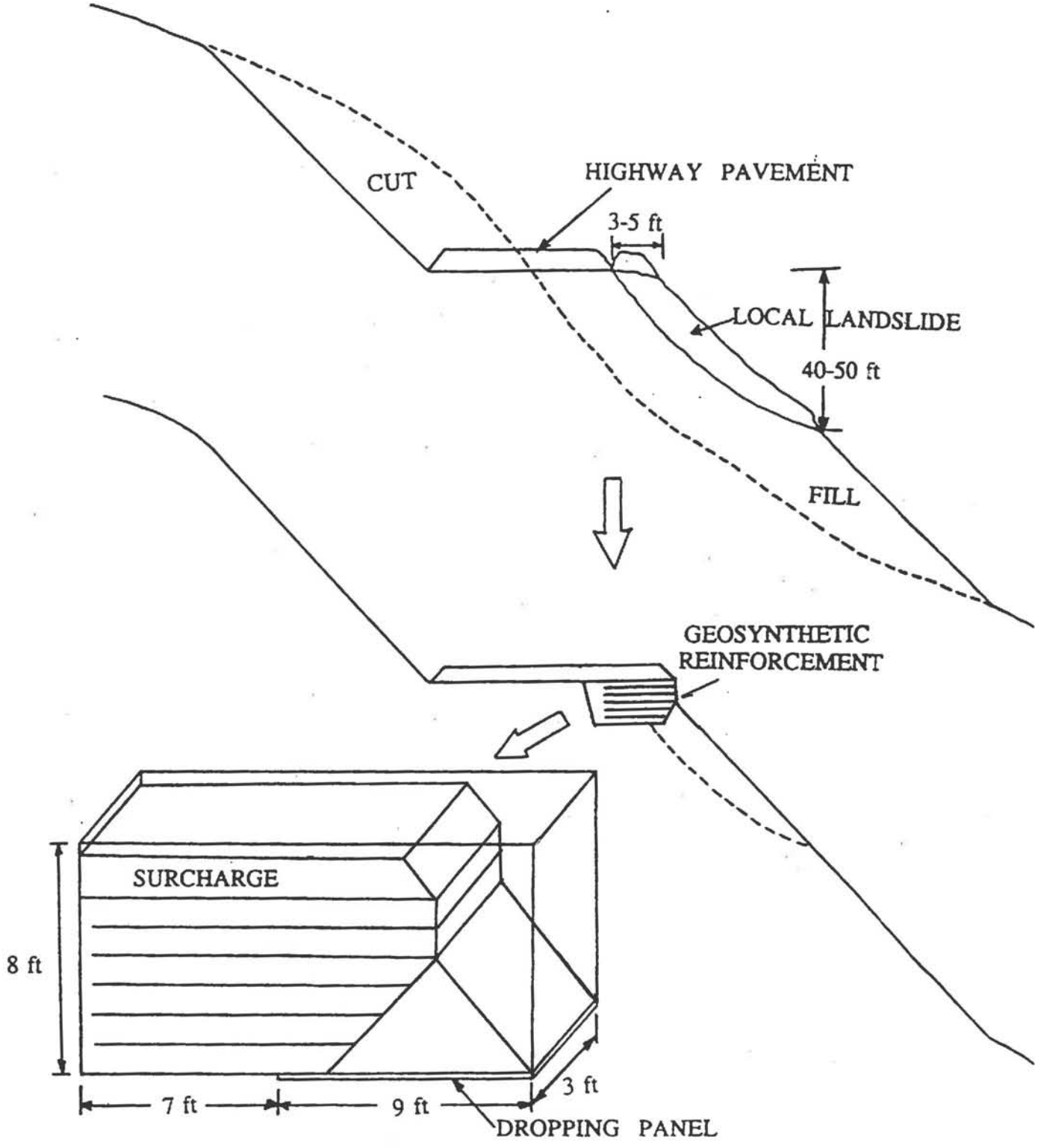

Figure 1.2 Schematic Diagram of the CTI Deep Patch Technique

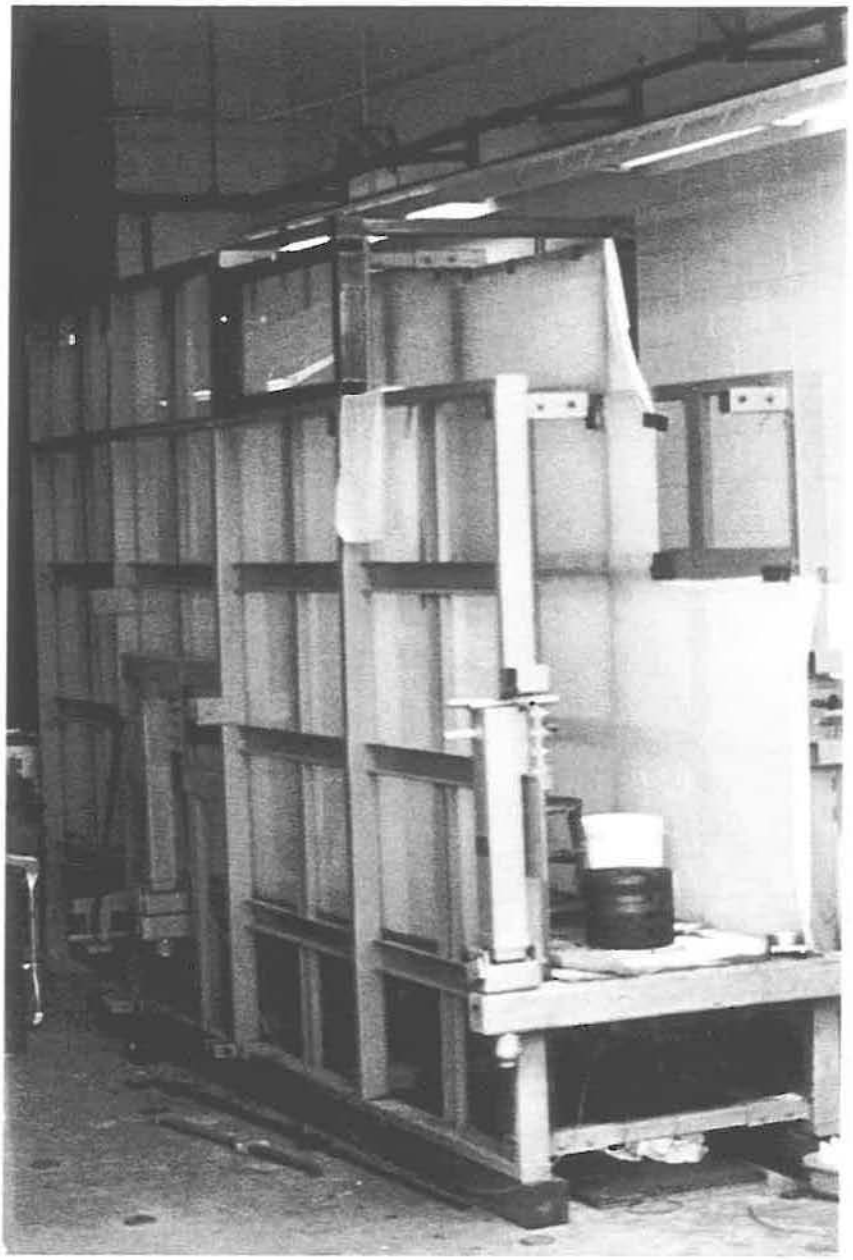

Figure 2.1 The Deep Patch Test Apparatus

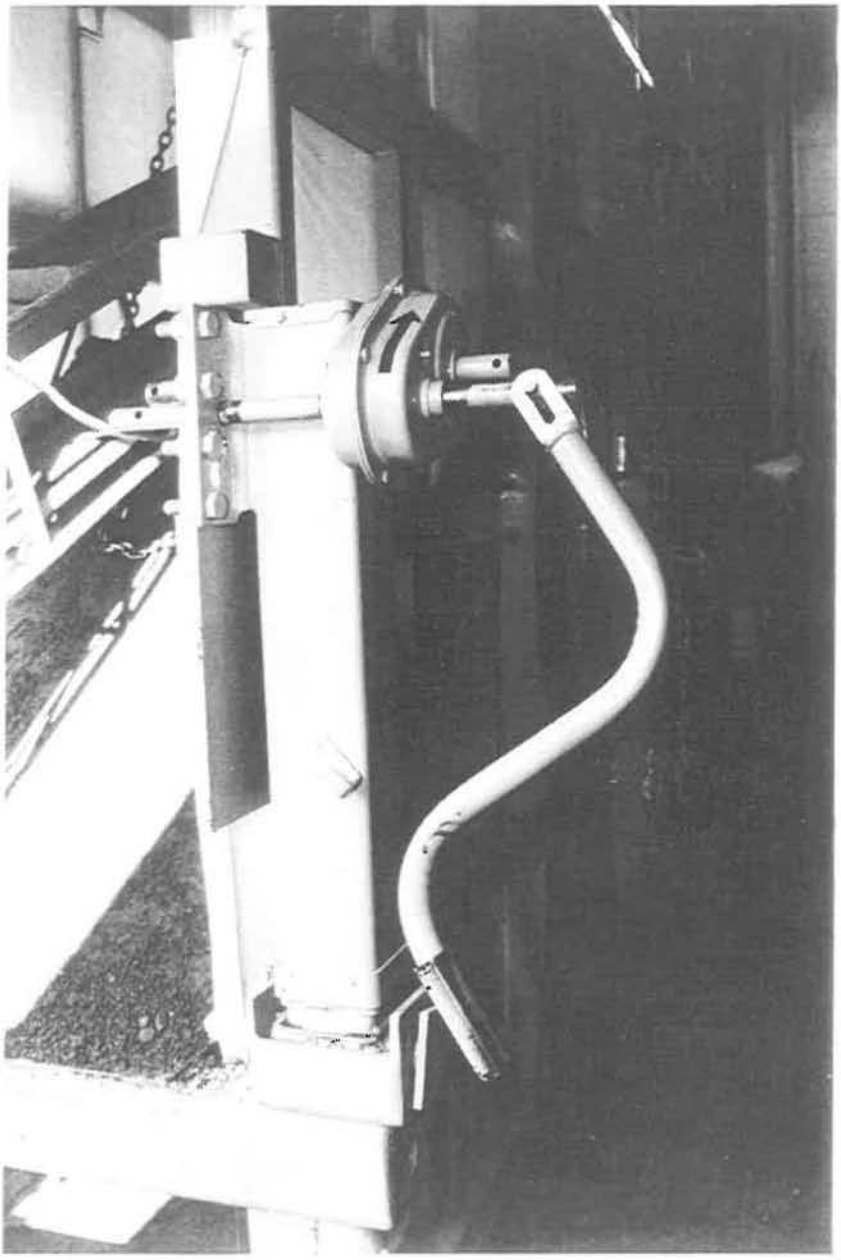

Figure 2.2 The Front Crank which Operates the Front Two Jacks

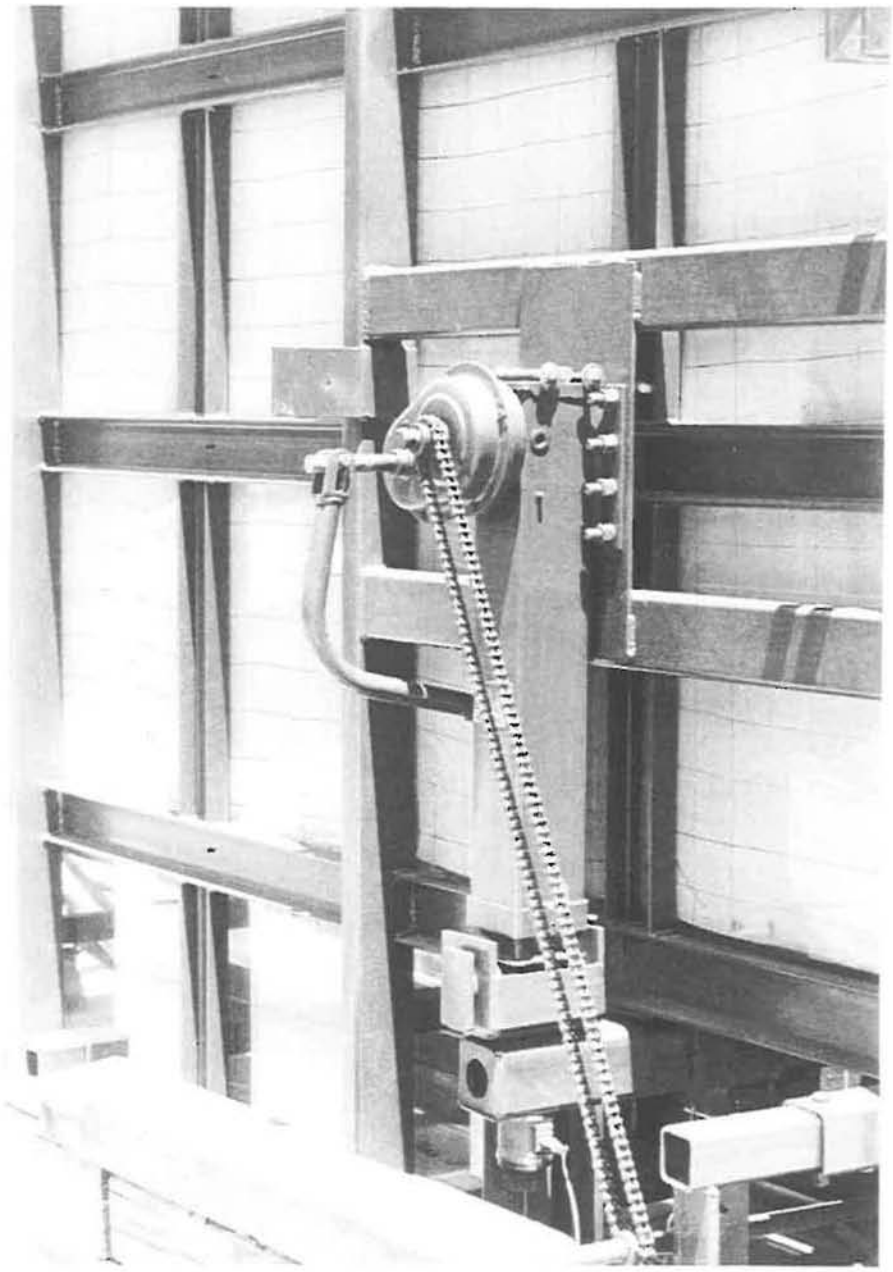

Figure 2.3 The Back Crank which Operates the Front Two Jacks

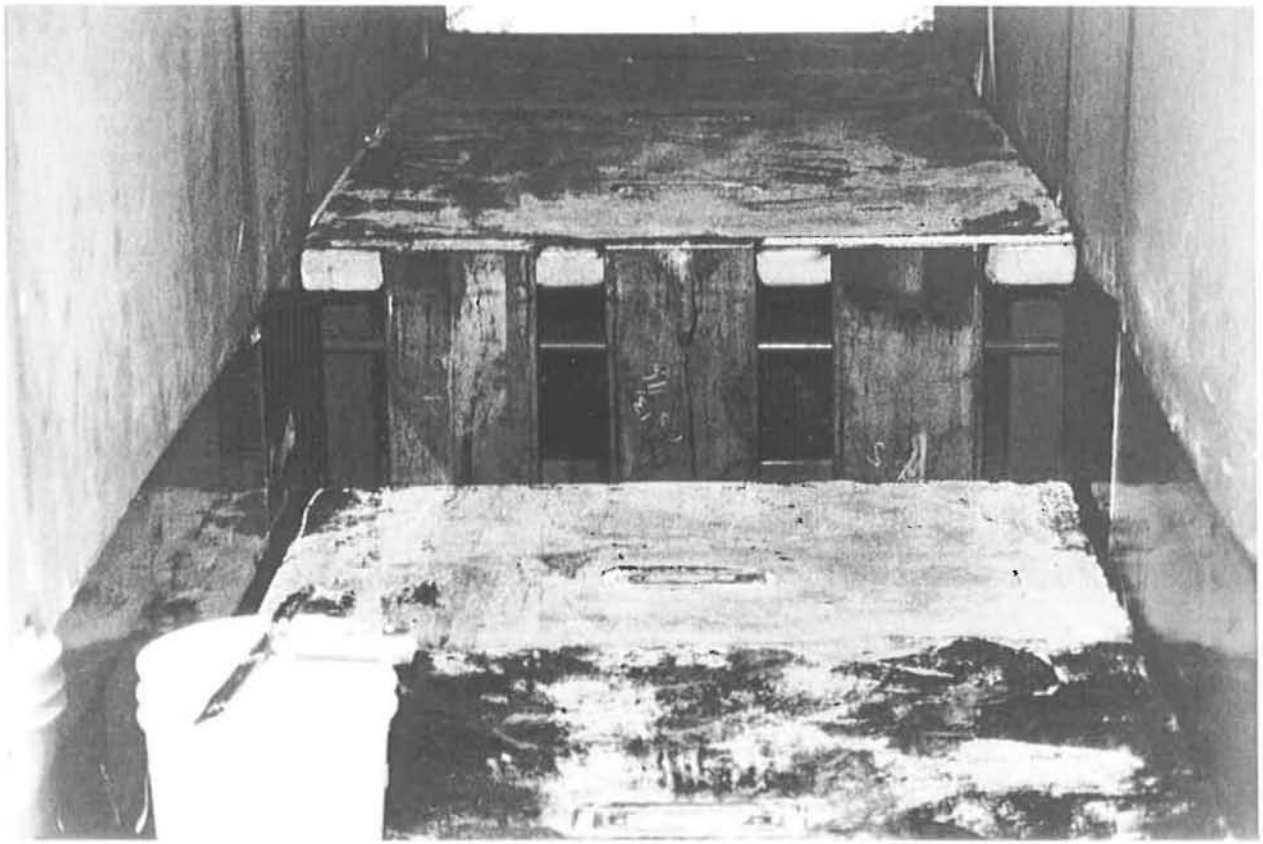

Figure 2.4 The Moveable Part of the Bottom Panel at 11 inch-Drop

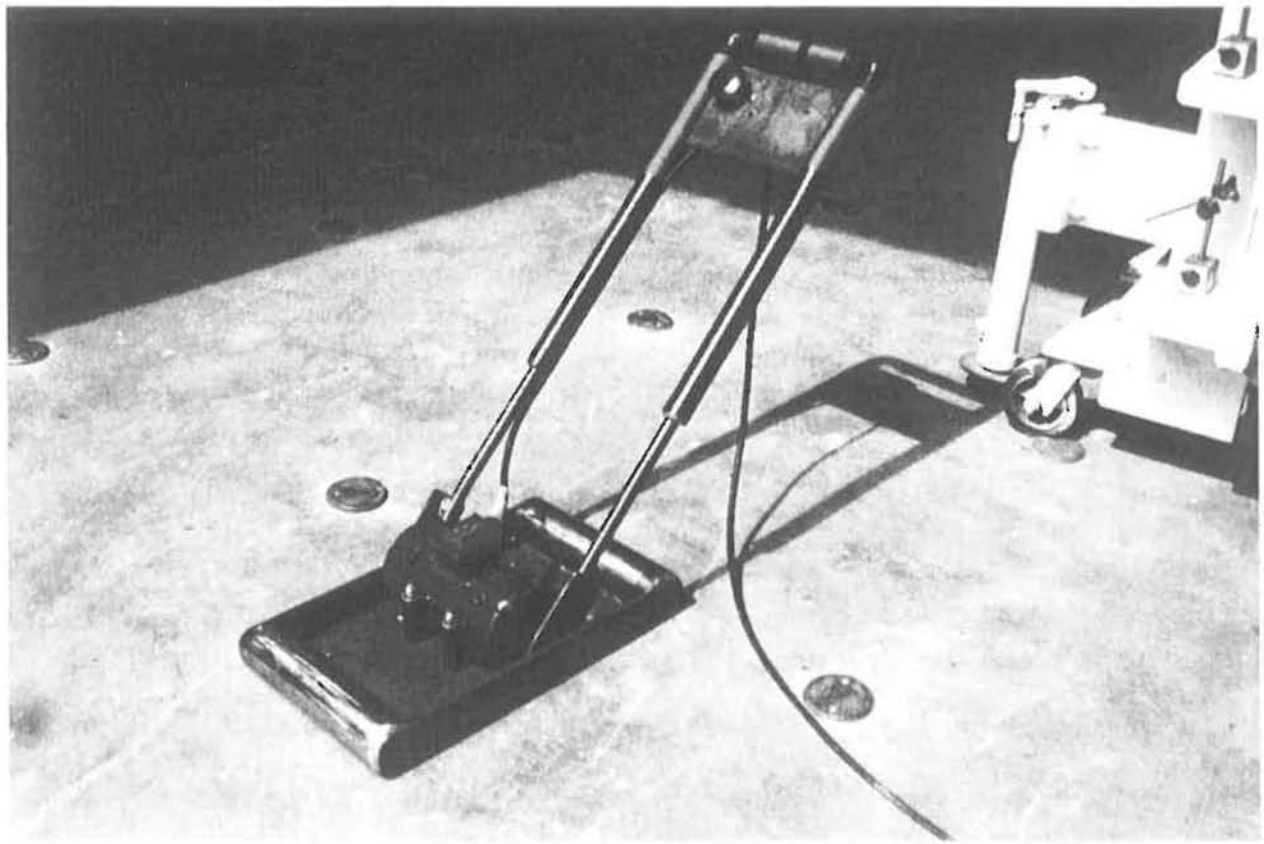

Figure 2.5 The Vibratory Plate Compactor

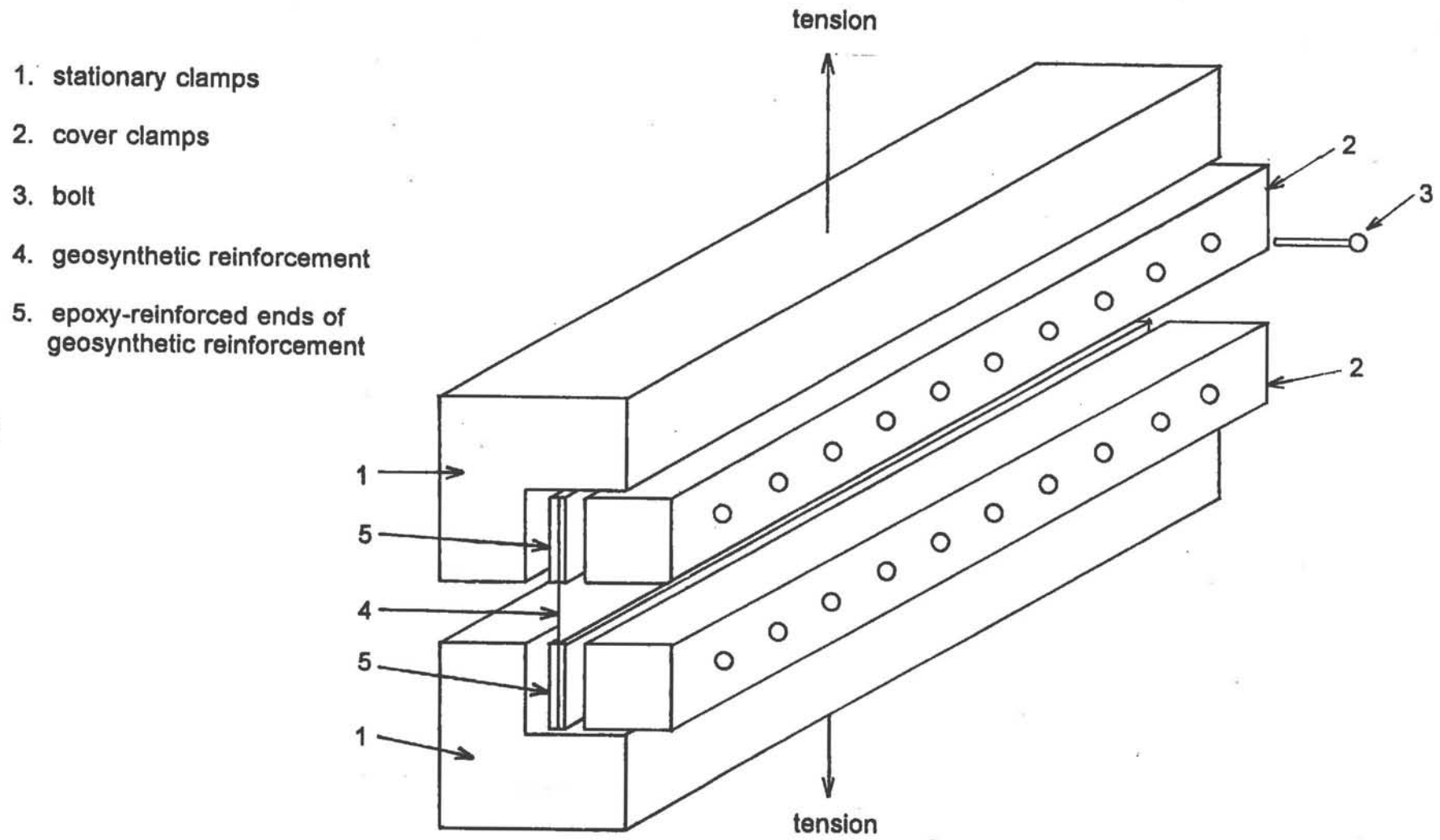

Figure 2.6 Schematic Diagram of the Uniaxial Load-Deformation Apparatus

Figure 2.7 The Uniaxial Load-Deformation Test

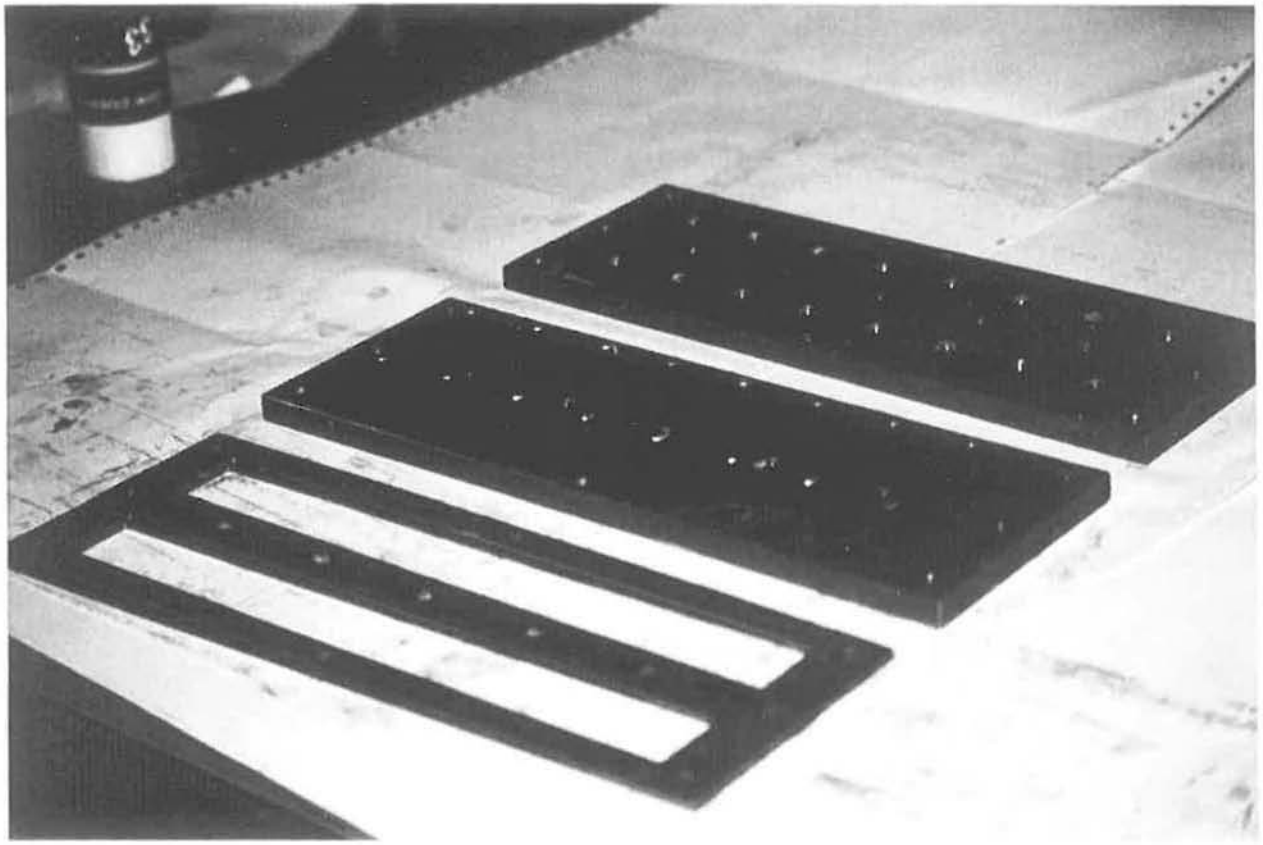

Figure 2.8 Steel Mold for Epoxy Application on the Two Ends of the Geotextile Specimen

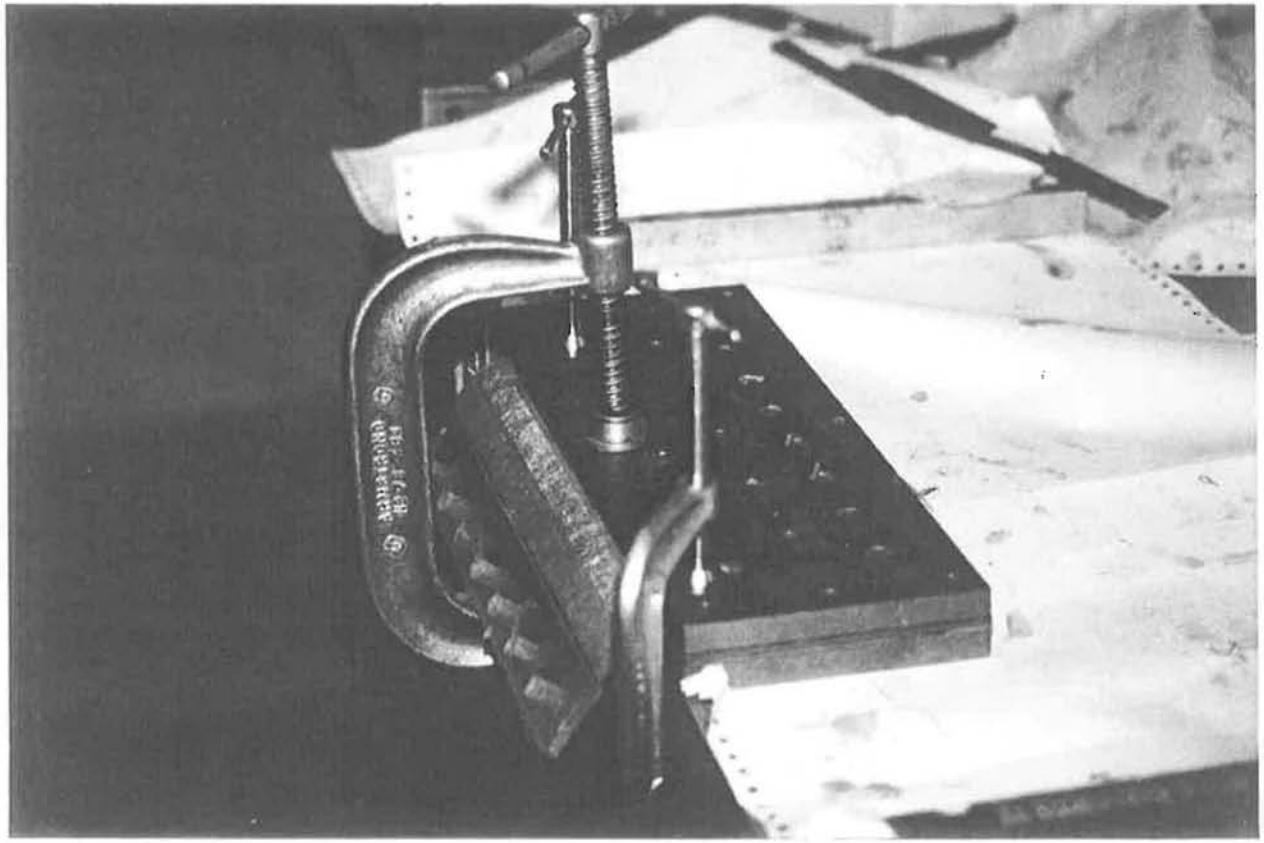

Figure 2.9 Assembly of Steel Mold for Epoxy Application on the Two Ends of the Geotextile Specimen

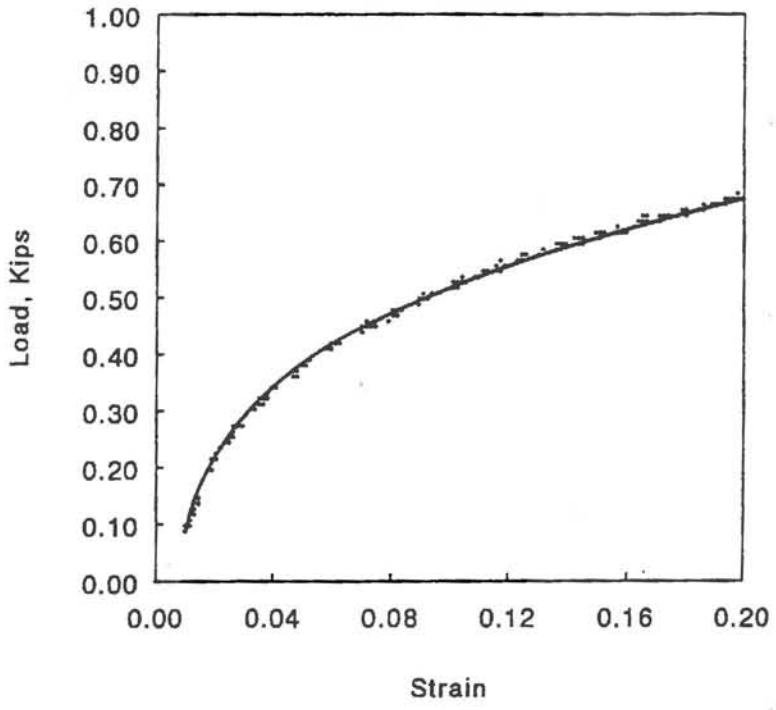

Figure 2.10 Load-Deformation Behavior of the Geotextile Reinforcement

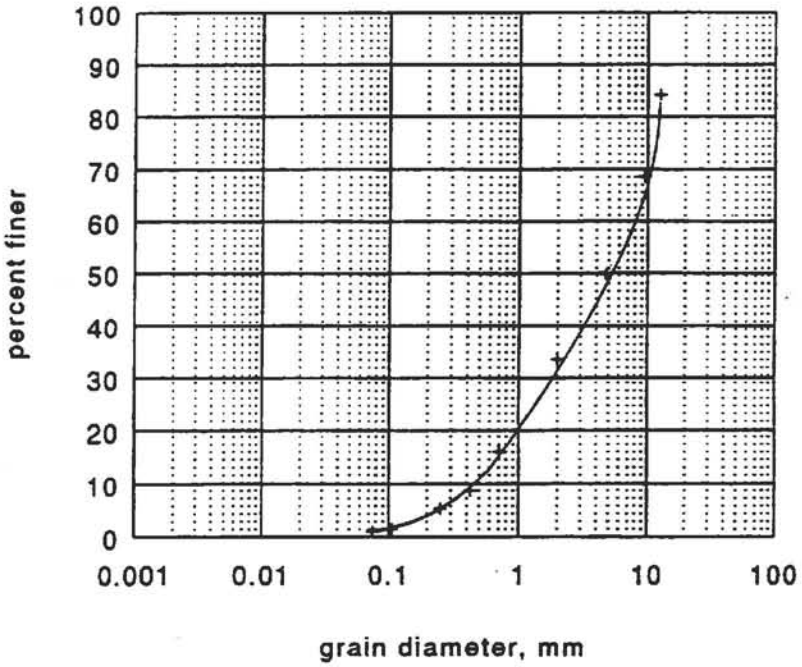

Figure 2.11 Grain Size Distribution Curve of the Gravelly Sand

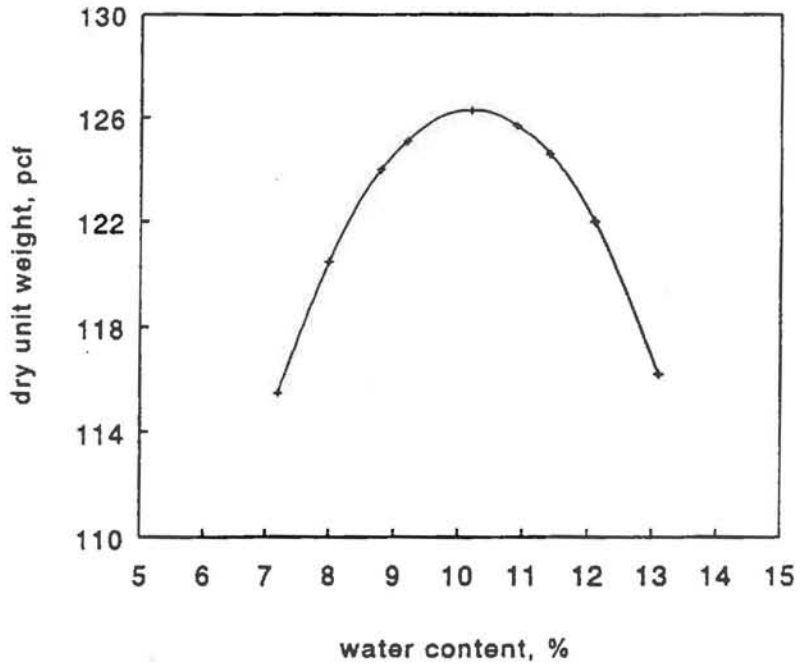

Figure 2.12 Compaction Curve of the Gravelly Sand

Figure 2.13(a) Triaxial Compression Test Results for the Gravelly Sand

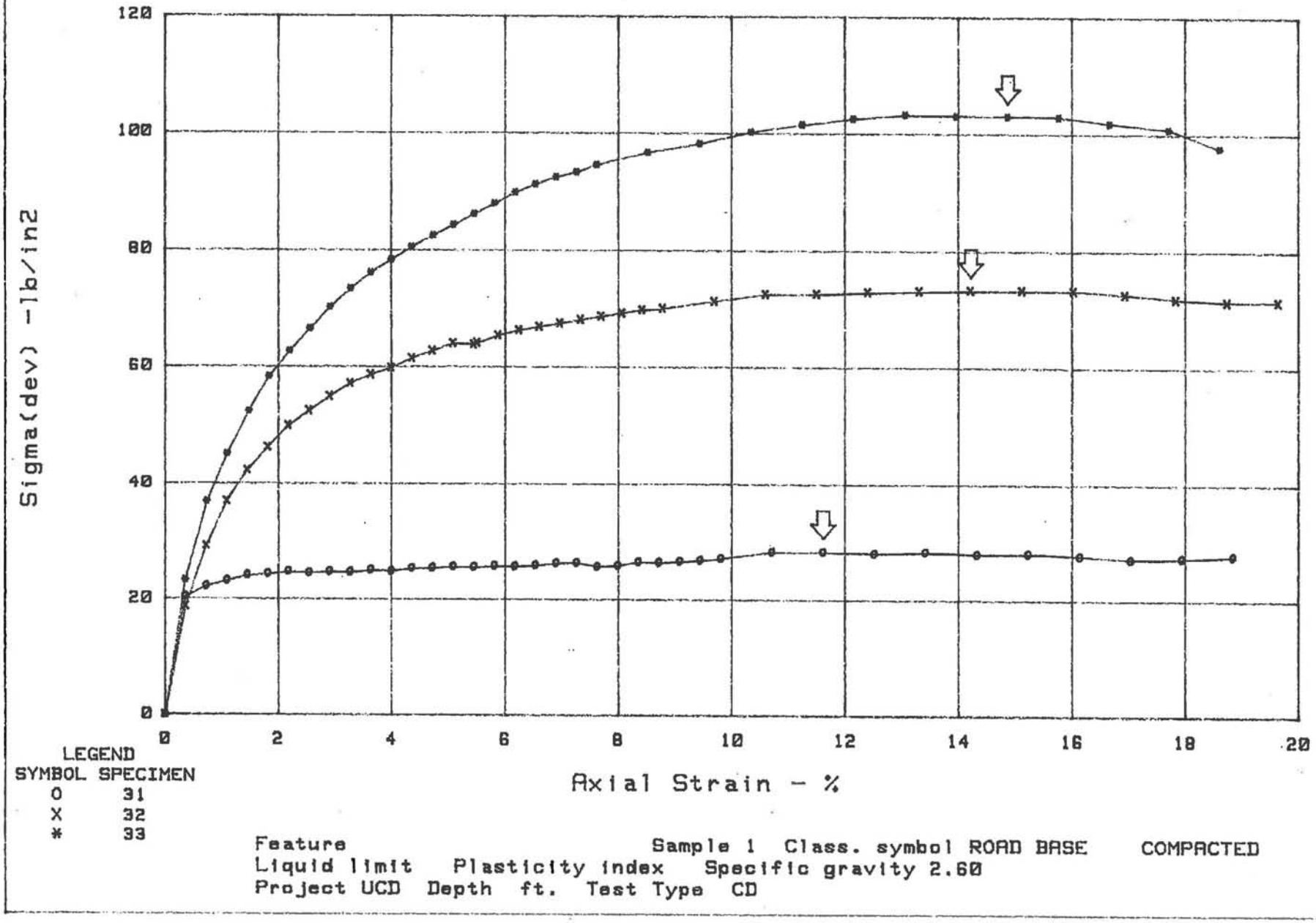

Figure 2.13(b) Triaxial Compression Test Results for the Gravelly Sand

10 Feb 1994
15:54:29

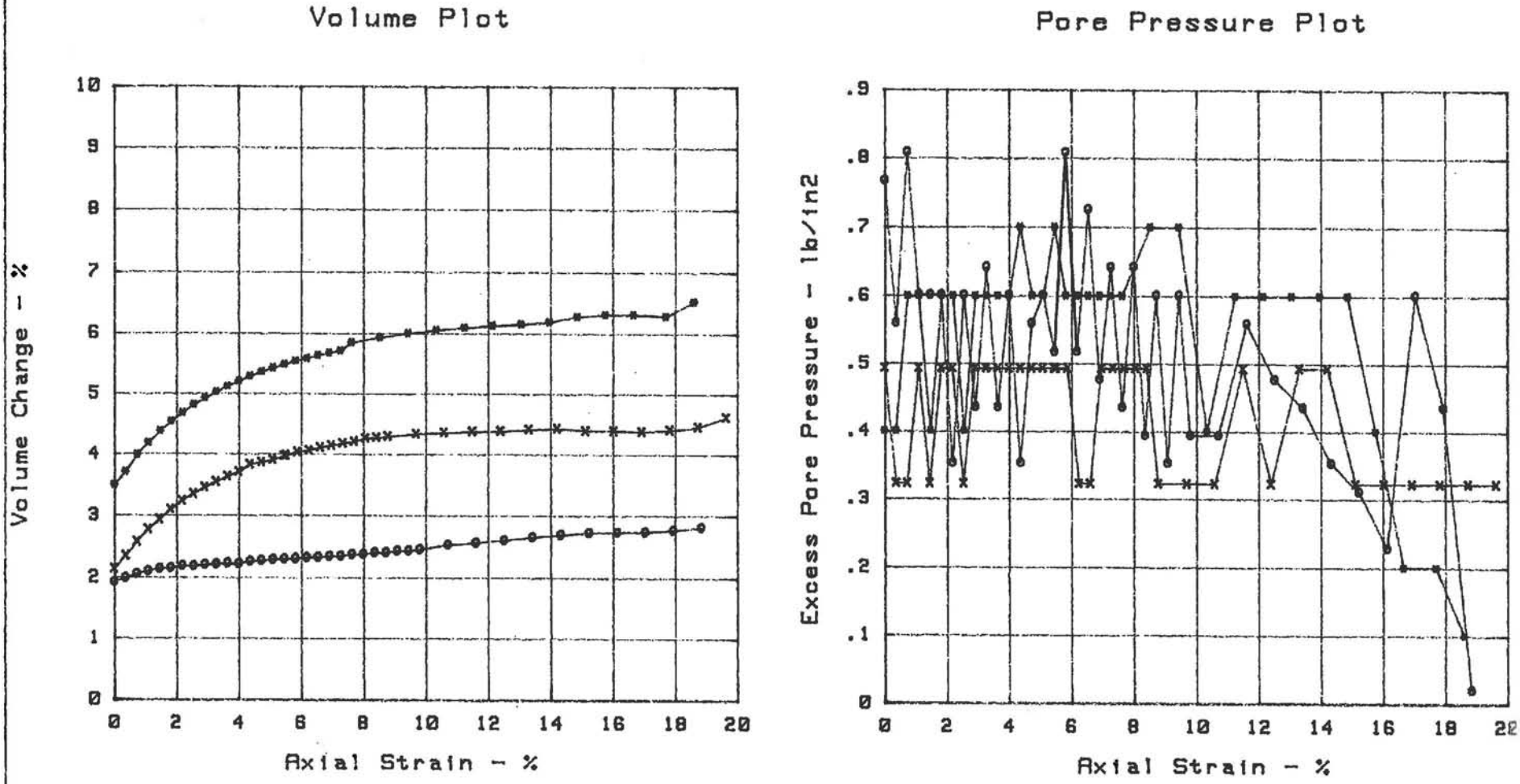

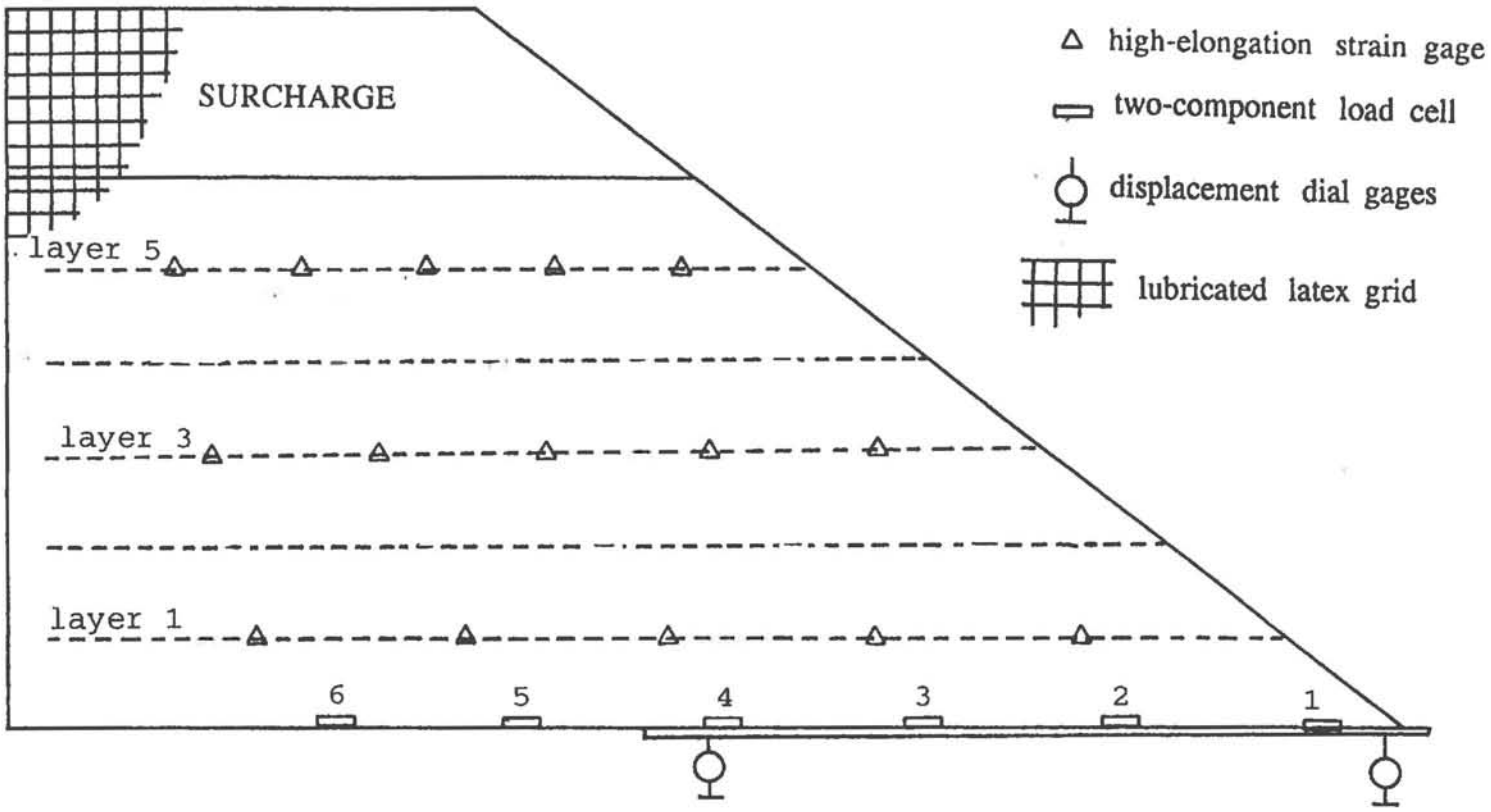

Figure 2.14 Instrumentation of the USFS Deep Patch Test

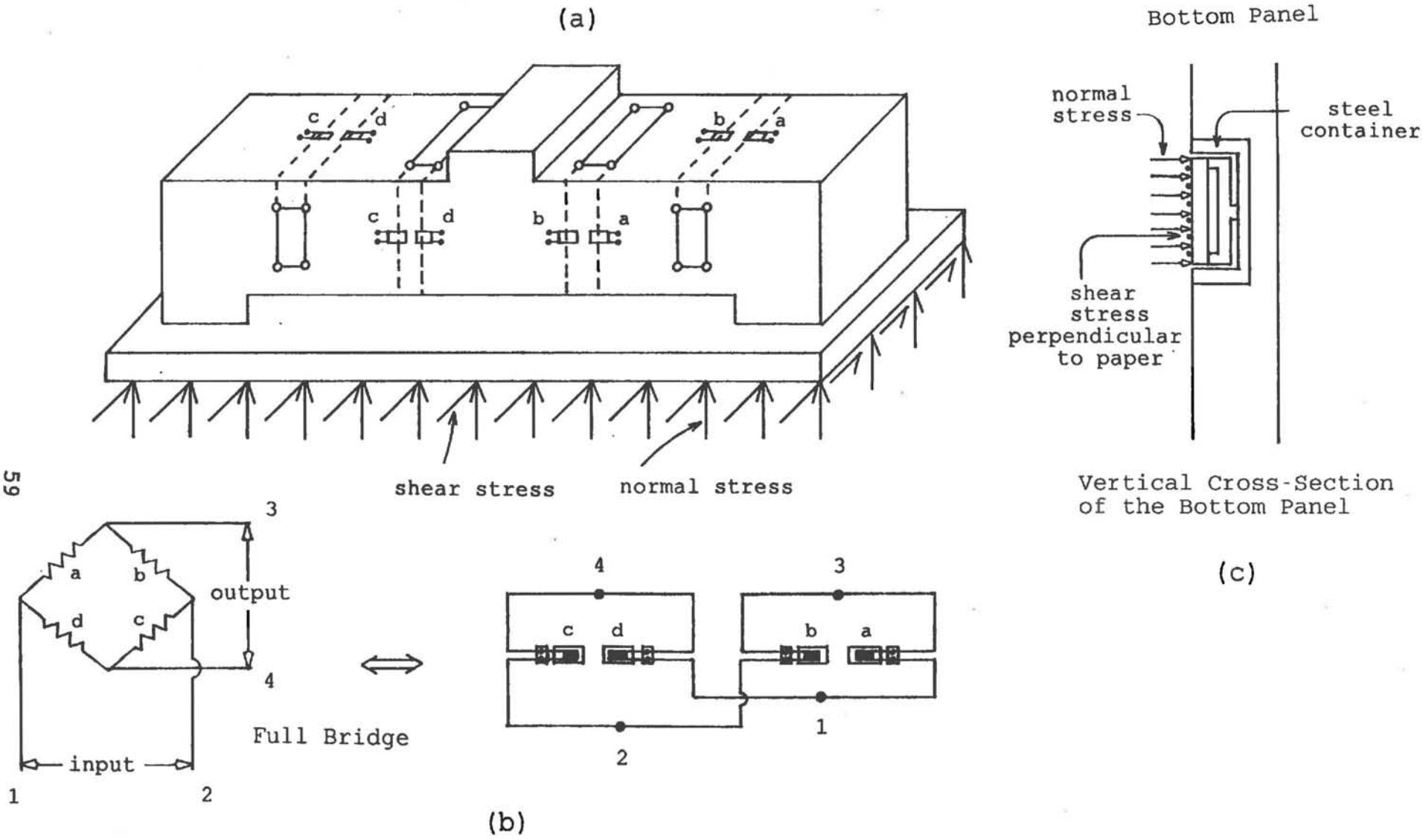

Figure 2.15 Schematic Diagram of the Two-Component Load Cell

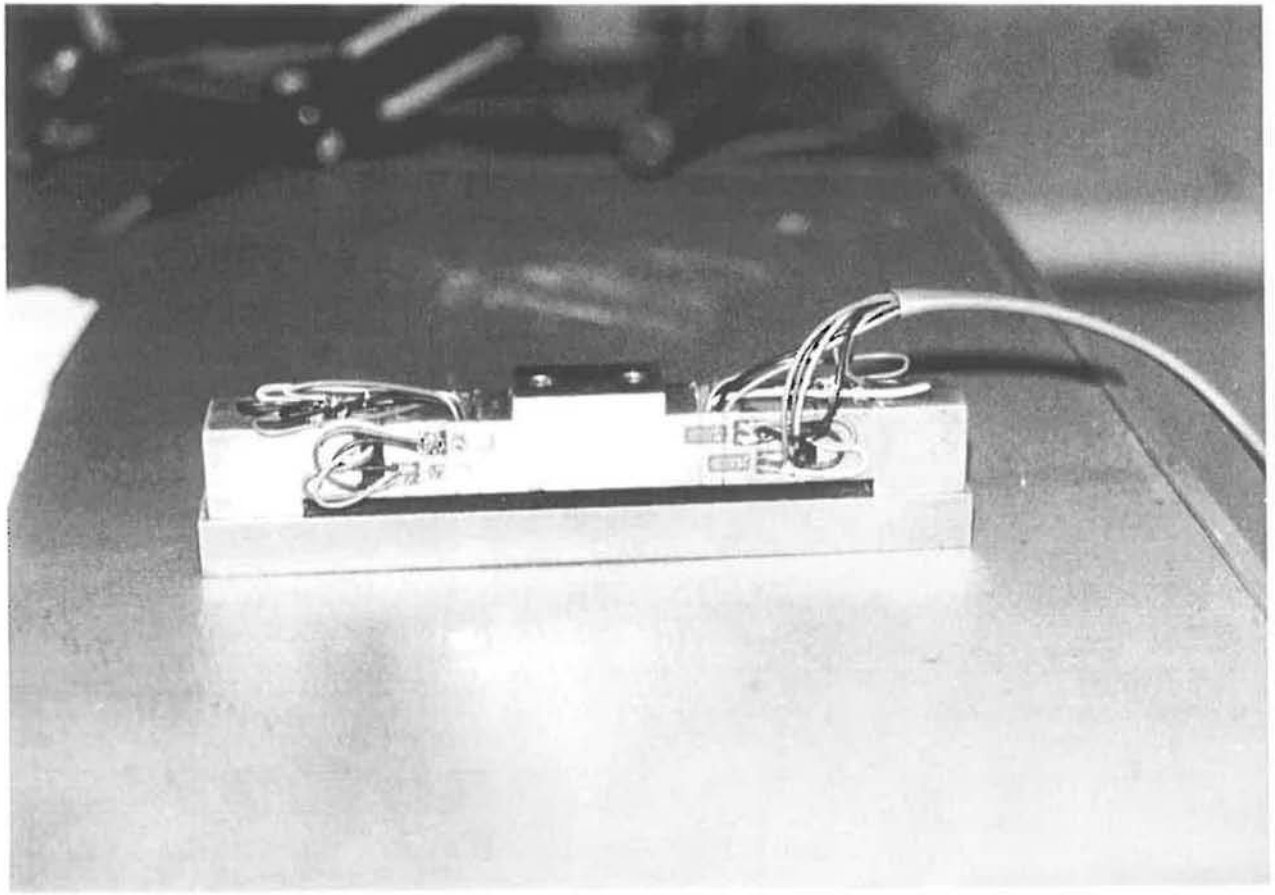

Figure 2.16 Instrumentation of the Two-Component Load Cell

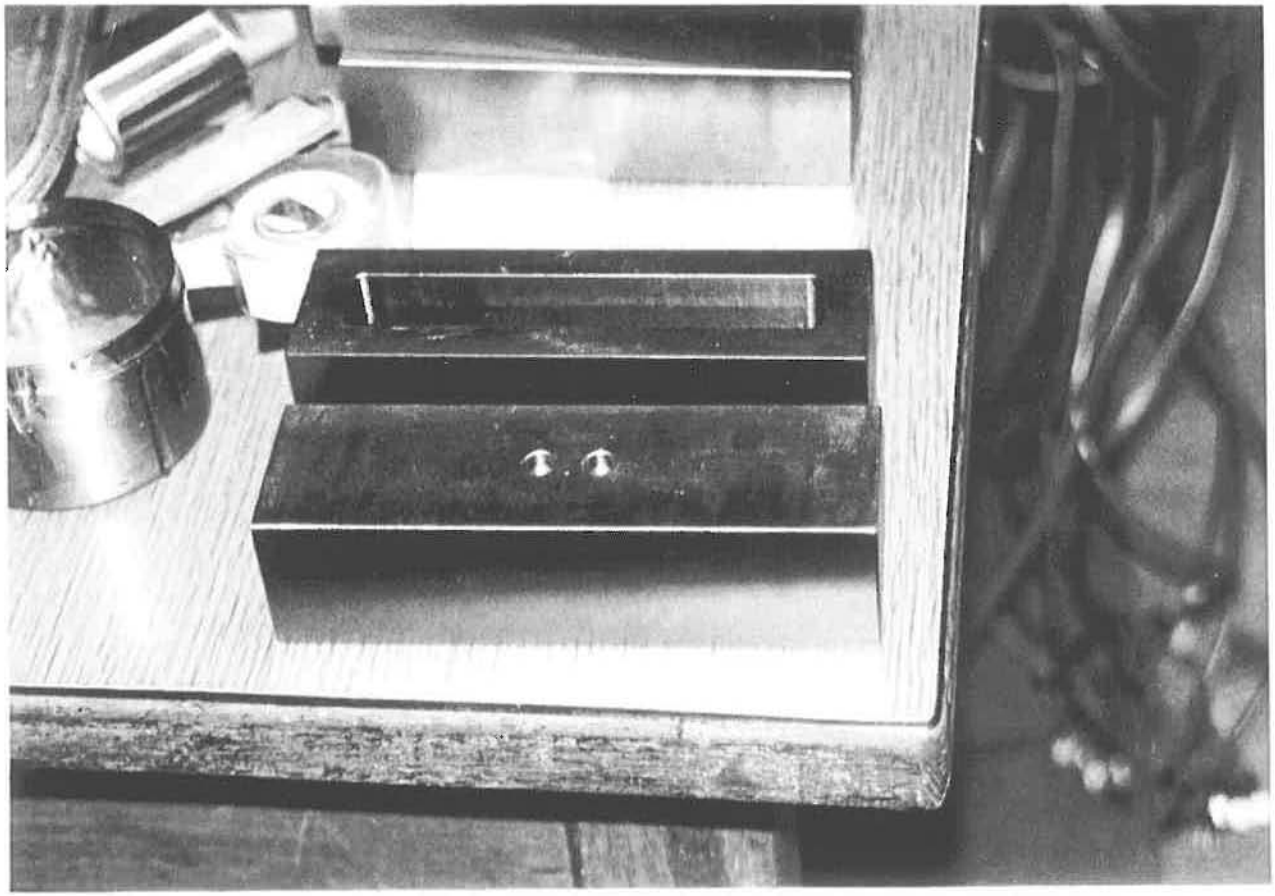

Figure 2.17 Steel Box for Load Cell Protection

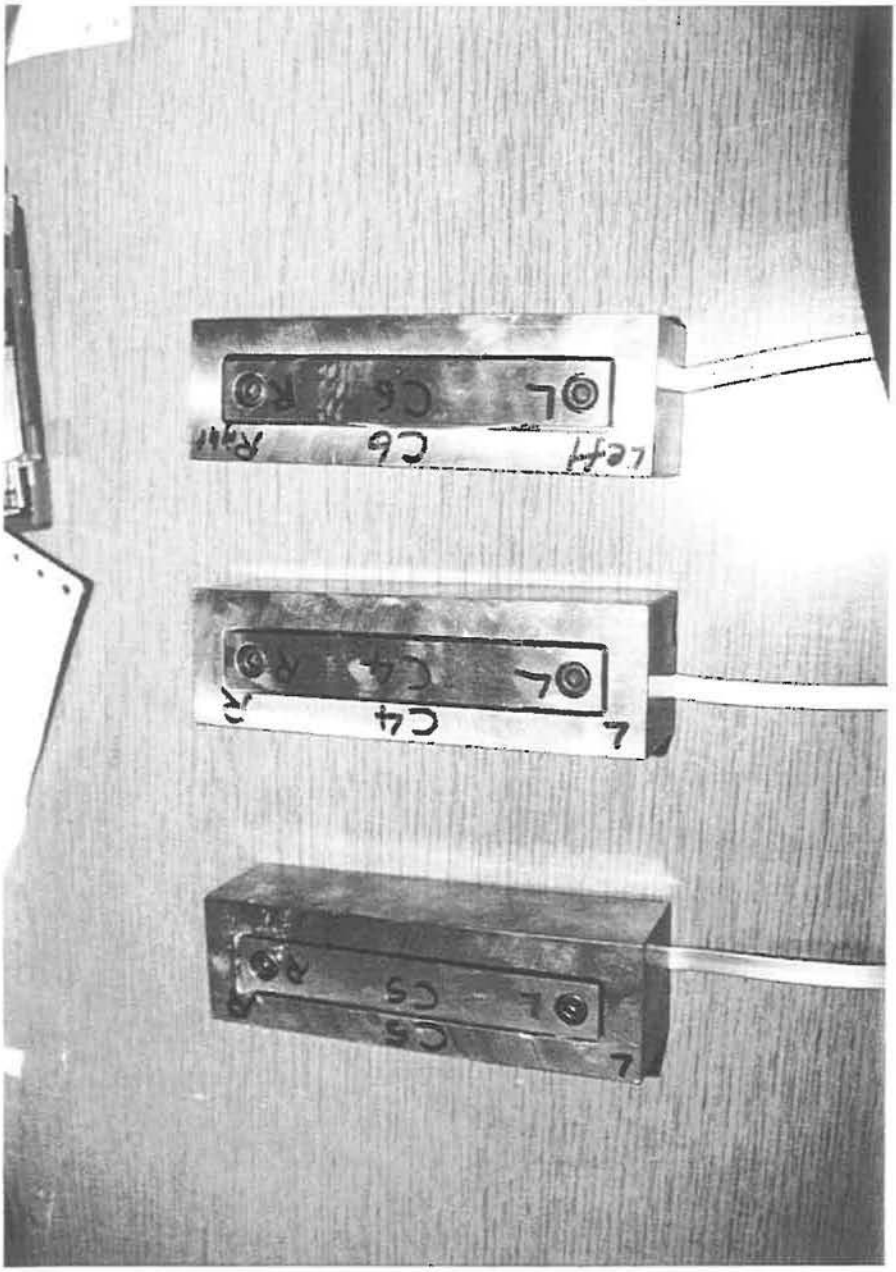

Figure 2.18 The Load Cell Inside the Protective Steel Box

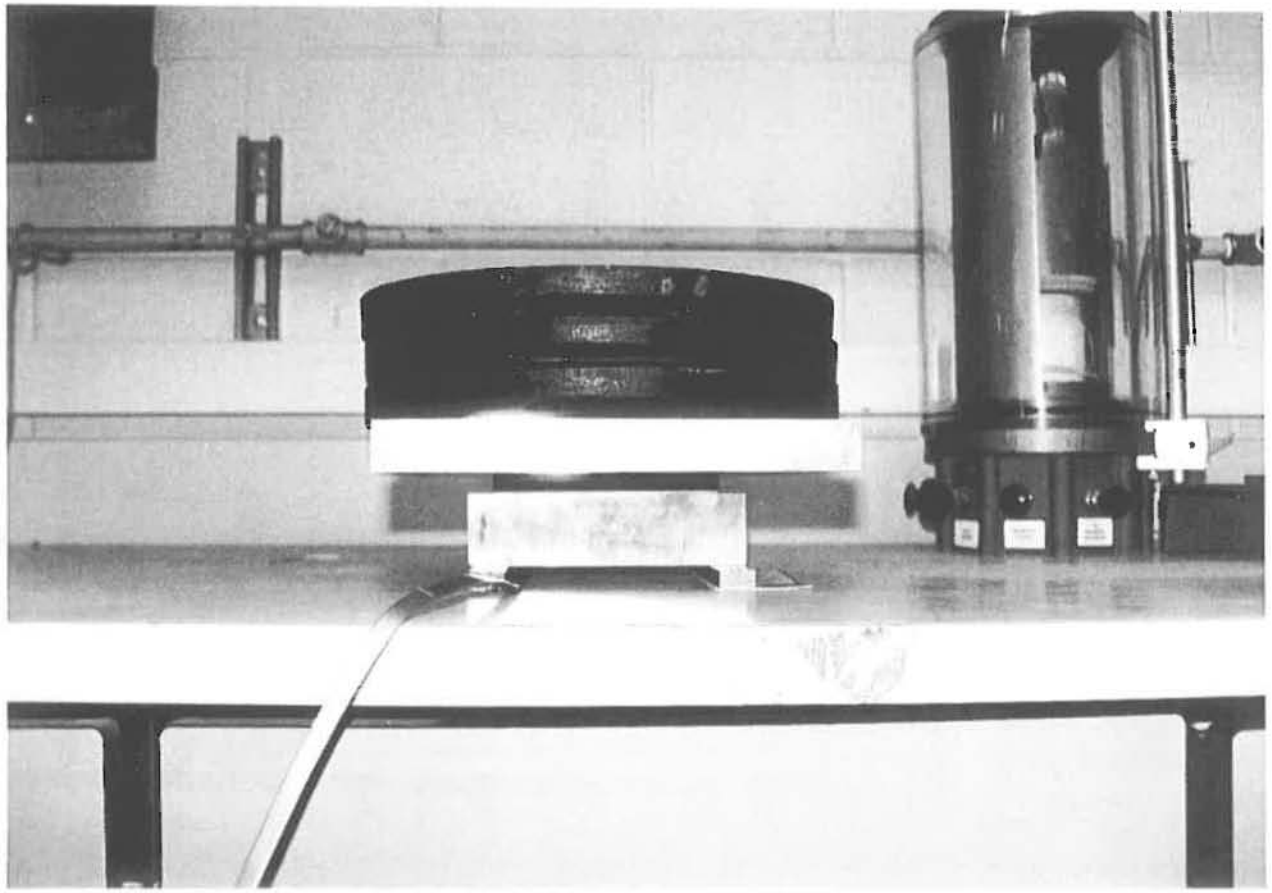

Figure 2.19 Normal Stress Calibration of Load Cell

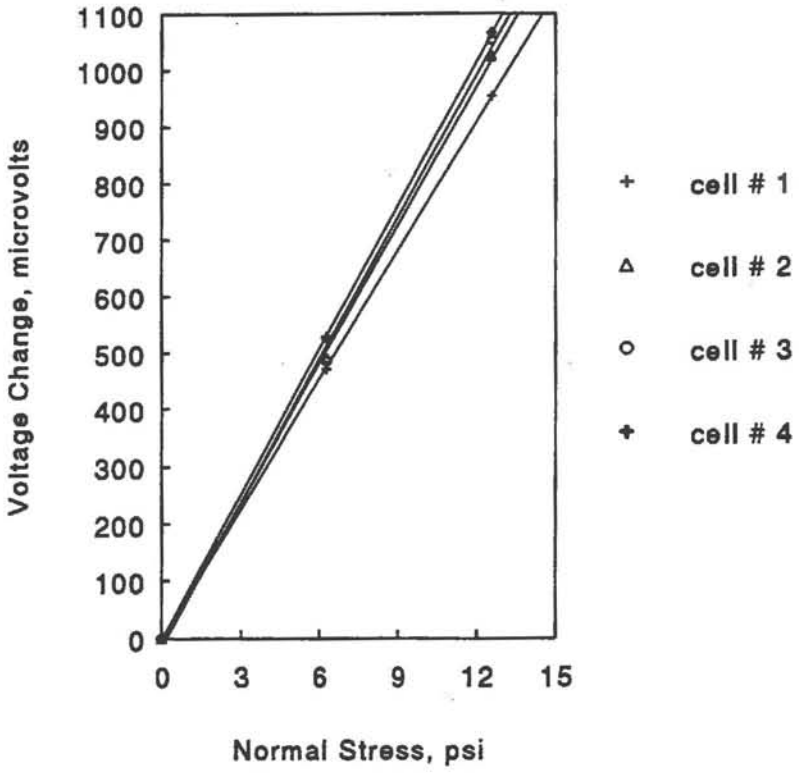

Figure 2.20 Normal Stress Calibration Curves for Load Cell

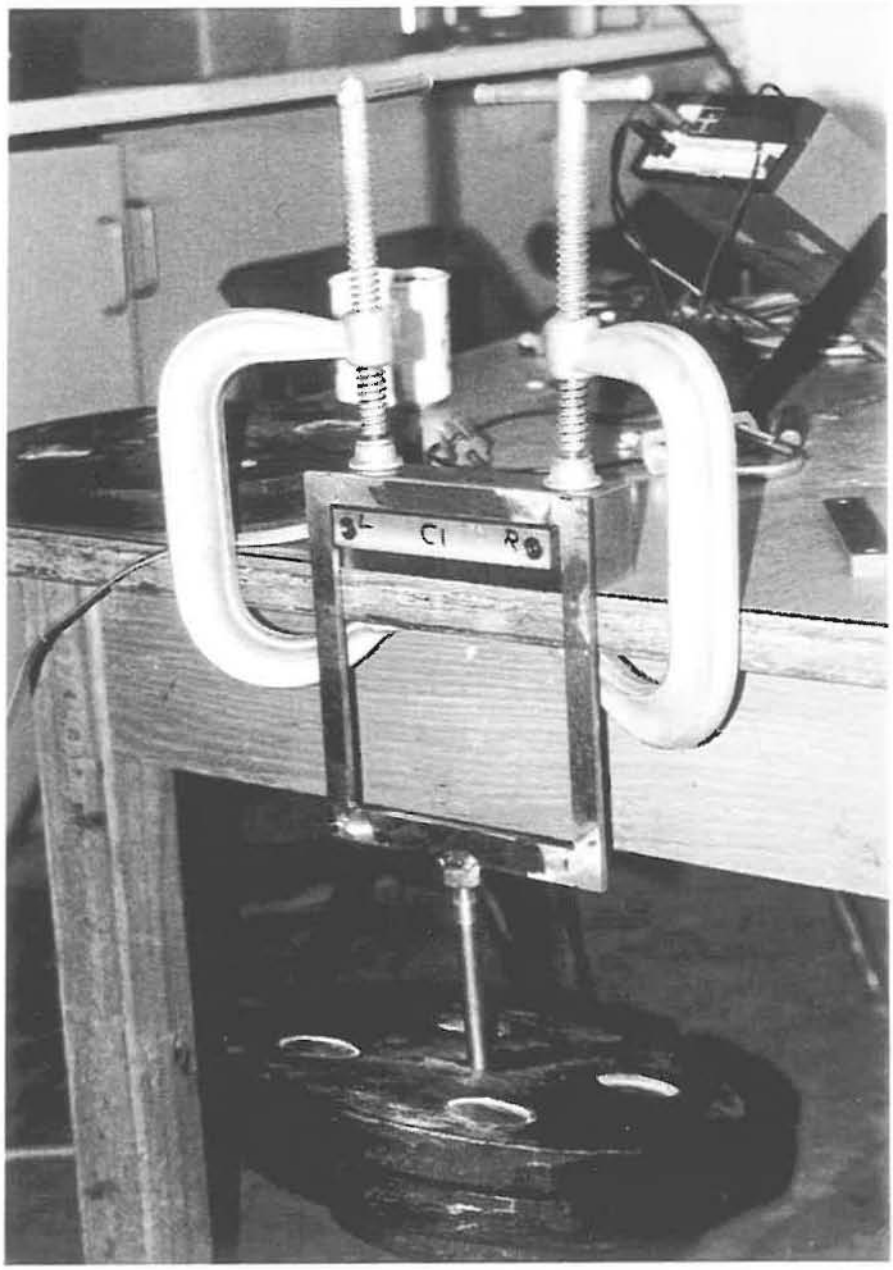

Figure 2.21 Shear Stress Calibration of Load Cell

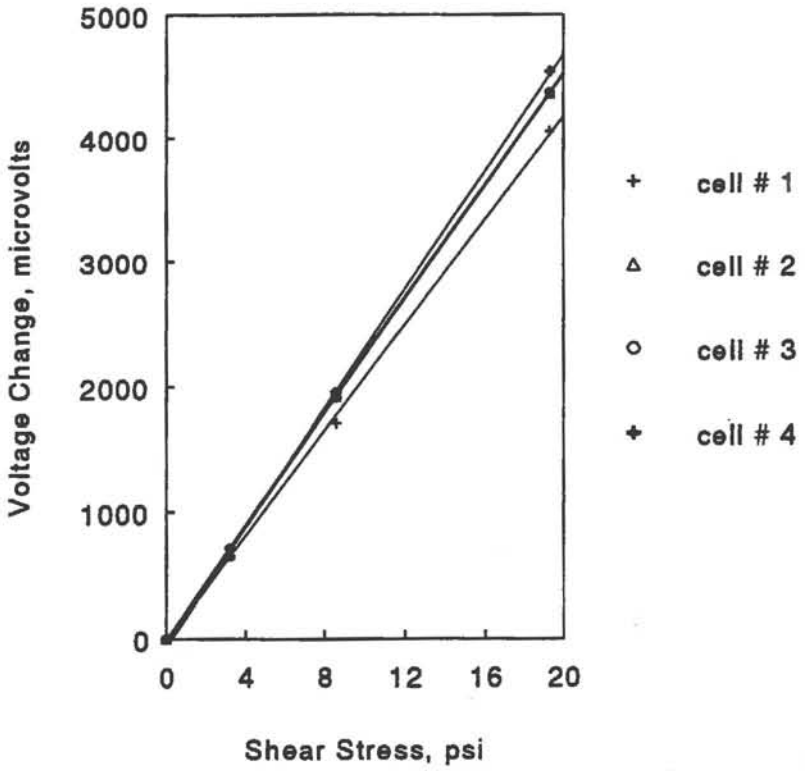

Figure 2.22 Shear Stress Calibration Curves for Load Cell

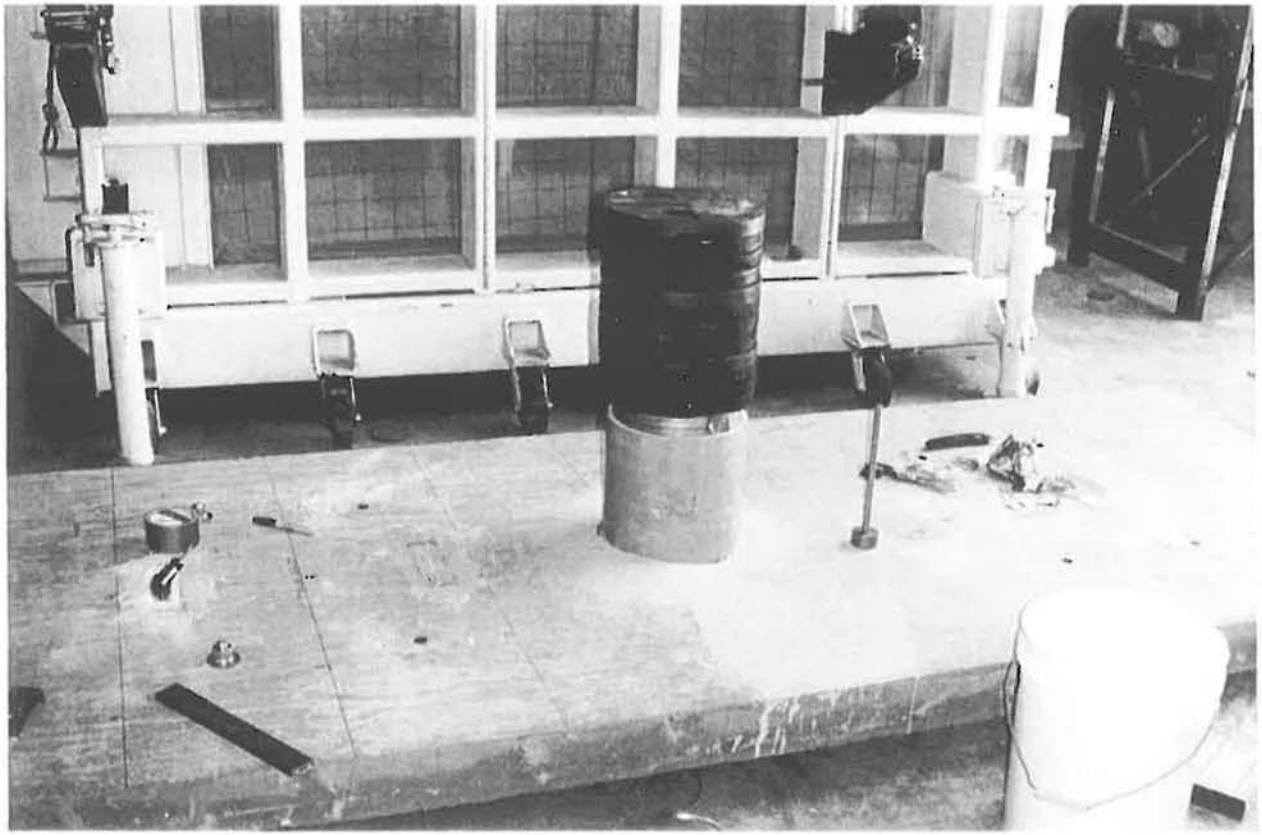

Figure 2.23 In-Soil Calibration of Load Cell

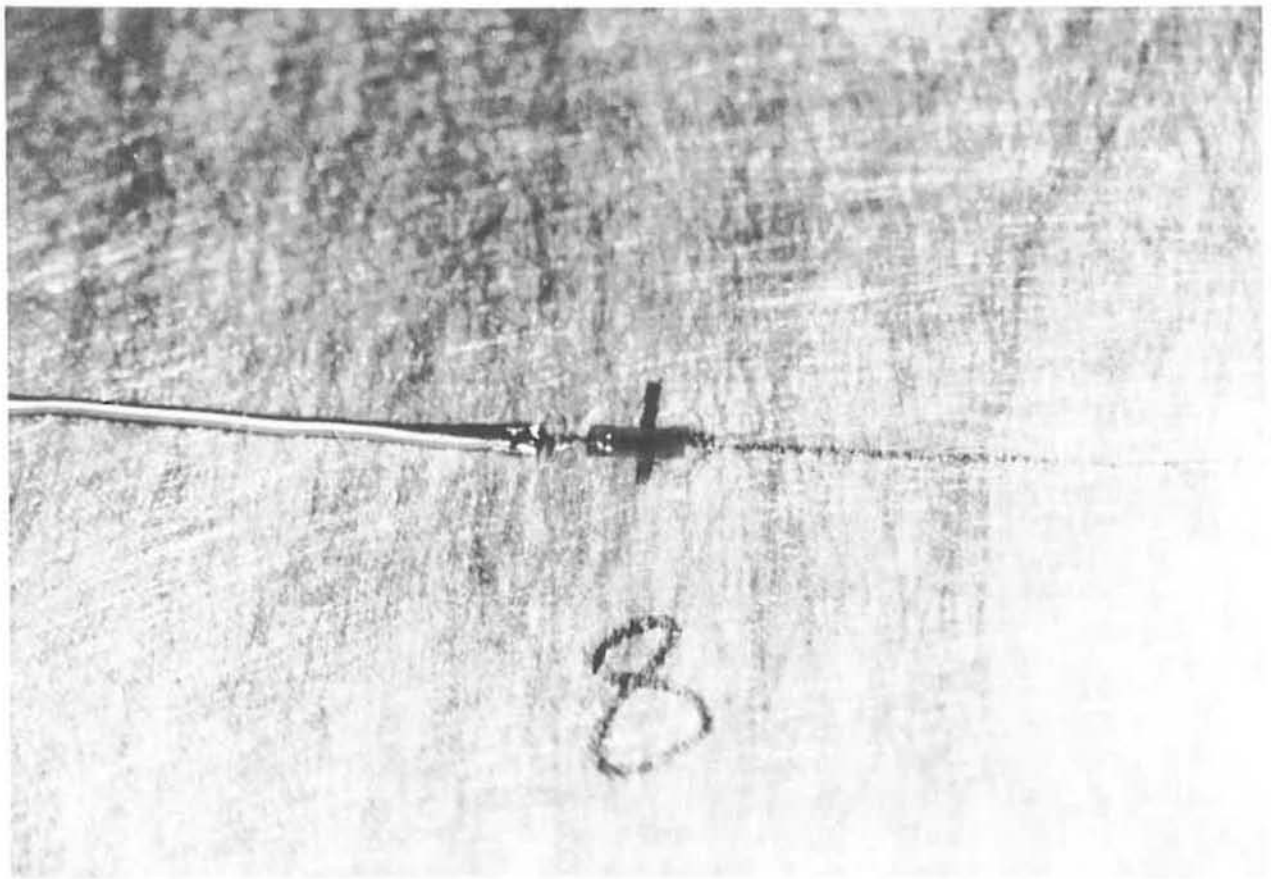

Figure 2.24 Strain Gage Mounting Method

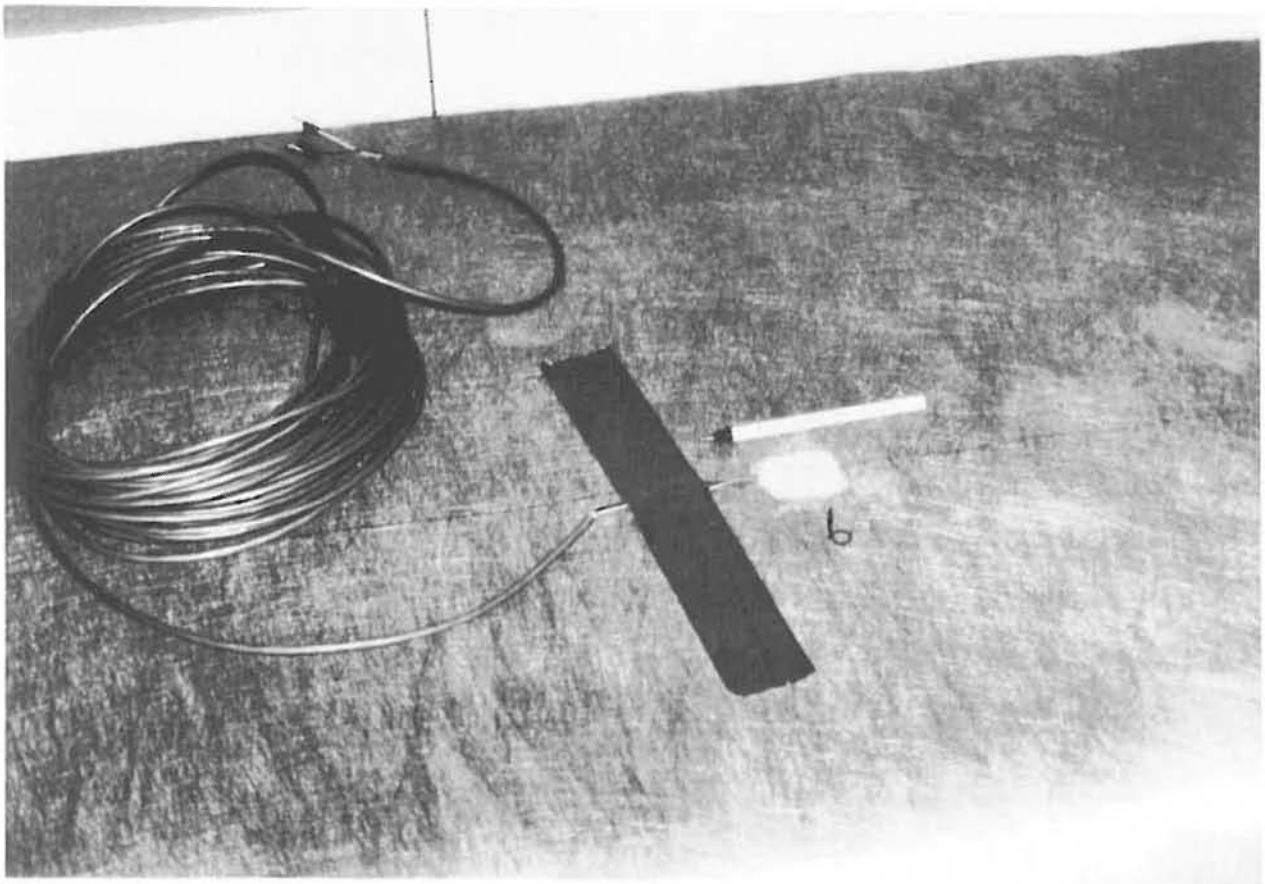

Figure 2.25 Strain Gage Covered with the Protective Mixture

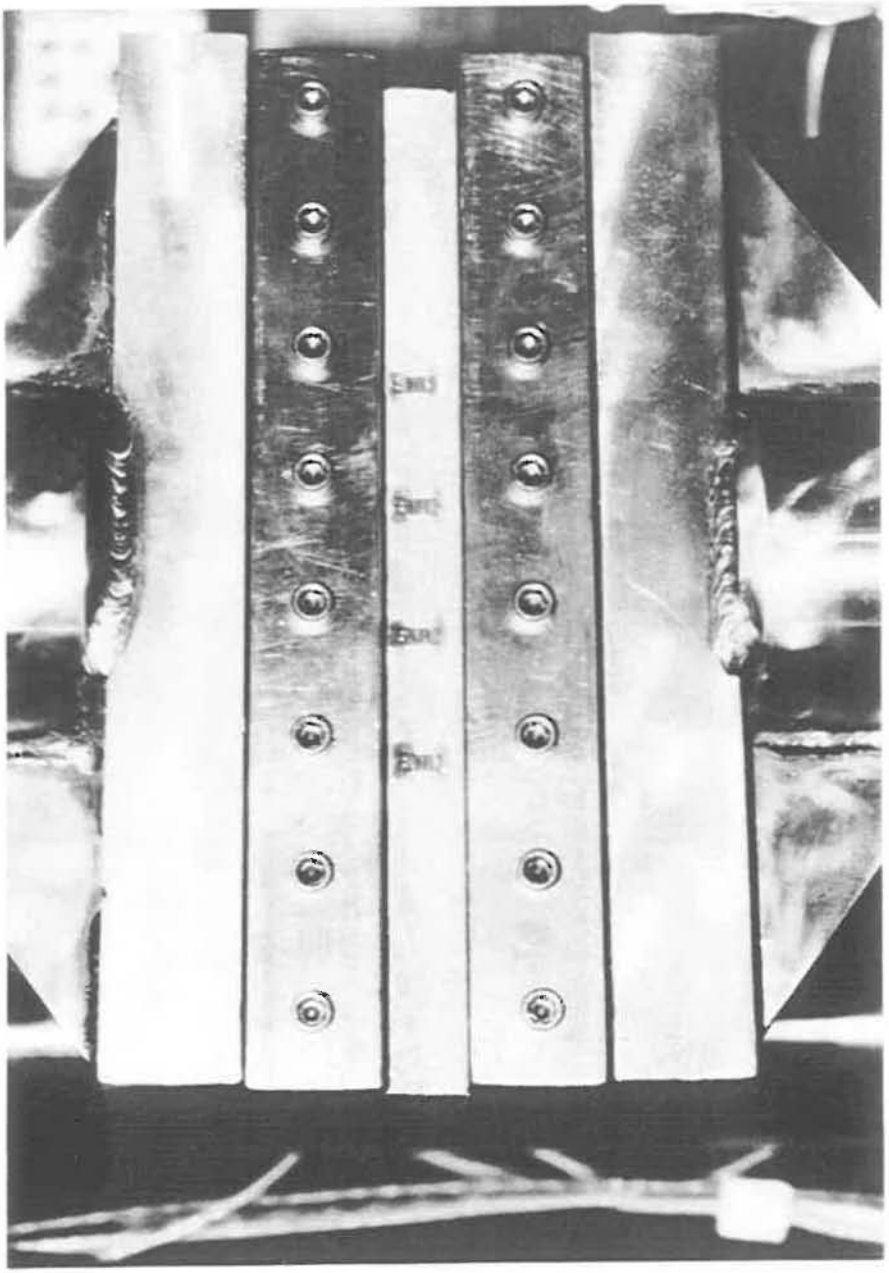

Figure 2.26 Strain Gage Calibration in the Uniaxial Load-Deformation Test

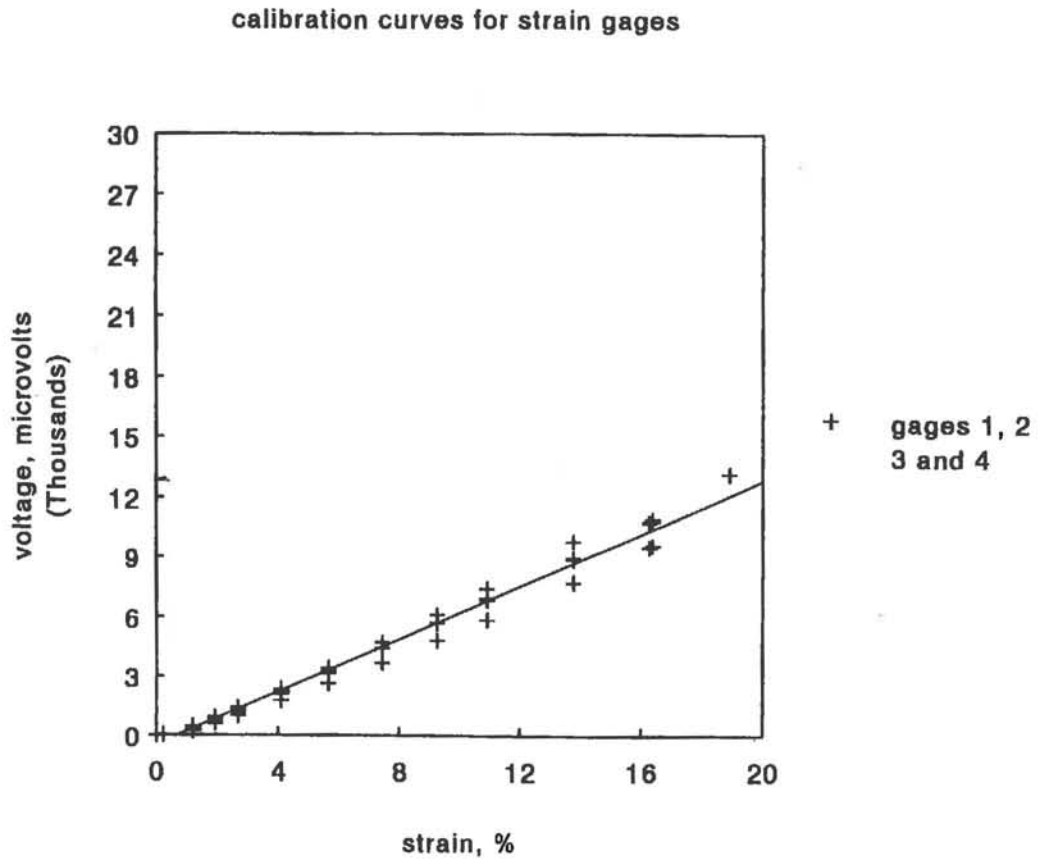

Figure 2.27 Calibration Curve for Strain Gage

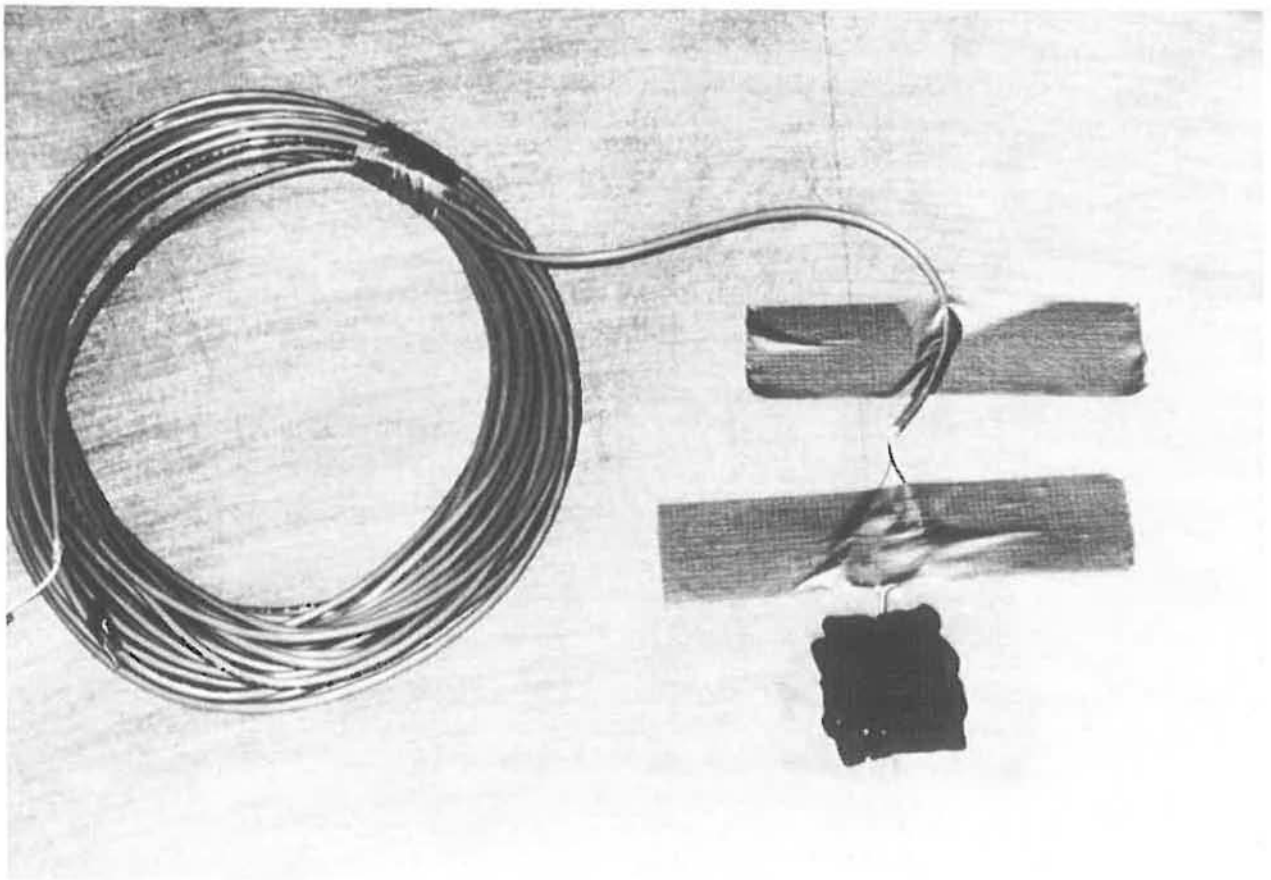

Figure 2.28 Environmental and Mechanical Protection of Strain Gages Using a layer of Neoprene Rubber

Figure 2.29 Geotextile Layer Instrumented with Strain Gages

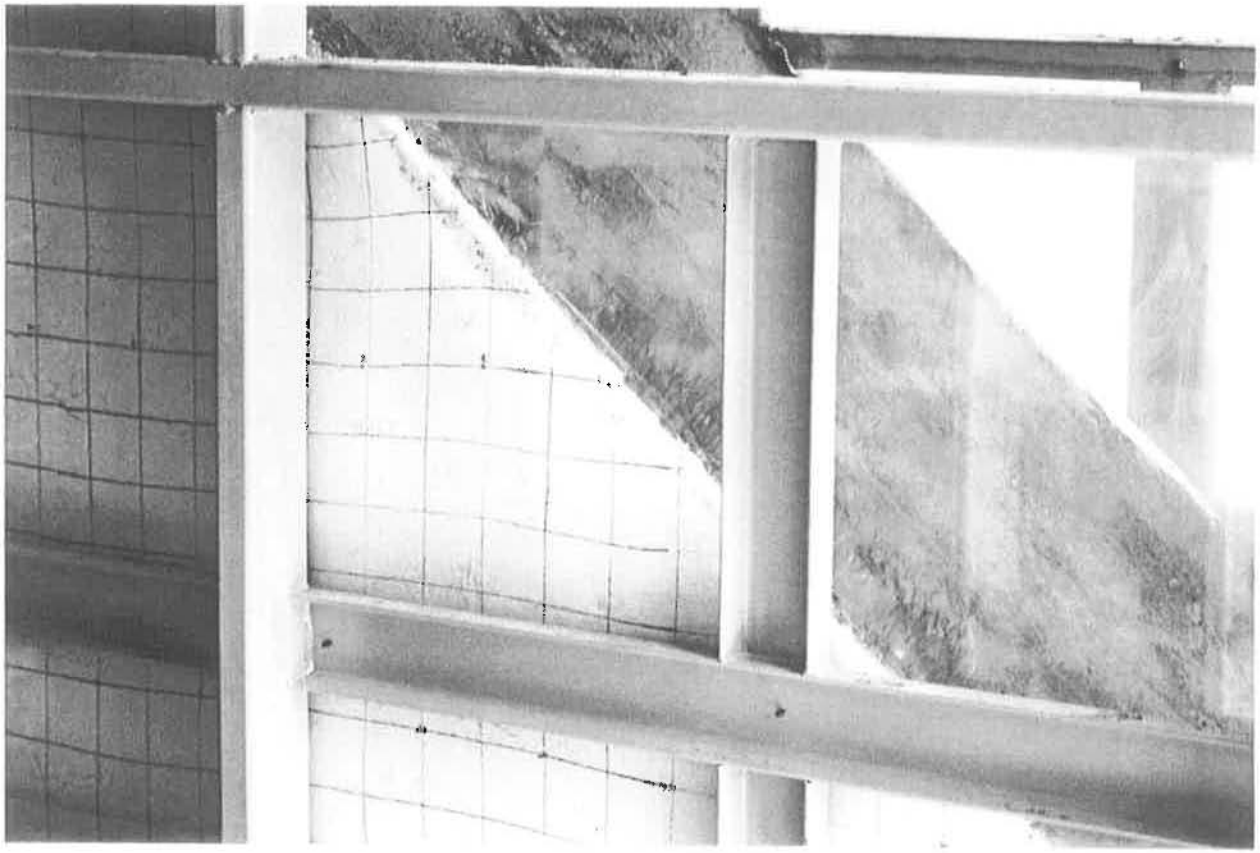

Figure 2.30 Lubricated Side-Wall Grid System (close-up)

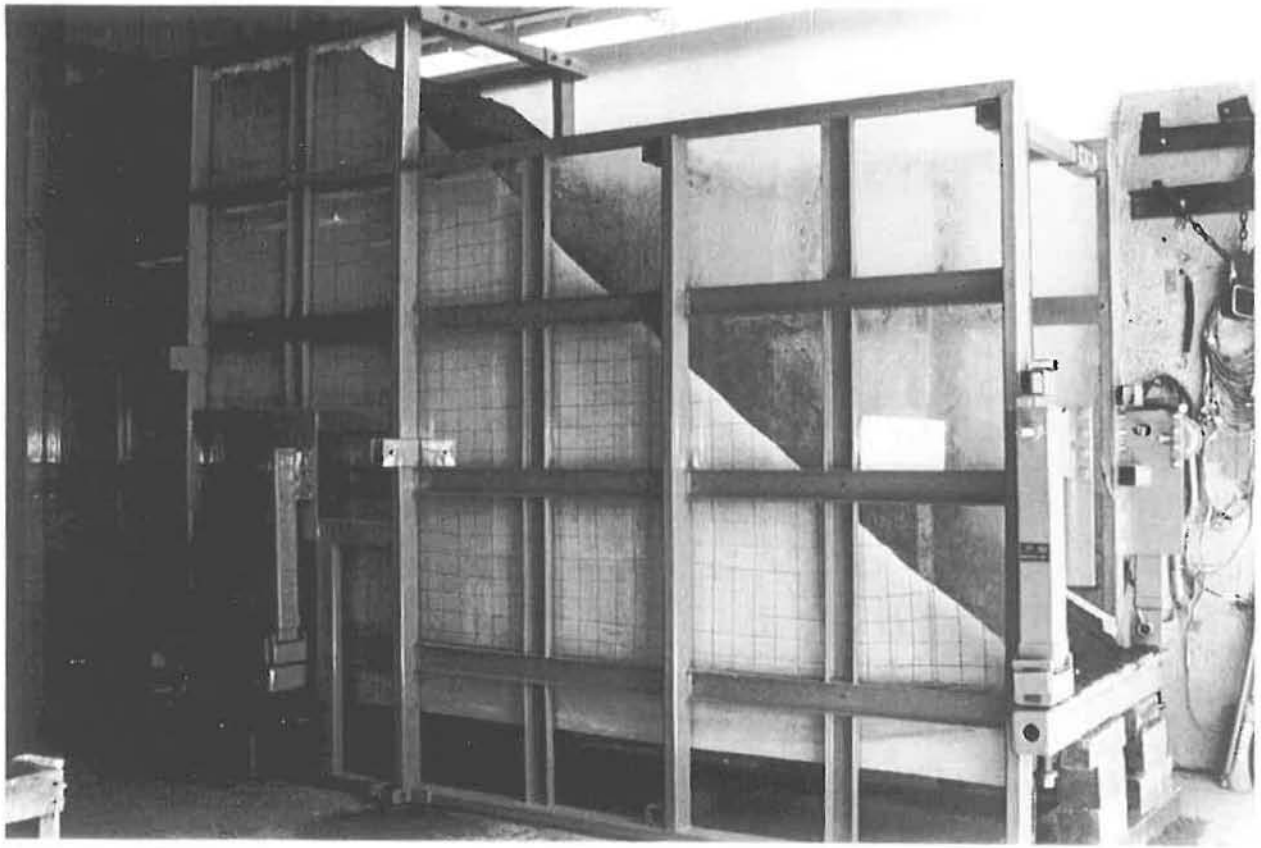

Figure 2.31 Lubricated Side-Wall Grid System

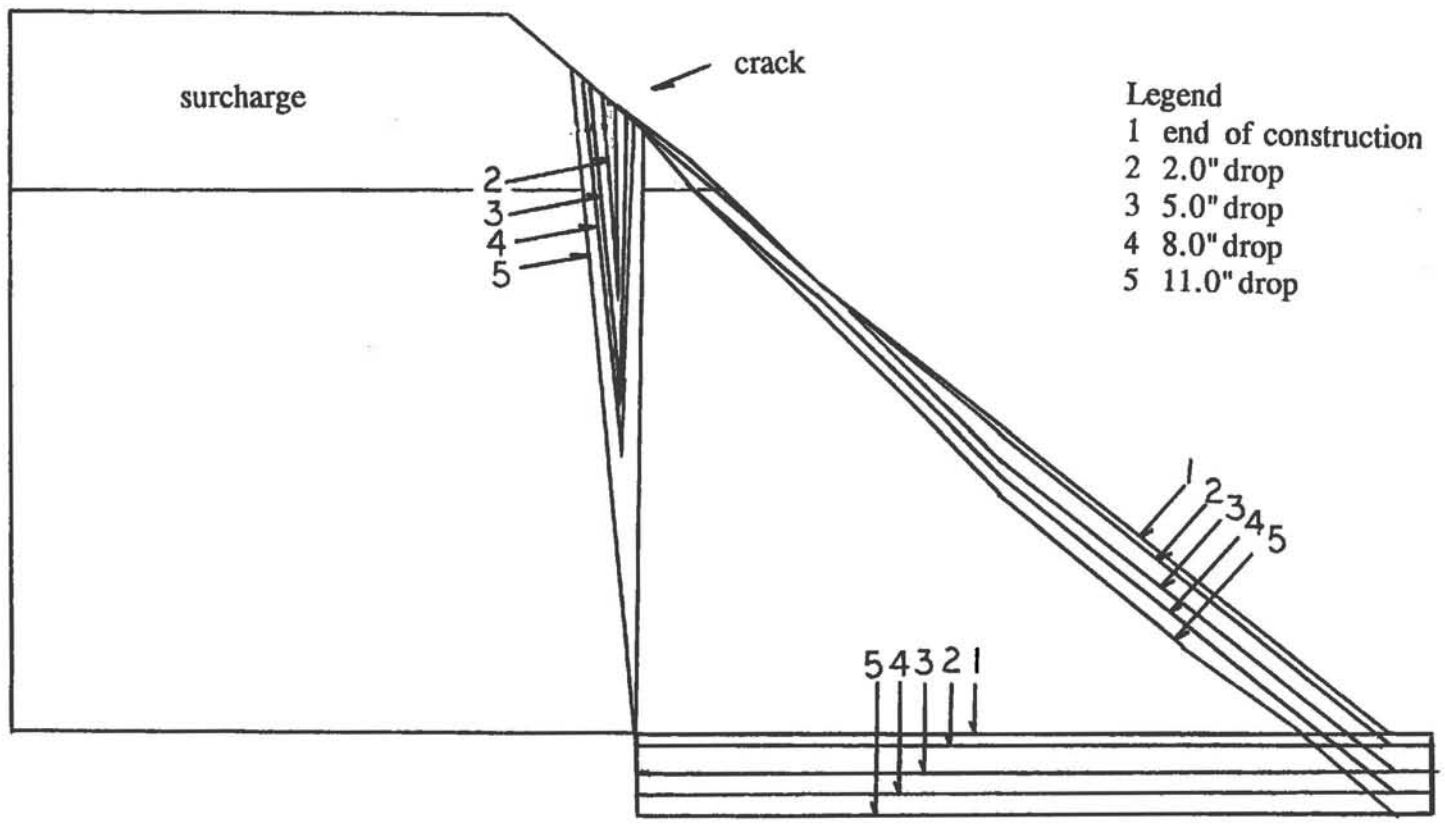

Figure 2.32 Displacement Field of the Backfill in the Unreinforced USFS Deep Patch Test

Figure 2.33 The Crack Corresponding to 11 inch-Drop in the Unreinforced USFS Deep Patch Test

w/ Reinforcement

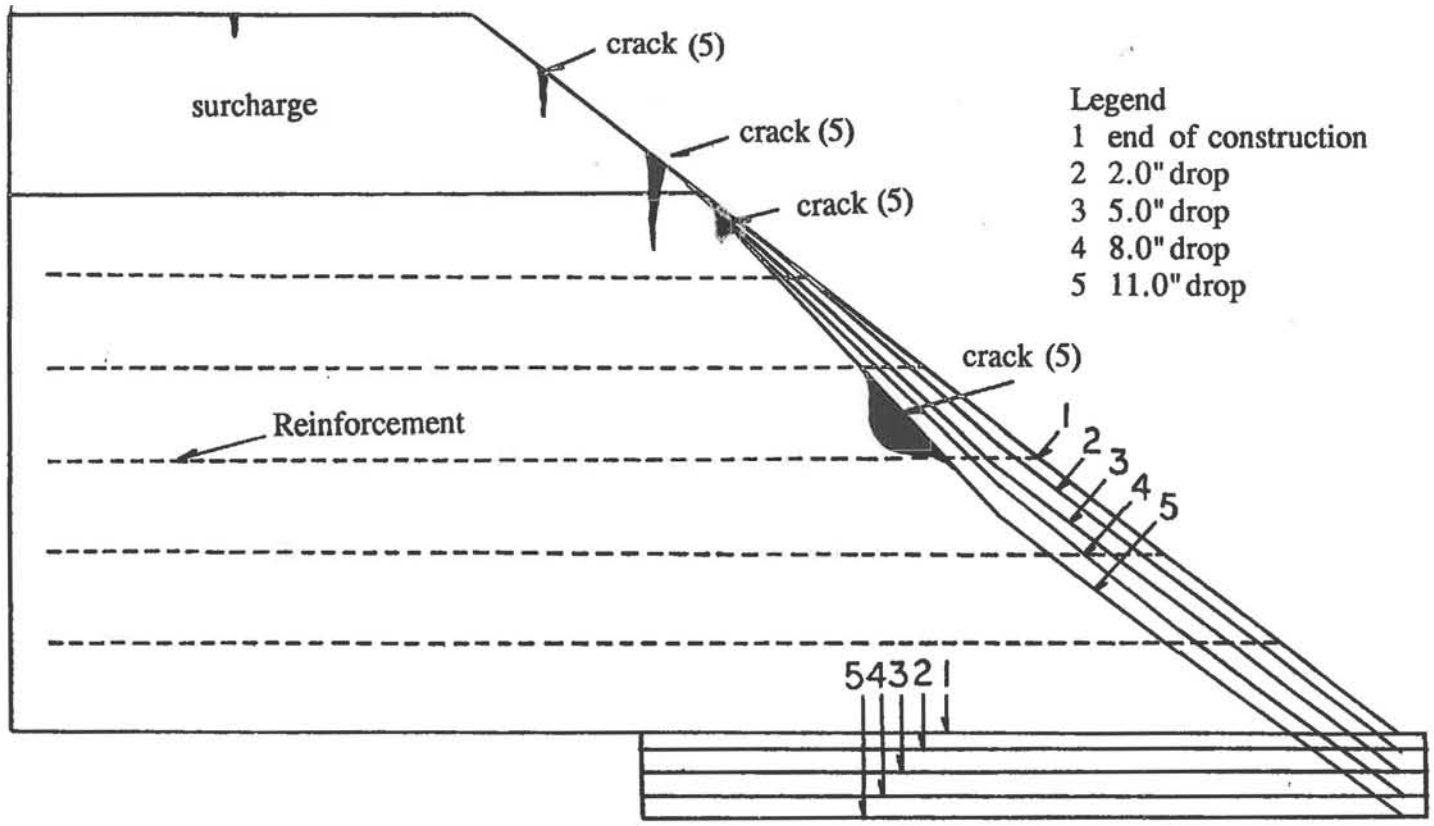

Figure 2.34 Displacement Field of the Backfill in the Reinforced USFS Deep Patch Test

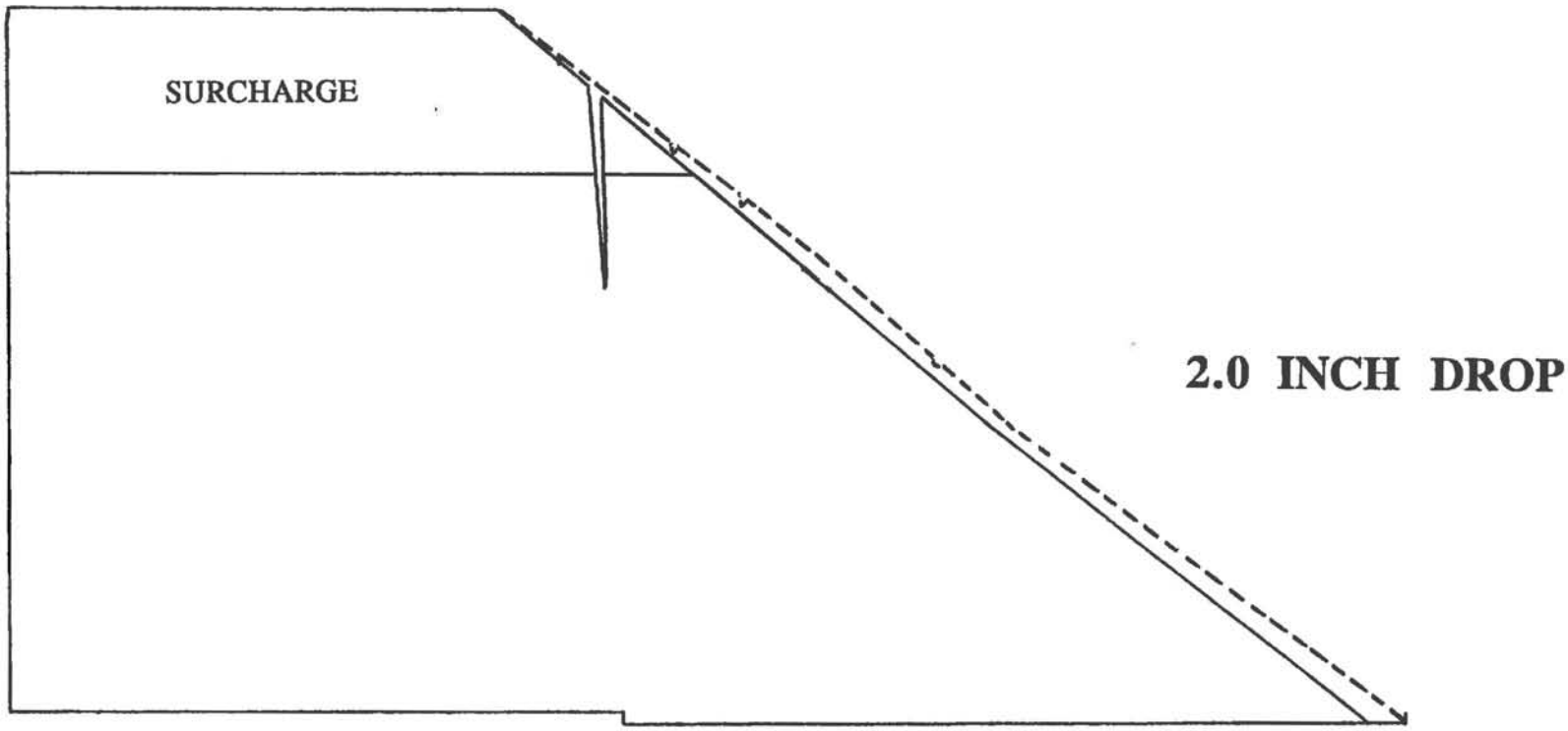

Figure 2.35(a) Comparison of Crack Propagation in the Two Tests at 2 inch-Drop

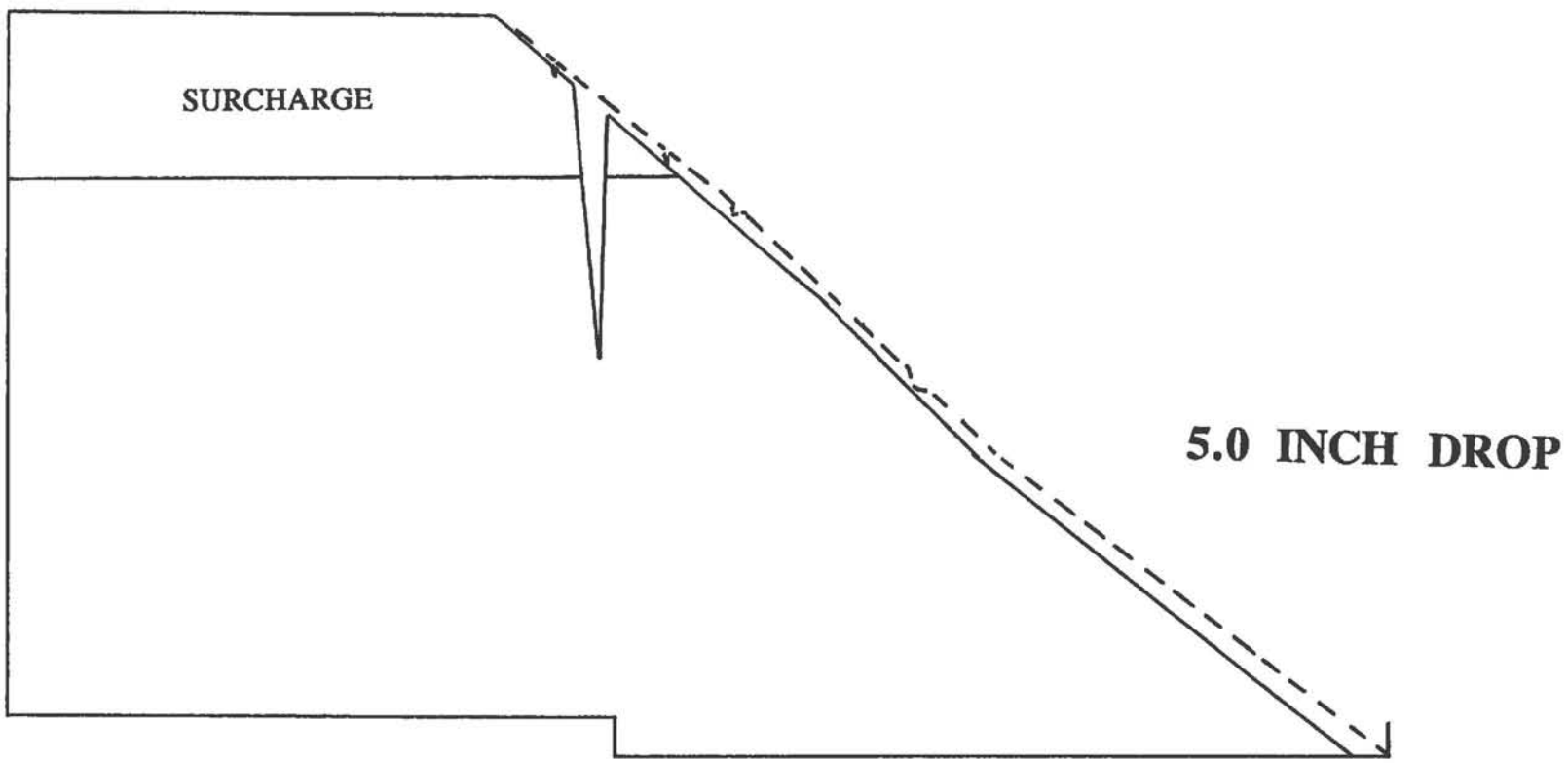

Figure 2.35(b) Comparison of Crack Propagation in the Two Tests at 5 inch-Drop

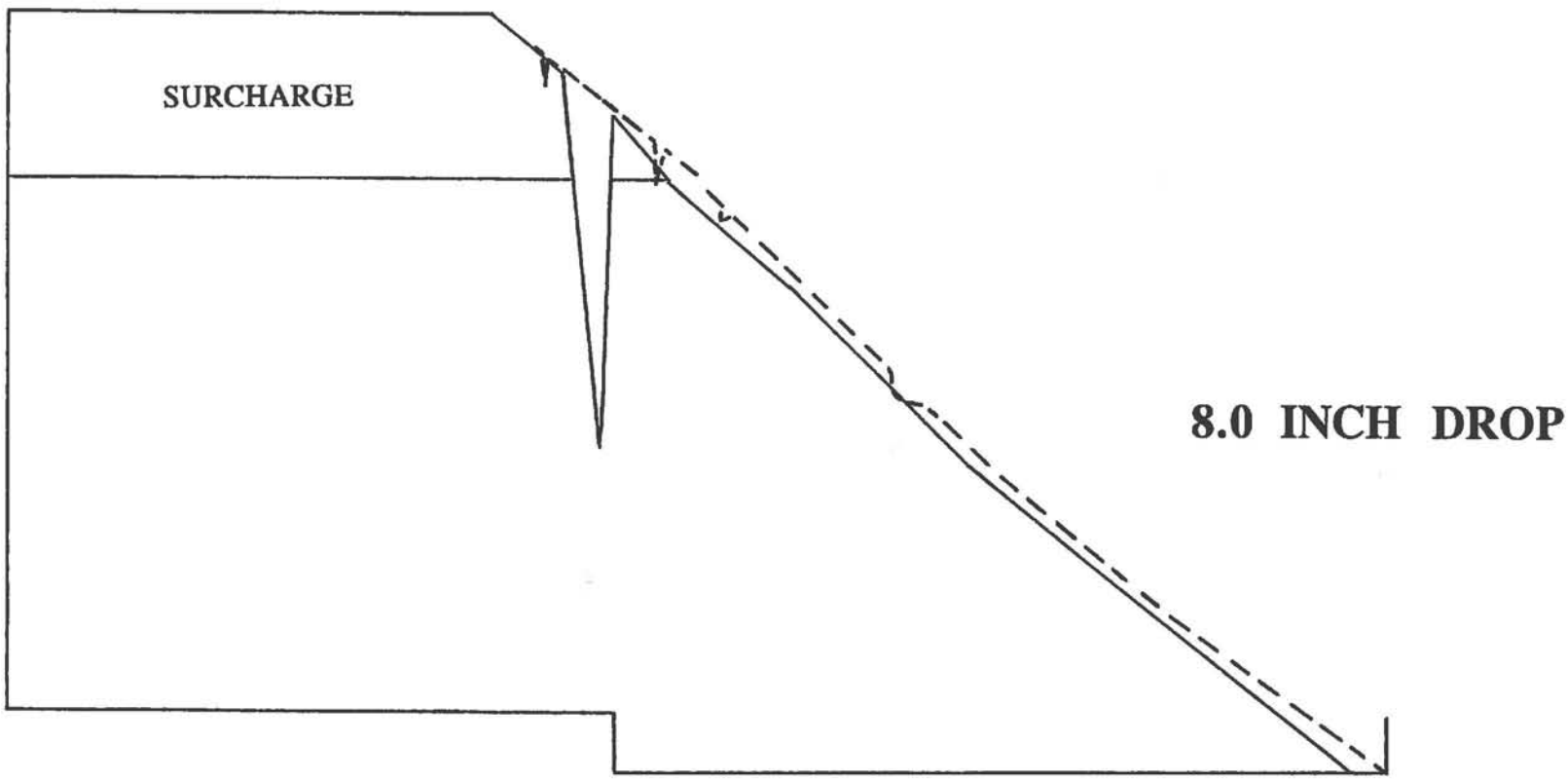

Figure 2.35(c) Comparison of Crack Propagation in the Two Tests at 8 inch-Drop

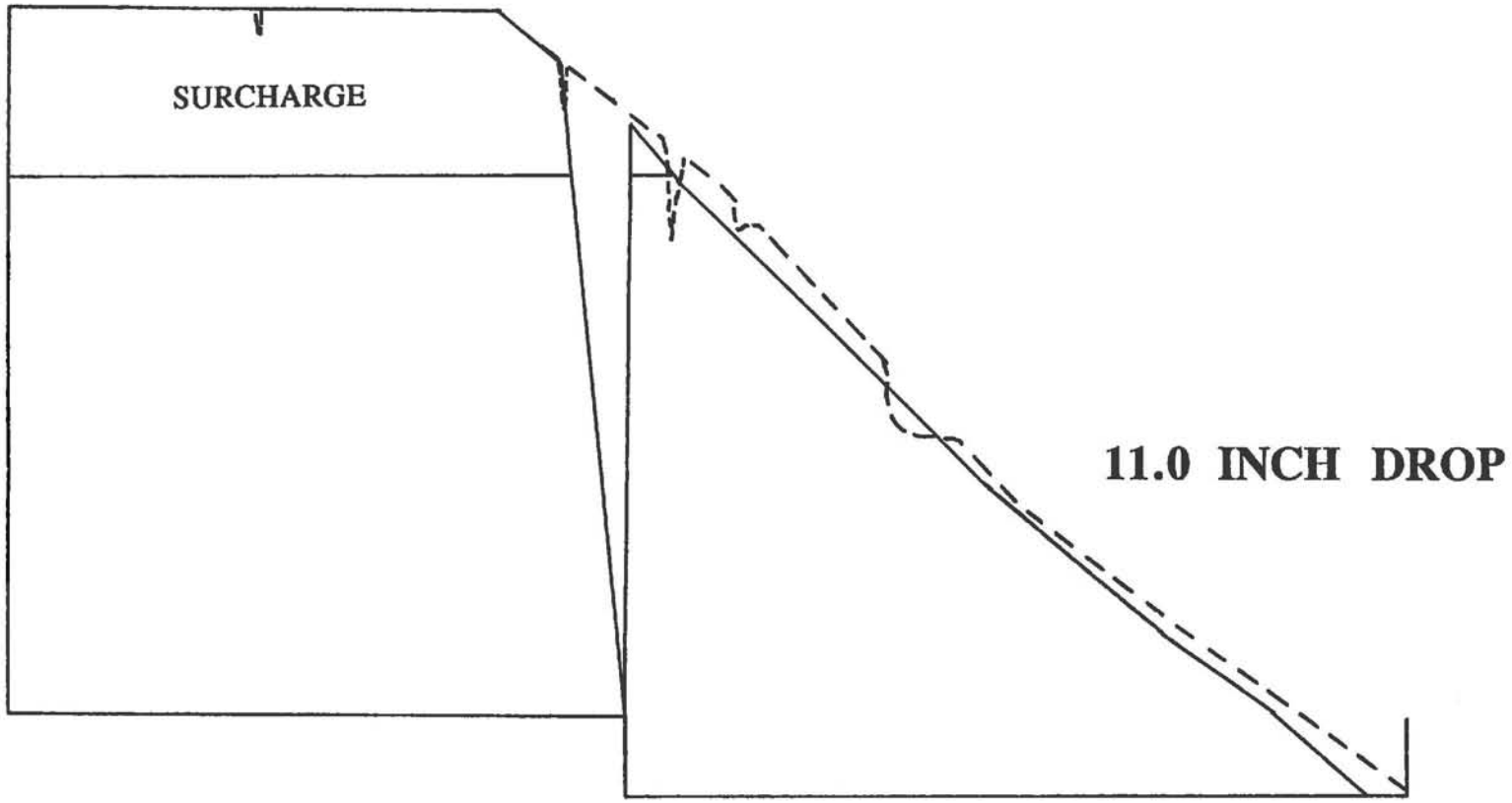

Figure 2.35(d) Comparison of Crack Propagation in the Two Tests at 11 inch-Drop

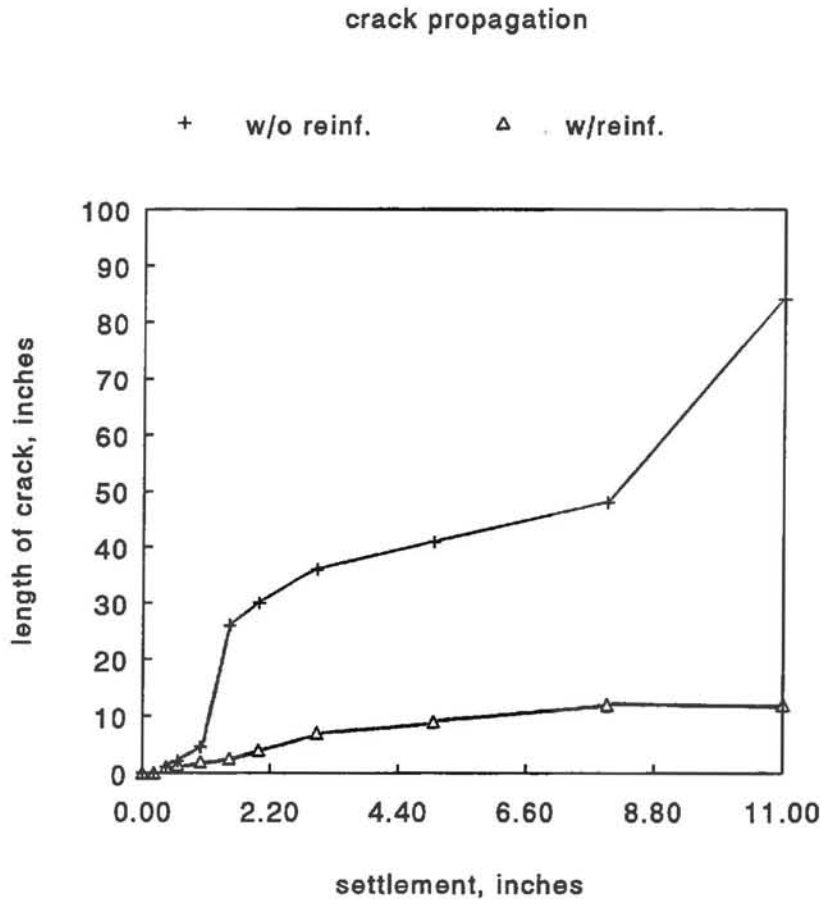

Figure 2.36 Comparison of Crack Propagation in the Two Tests

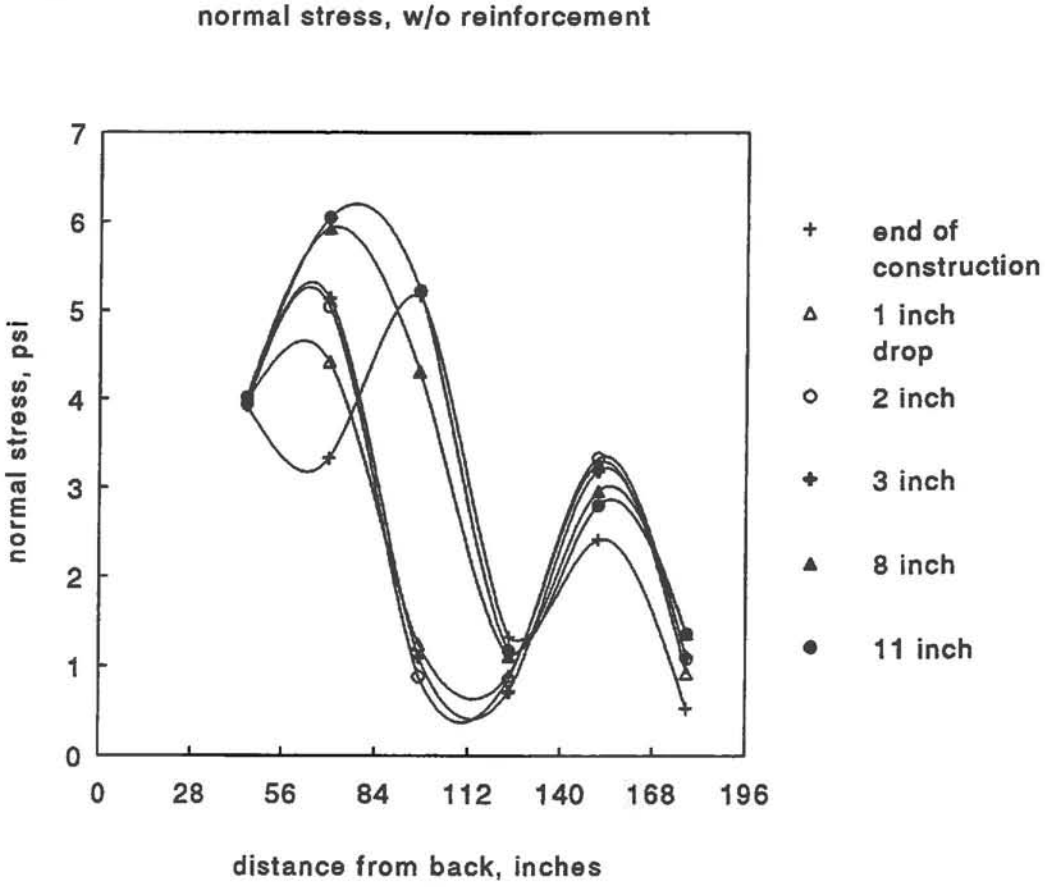

Figure 2.37 Distribution of Normal Stresses along the Bottom Panel in the Unreinforced USFS Deep Patch Test

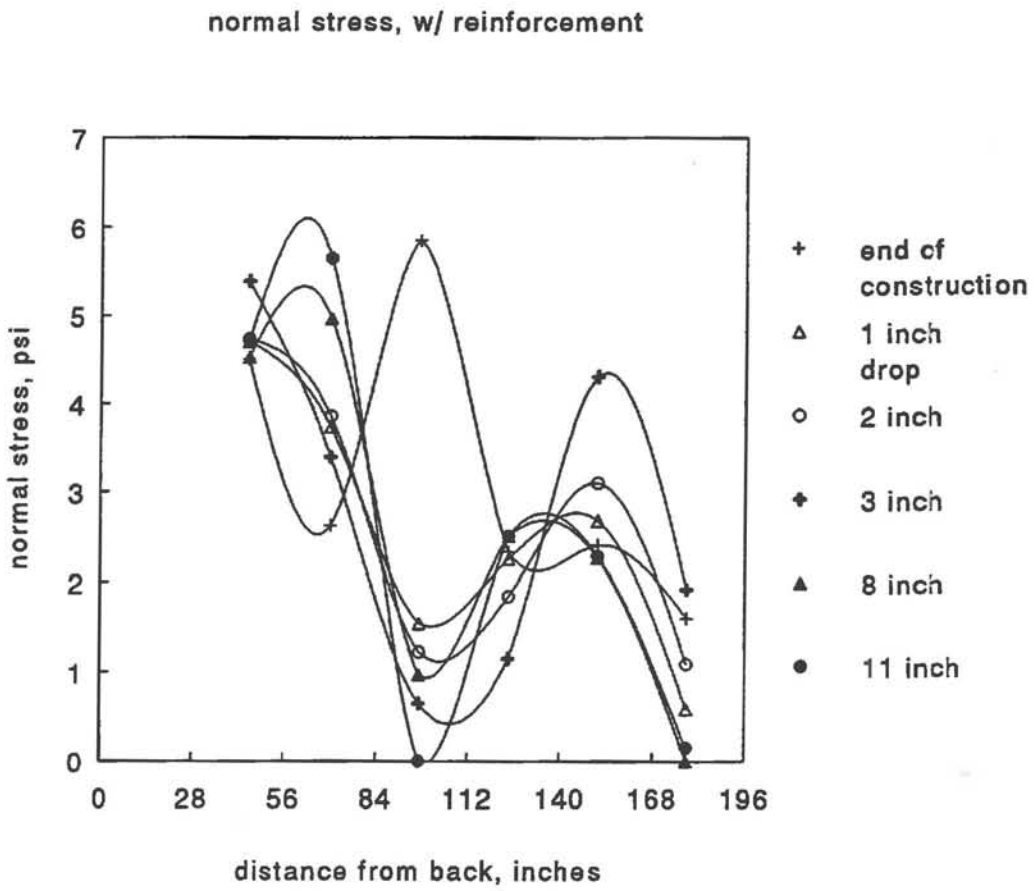

Figure 2.38 Distribution of Normal Stresses along the Bottom Panel in the Reinforced USFS Deep Patch Test

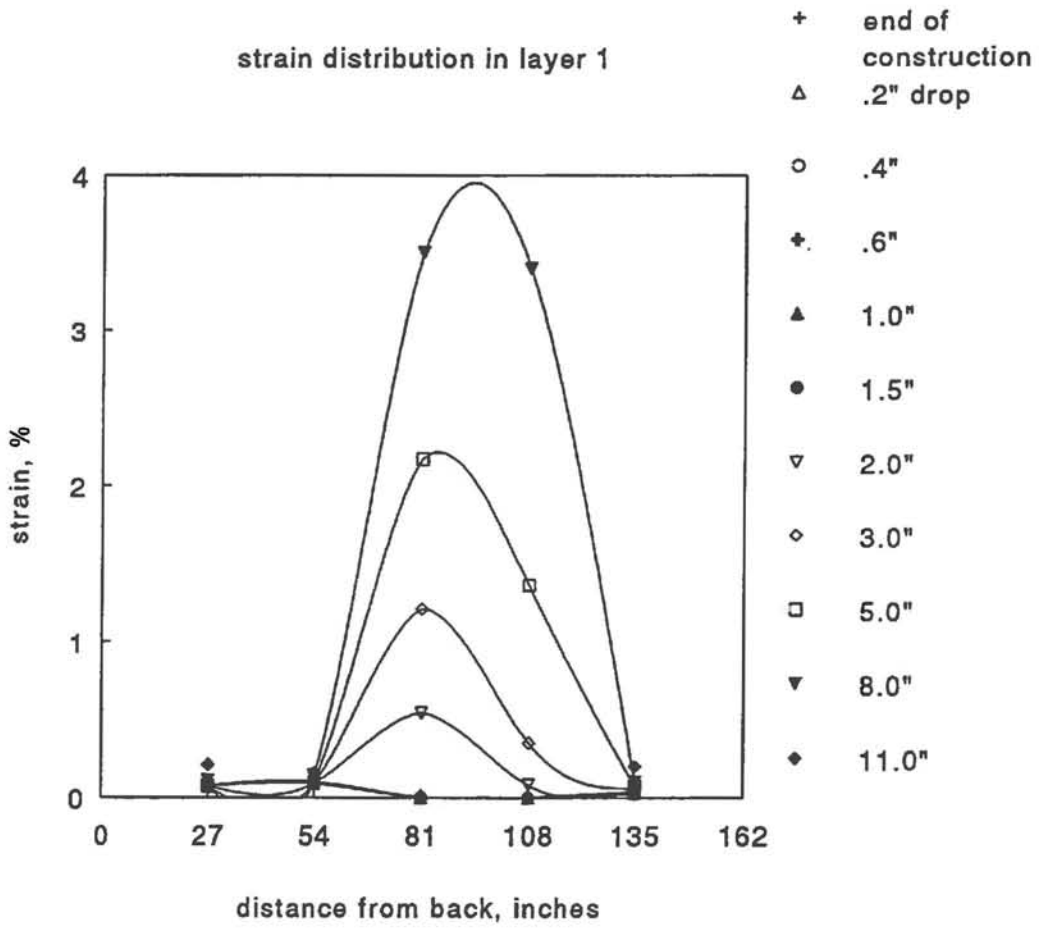

Figure 2.39(a) Distribution of Strain along the Geosynthetic Reinforcement Layer 1 in the Reinforced USFS Deep Patch Test

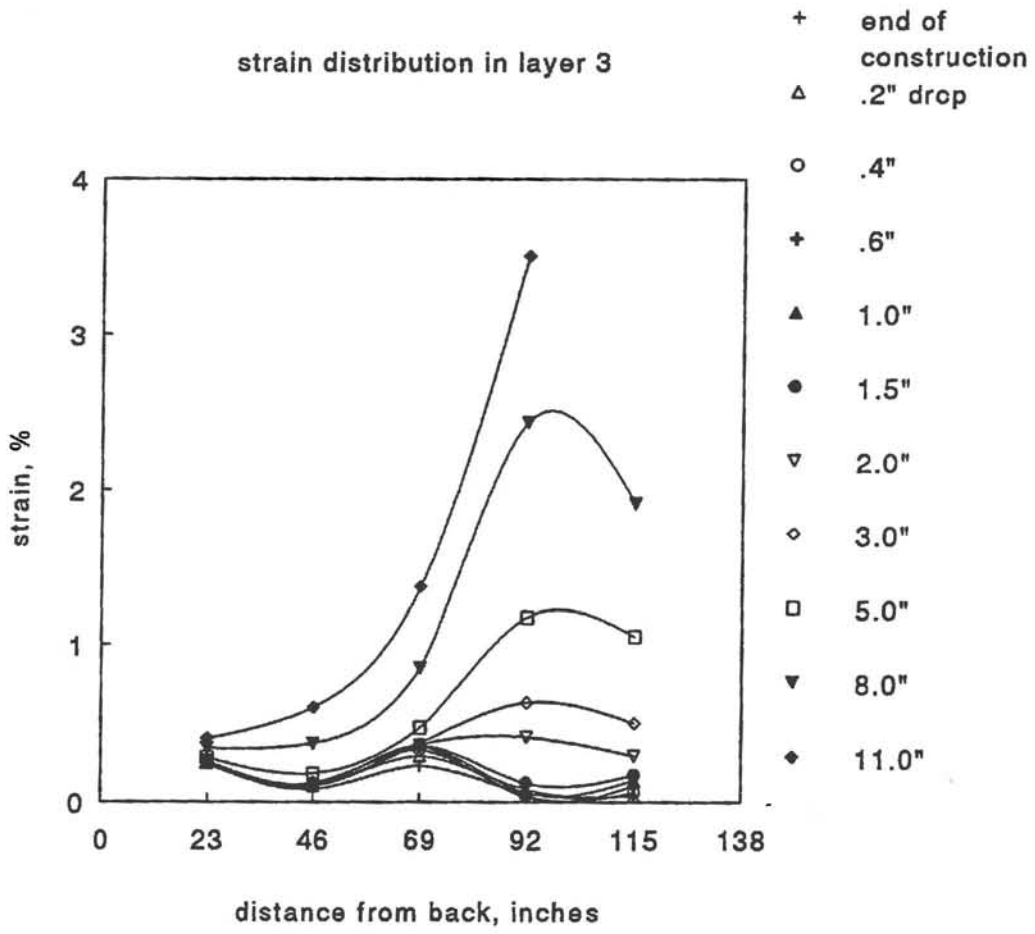

Figure 2.39(b) Distribution of Strain along the Geosynthetic Reinforcement Layer 3 in the Reinforced USFS Deep Patch Test

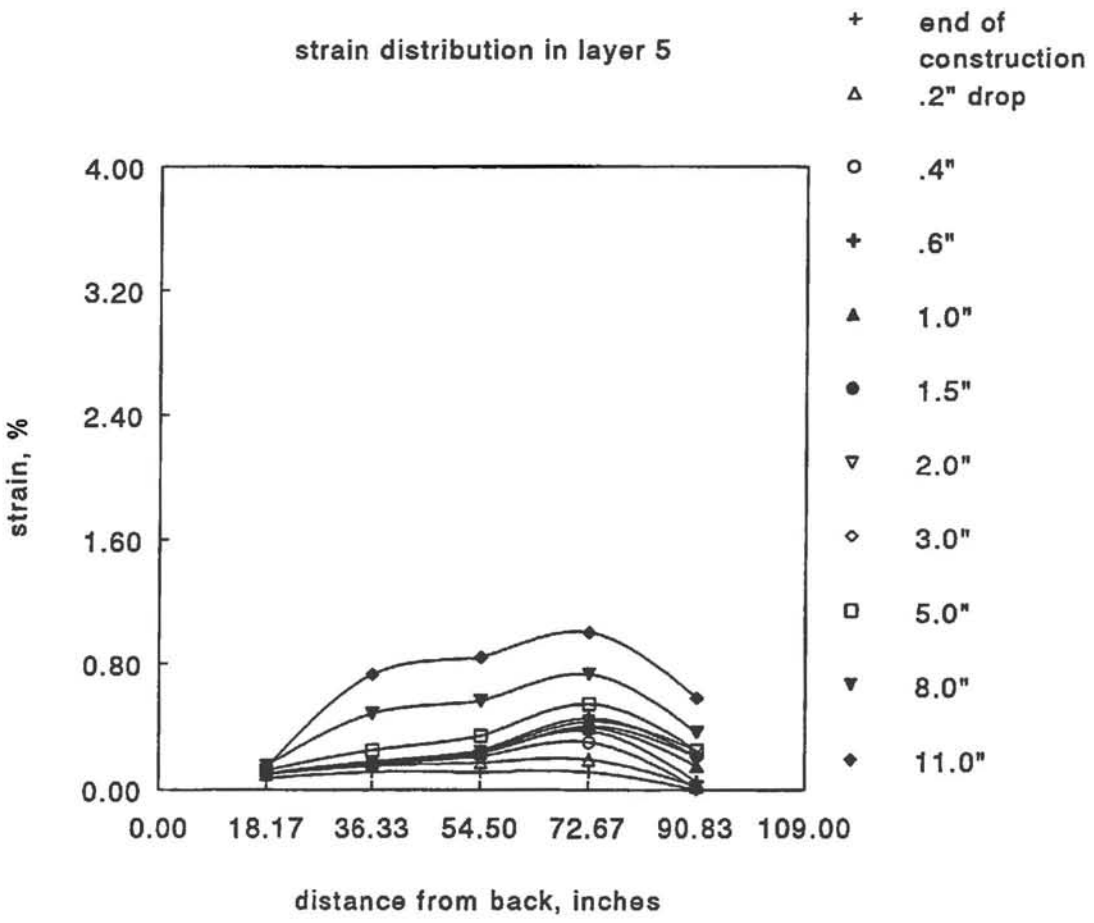

Figure 2.39(c) Distribution of Strain along the Geosynthetic Reinforcement Layer 5 in the Reinforced USFS Deep Patch Test

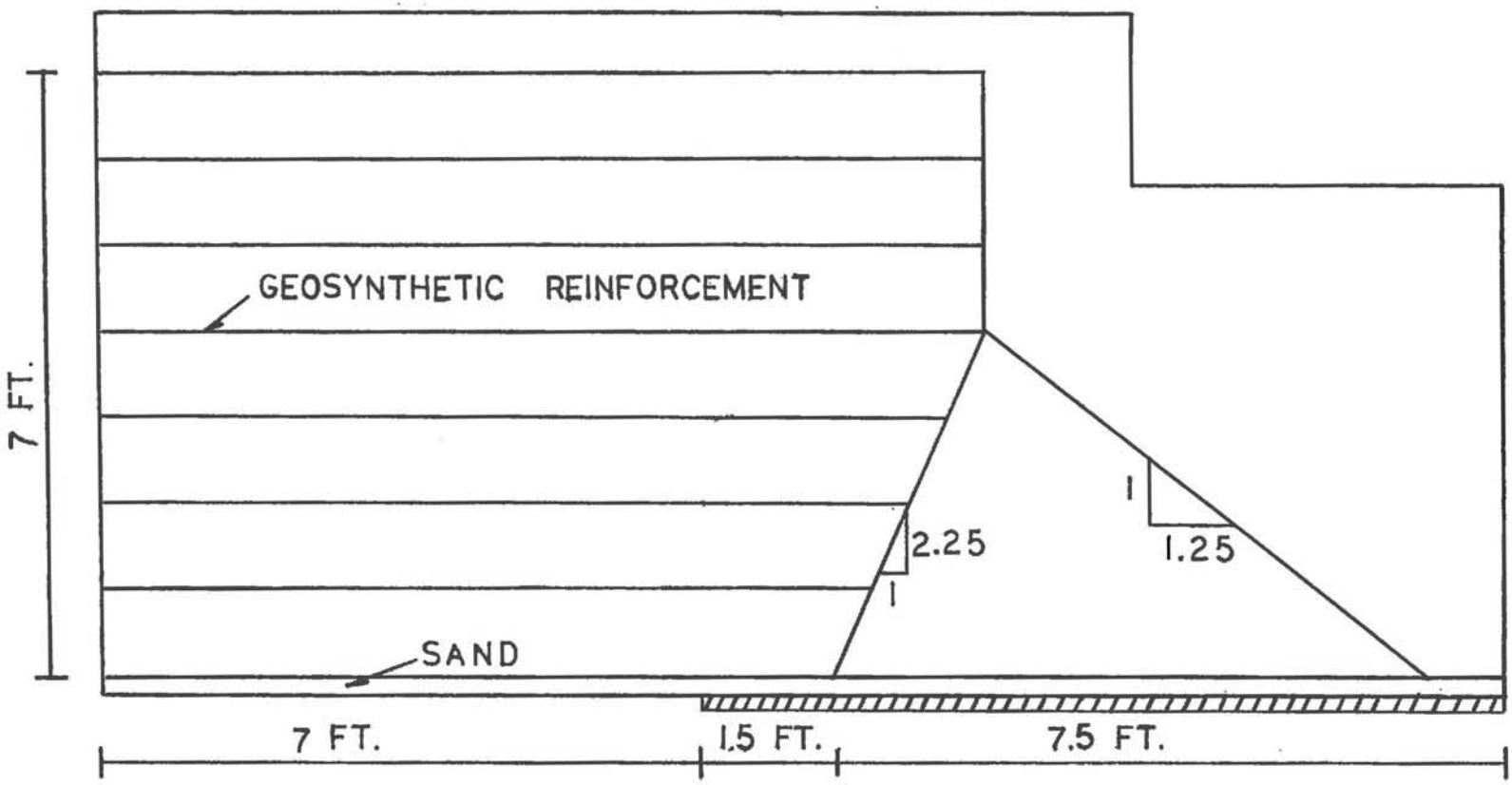

Figure 3.1 Schematic Diagram of the CTI Deep Patch Test

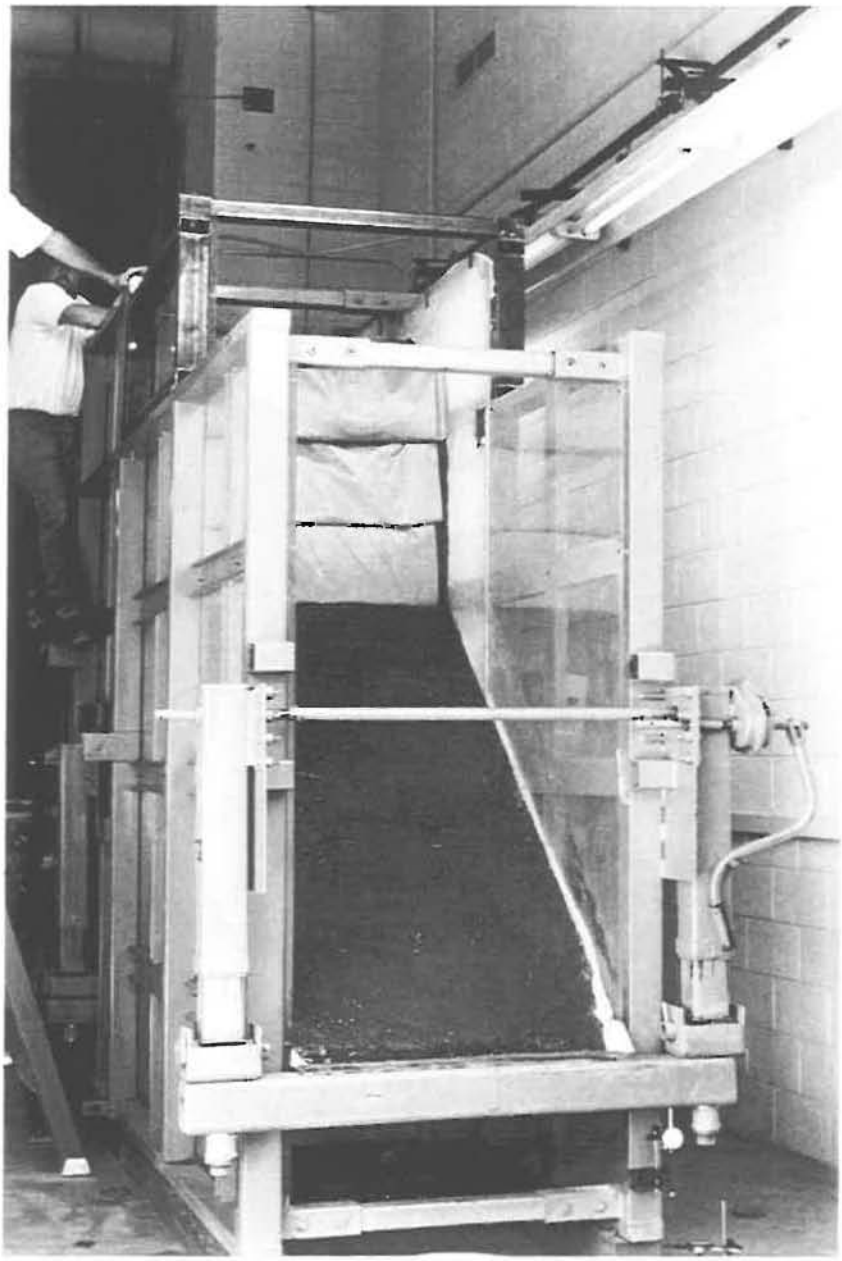

Figure 3.2 The CTI Deep Patch Test at End of Construction

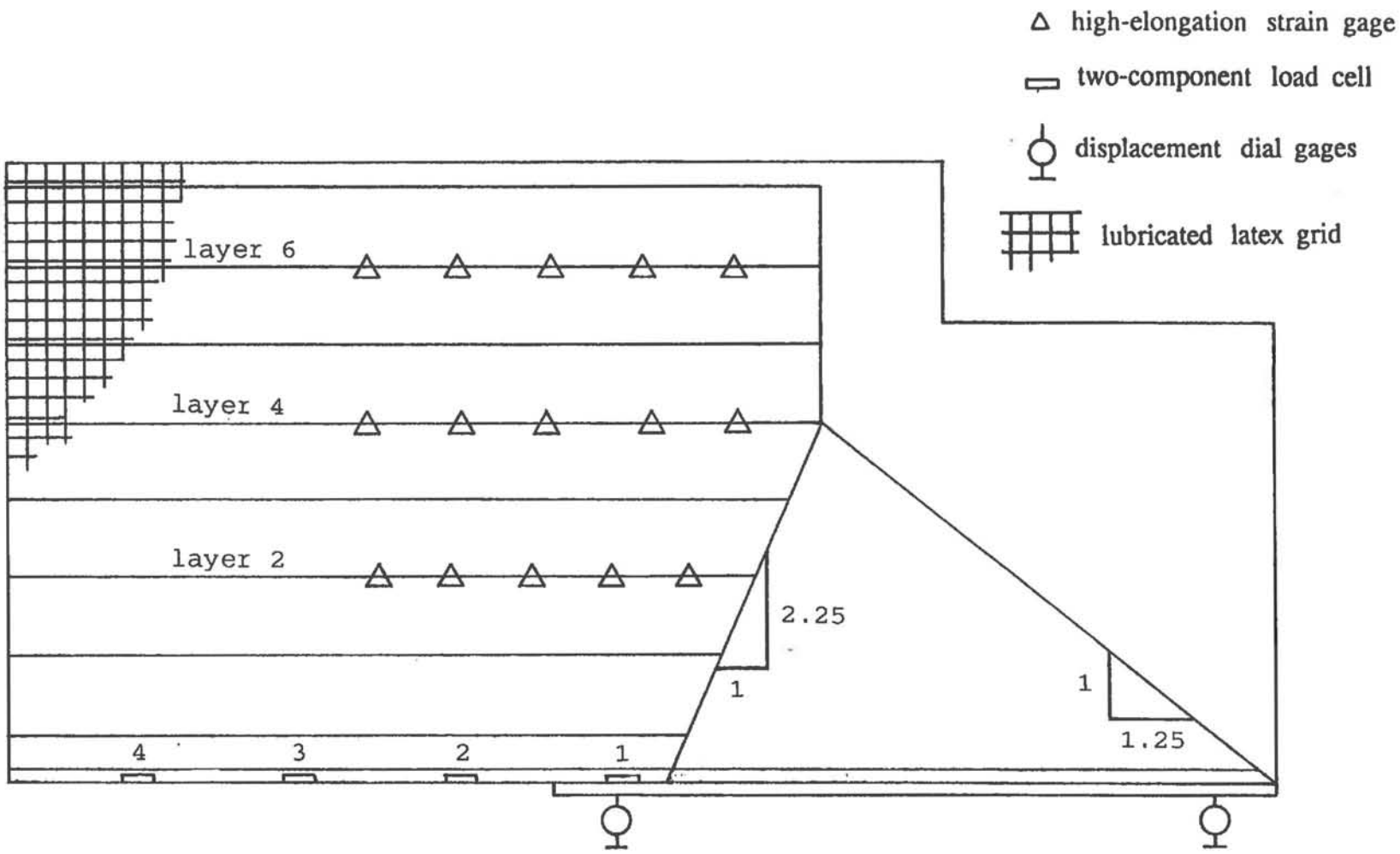

Figure 3.3 Instrumentation of the CTI Deep Patch Test

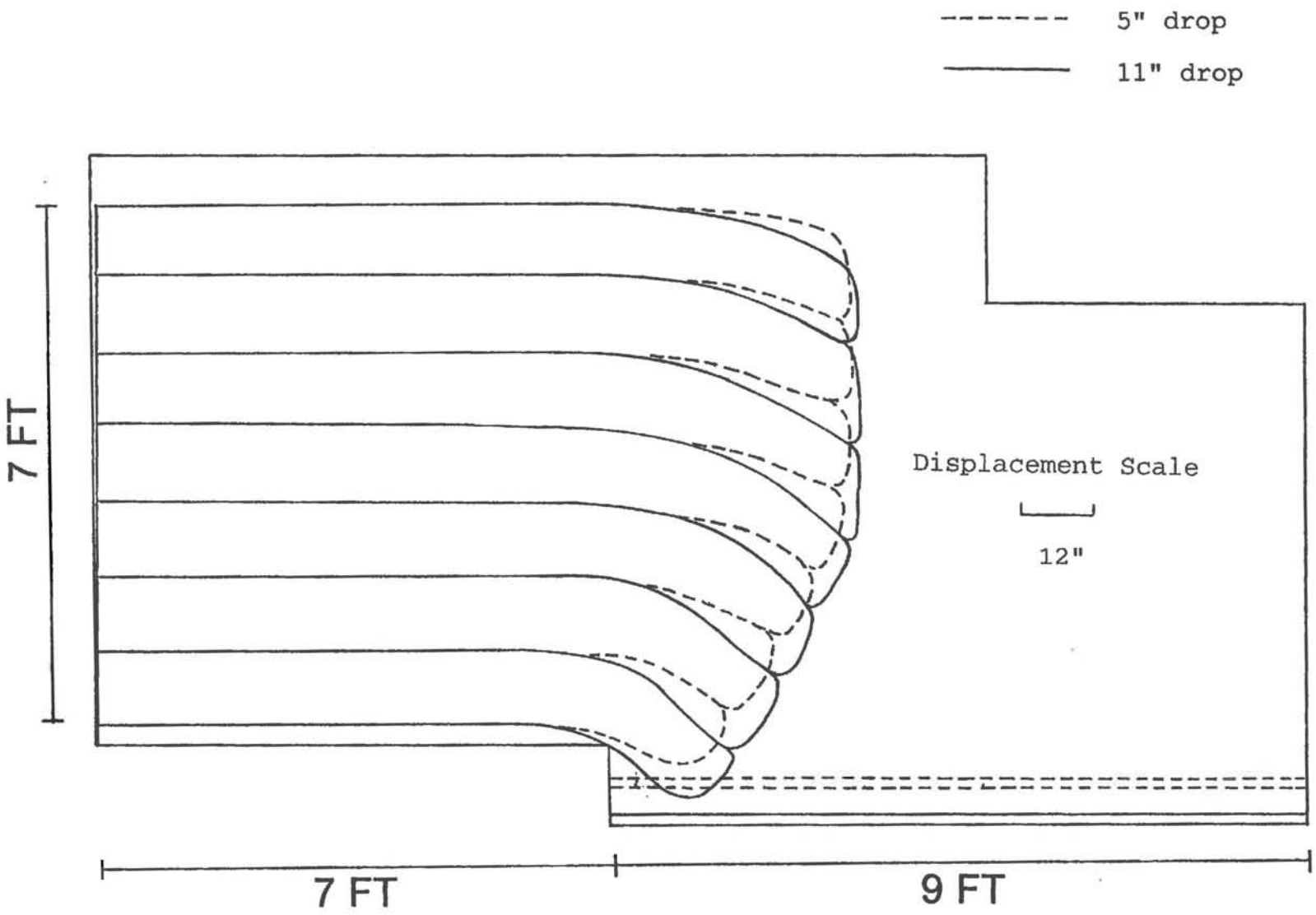

Figure 3.4 Displacement Field of the Backfill in the CTI Deep Patch Test with Road Base Backfill

Figure 3.5 The Deformed Face of the CTI Deep Patch Test with Road Base Backfill after Removing the Berm

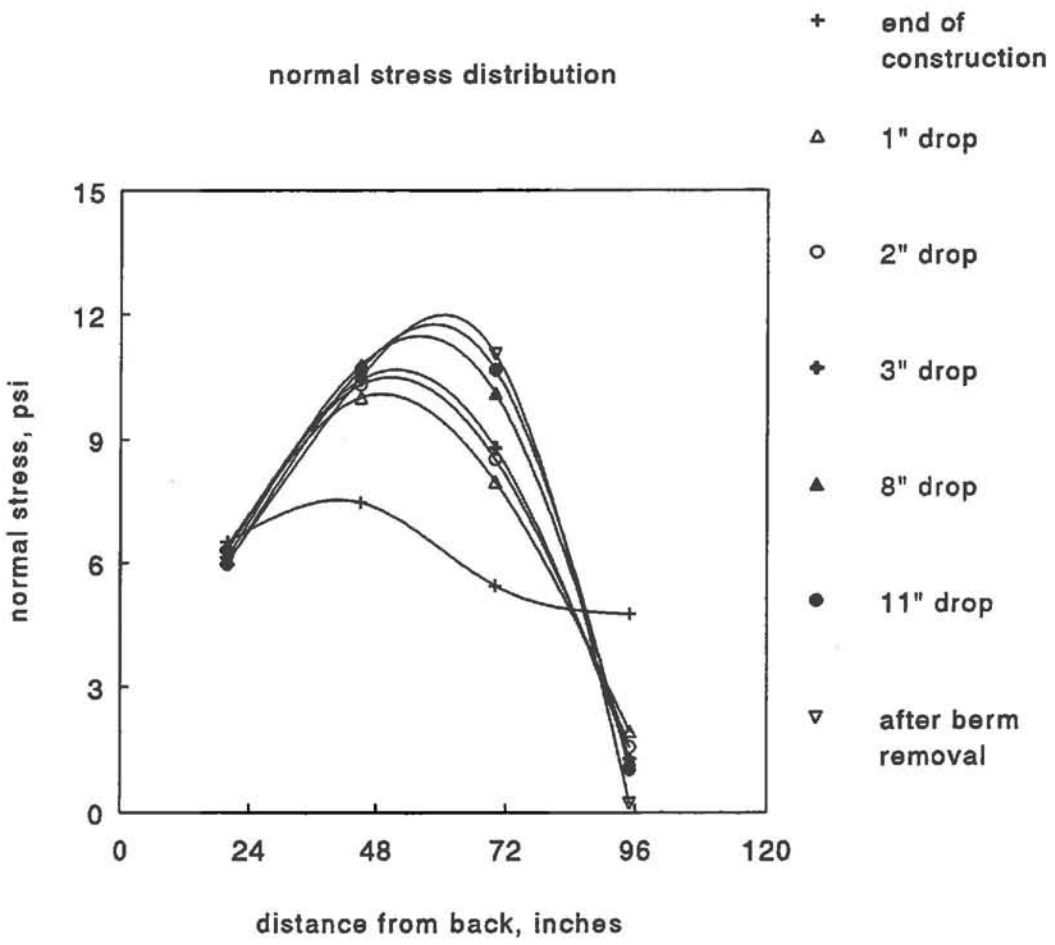

Figure 3.6 Distribution of Normal Stresses along the Bottom Panel in the CTI Deep Patch Test with Road Base Backfill

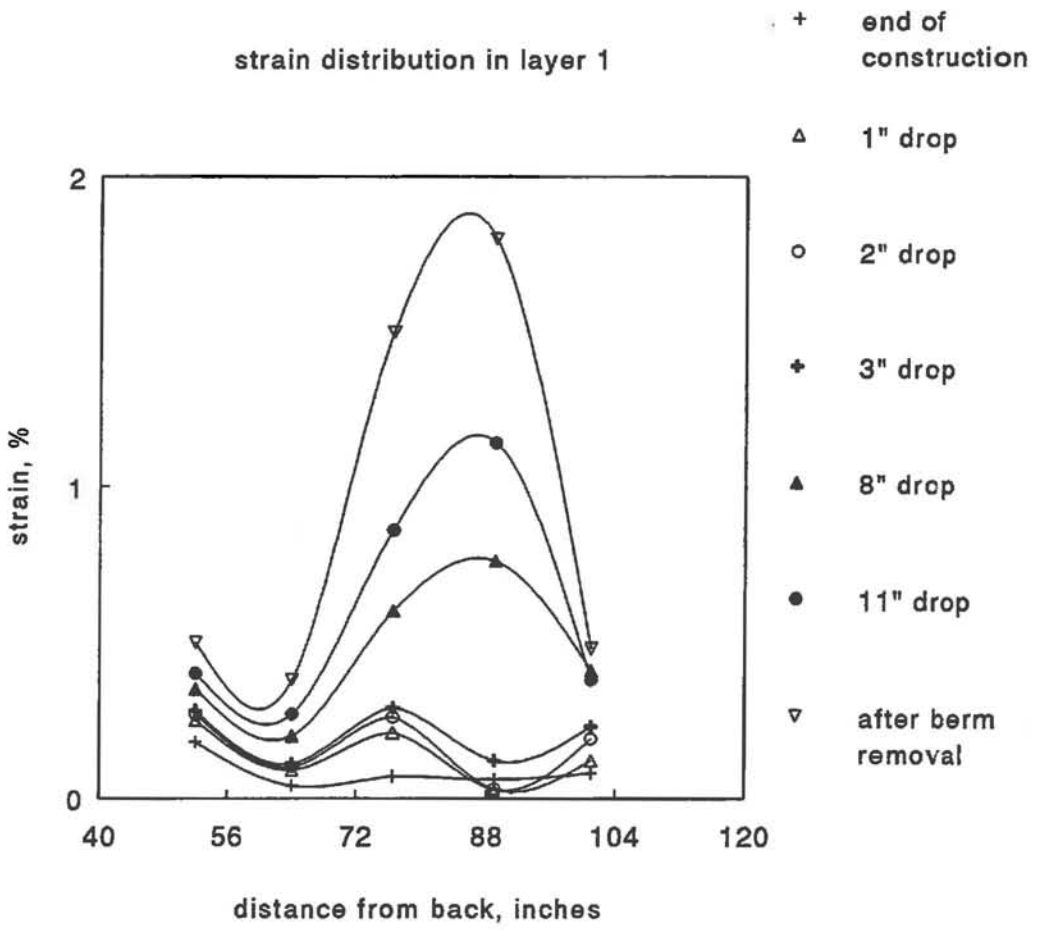

Figure 3.7(a) Distribution of Strain along the Geosynthetic Reinforcement Layer 2 in the CTI Deep Patch Test with Road Base Backfill

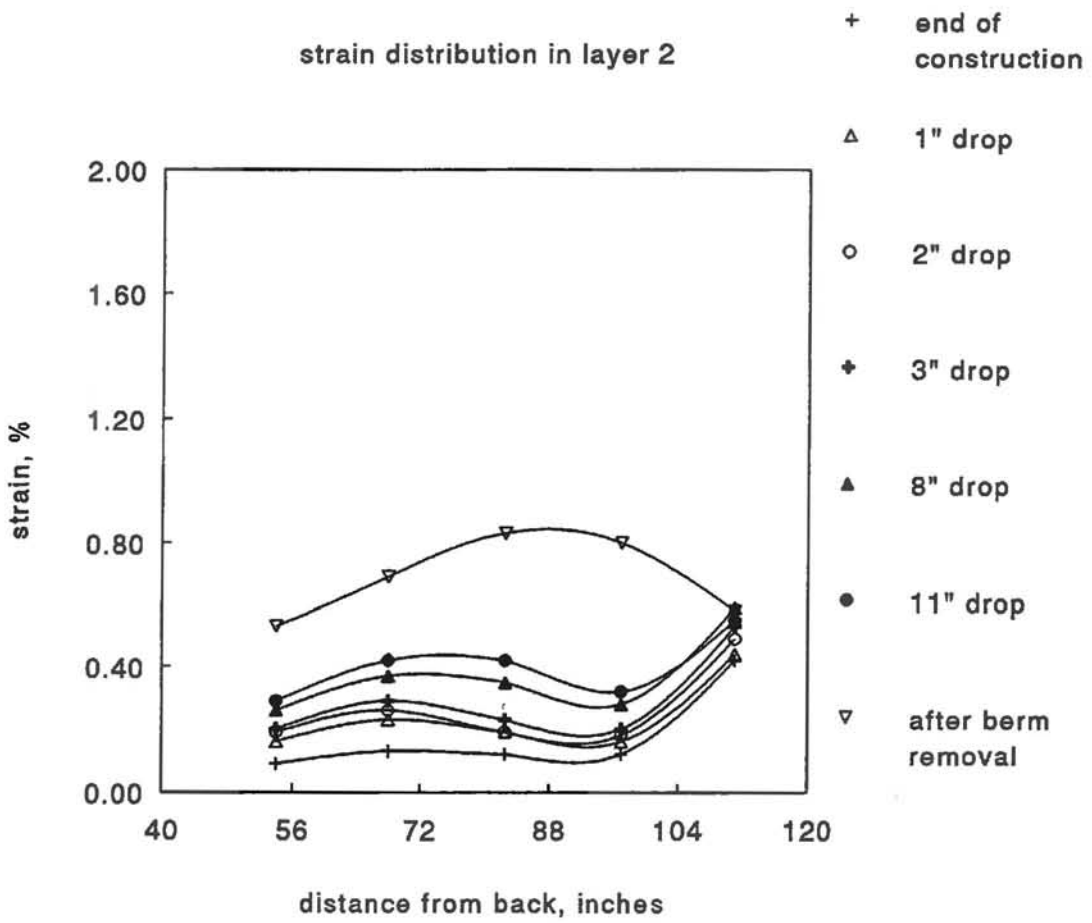

Figure 3.7(b) Distribution of Strain along the Geosynthetic Reinforcement Layer 2 in the CTI Deep Patch Test with Road Base Backfill

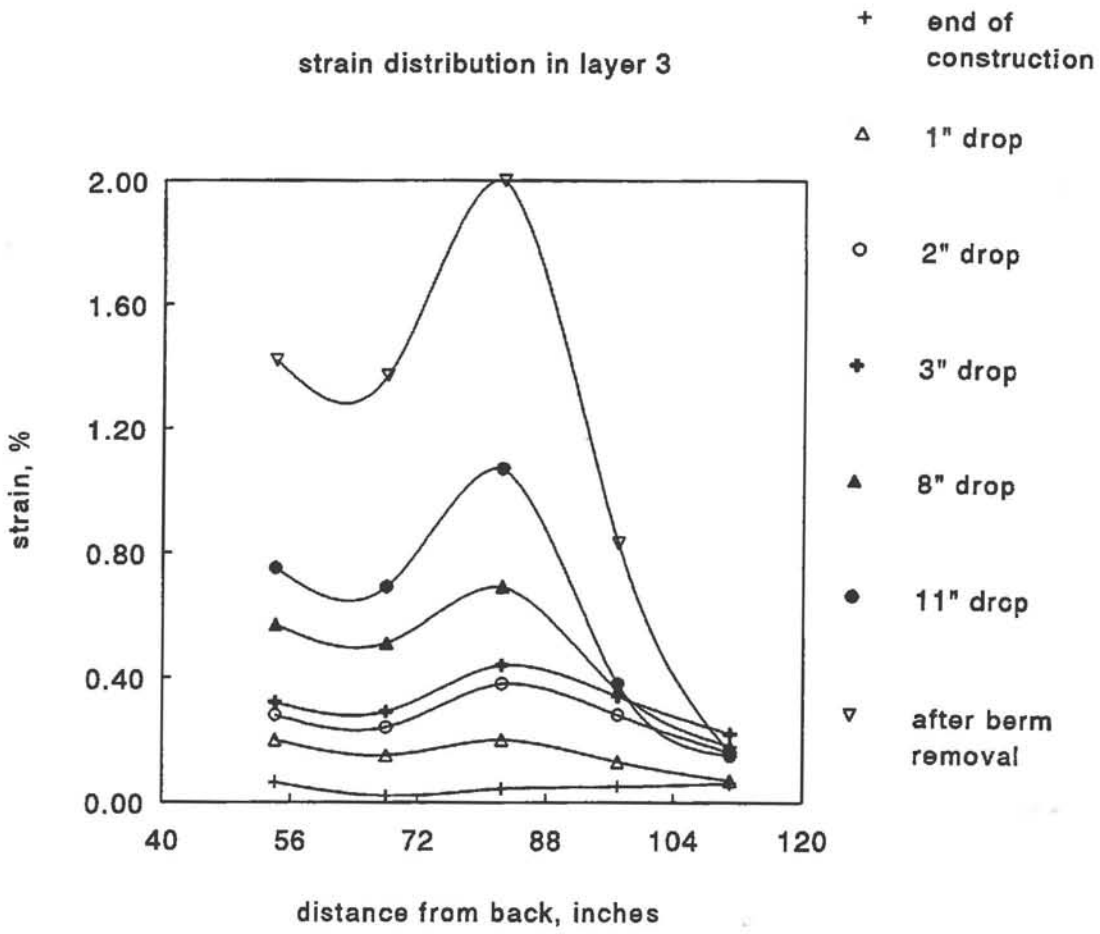

Figure 3.7(c) Distribution of Strain along the Geosynthetic Reinforcement Layer 6 in the CTI Deep Patch Test with Road Base Backfill

SILVERTHORNE, COLORADO
October 26, 1993

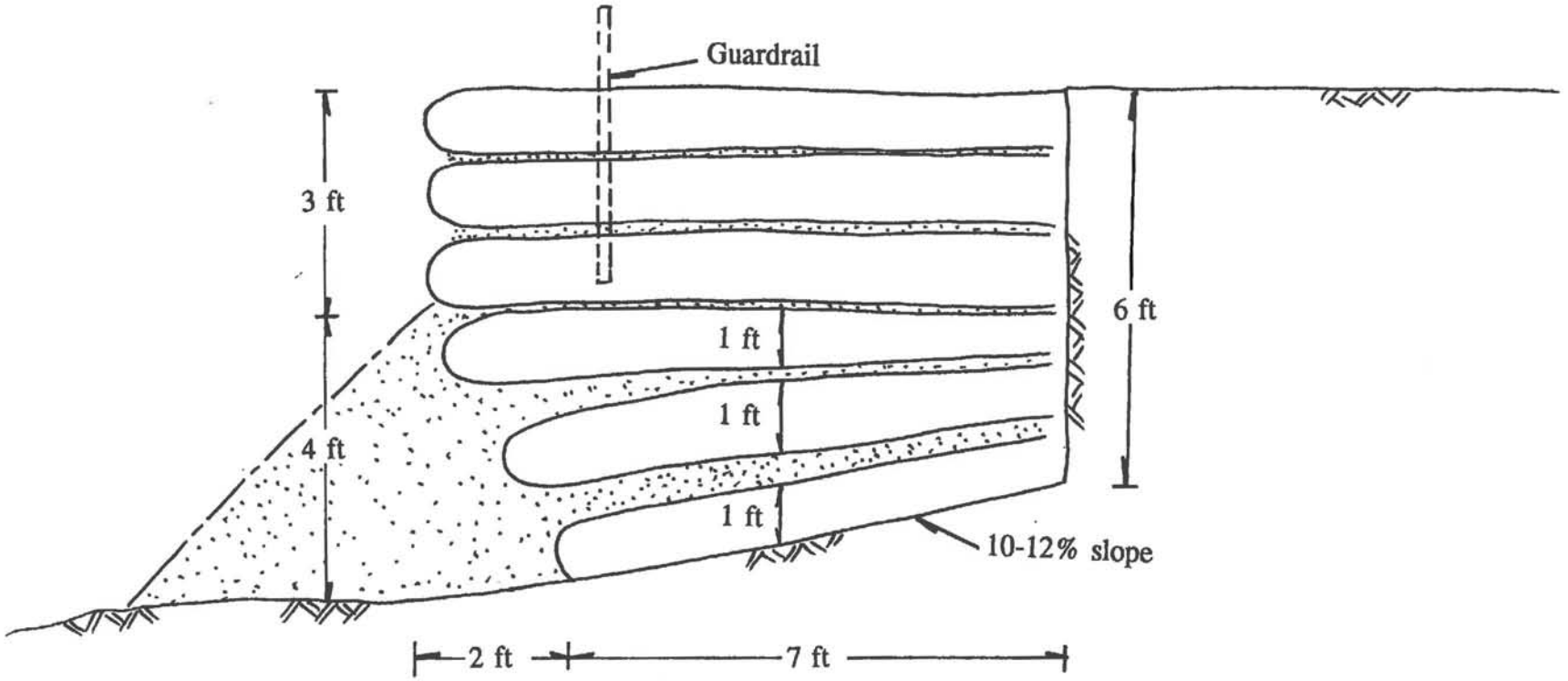

Figure 3.8 Configuration of the CTI Deep Patch in Silverthorne

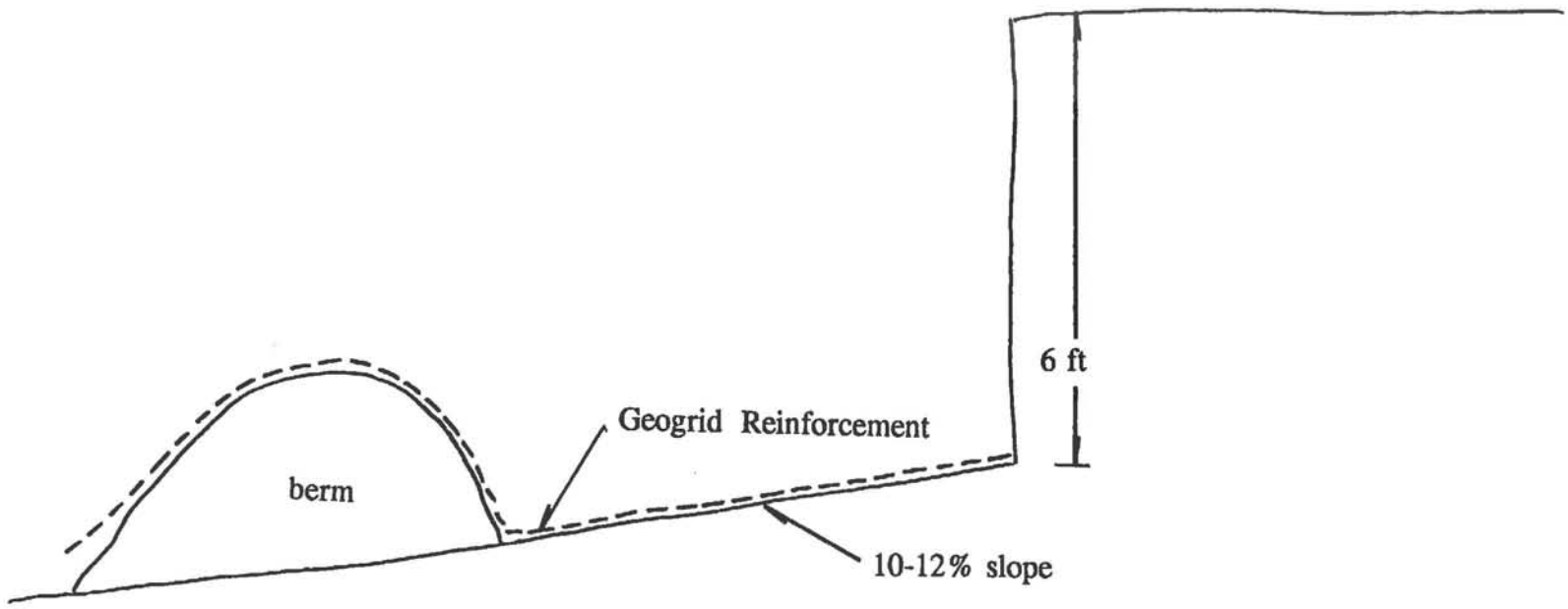

Figure 3.9 Construction Procedure of the CTI Deep Patch in Silverthorne

Figure 3.10 Construction of the CTI Deep Patch in Silverthorne

Figure 3.11 Construction of the CTI Deep Patch in Silverthorne

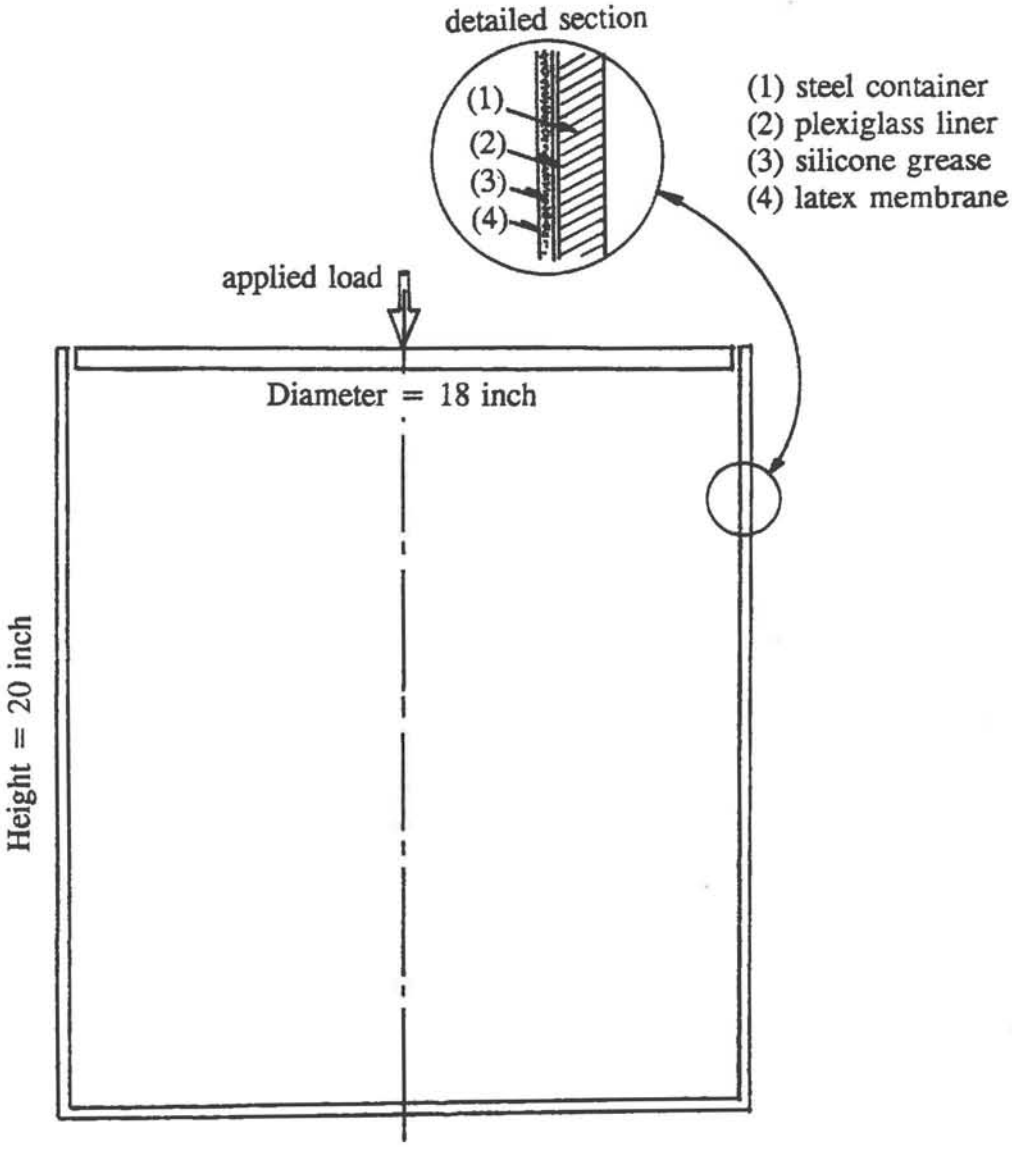

Figure 4.1 Schematic Diagram of the One-Dimensional Compression Test for Shredded Tire

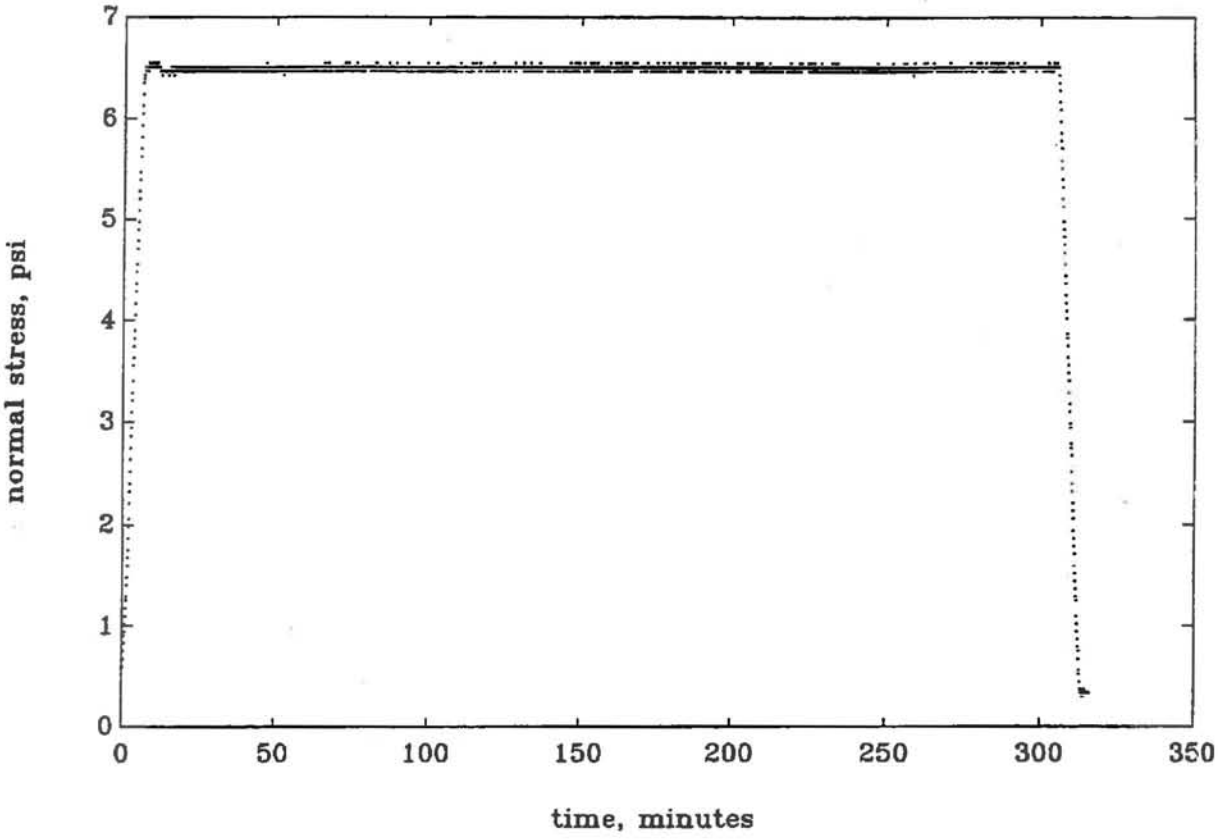

Figure 4.2 The Load History of the One-Dimensional Compression Test on Shredded Tire

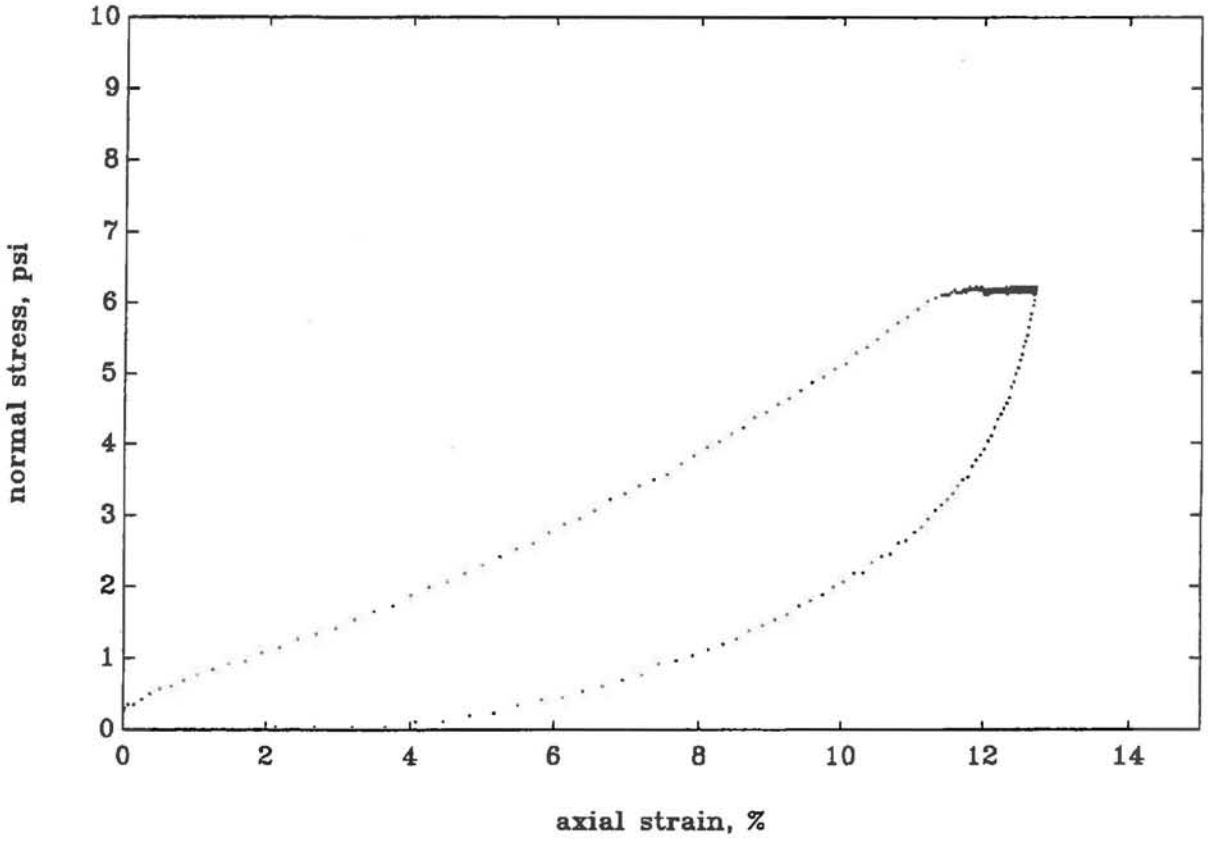

Figure 4.3 Stress-Strain Behavior of the Shredded Tire under One-Dimensional Compression

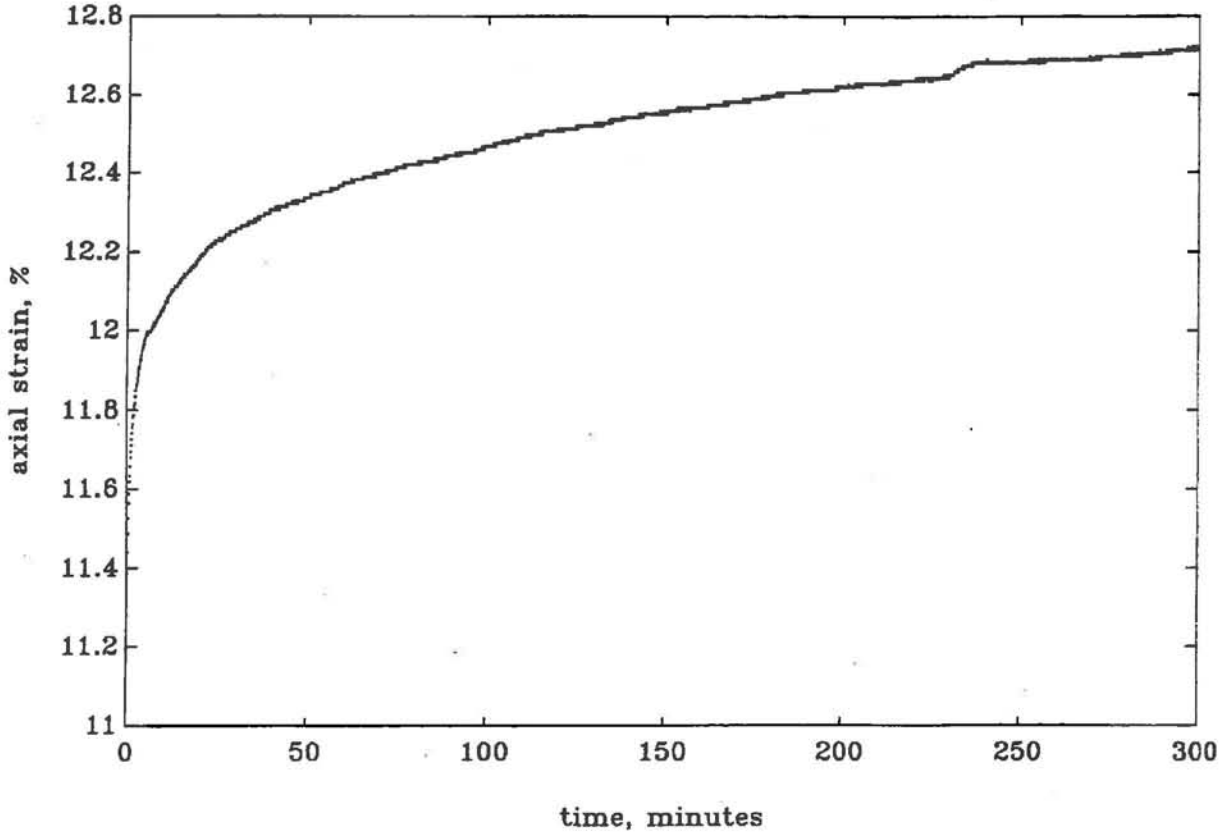

Figure 4.4 Creep Behavior of Shredded Tire under a Constant Stress of 6.3 psi (arithmetic)

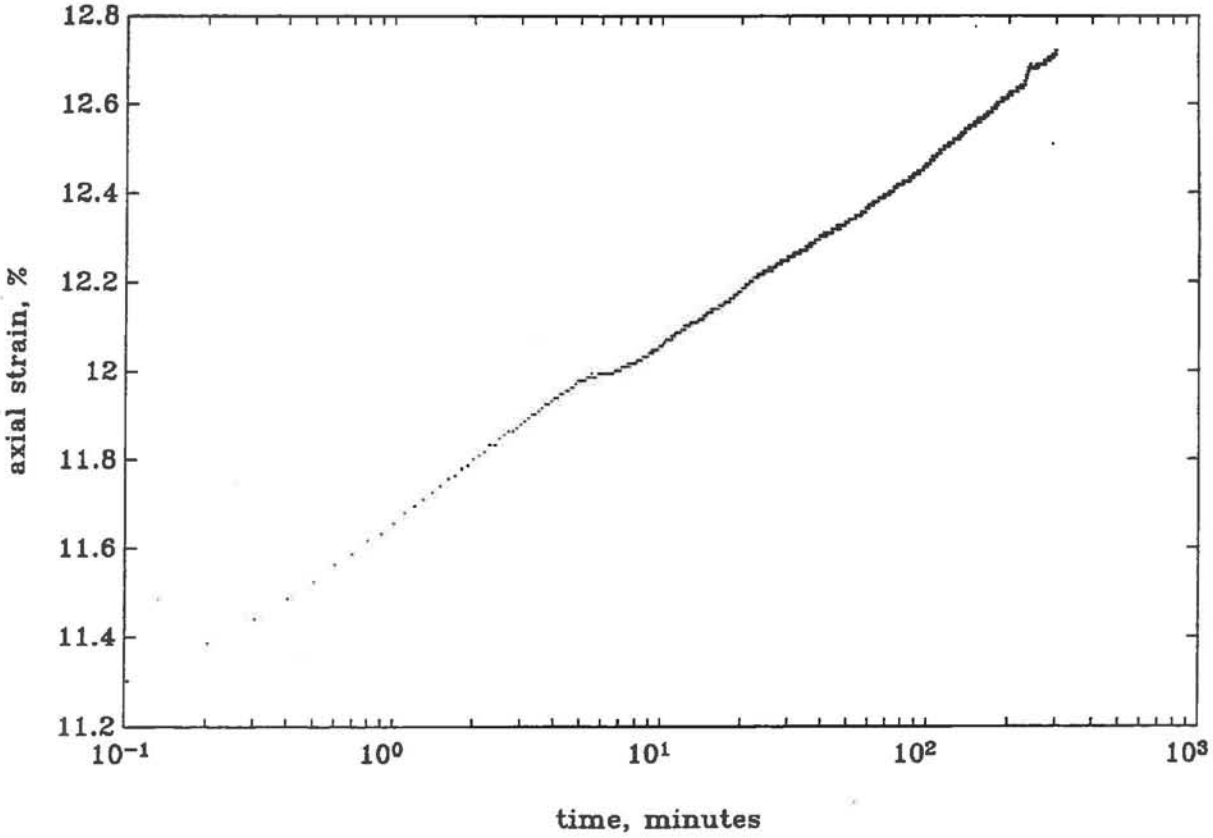

Figure 4.5 Creep Behavior of Shredded Tire under a Constant Stress of 6.3 psi (semi-logarithmic)

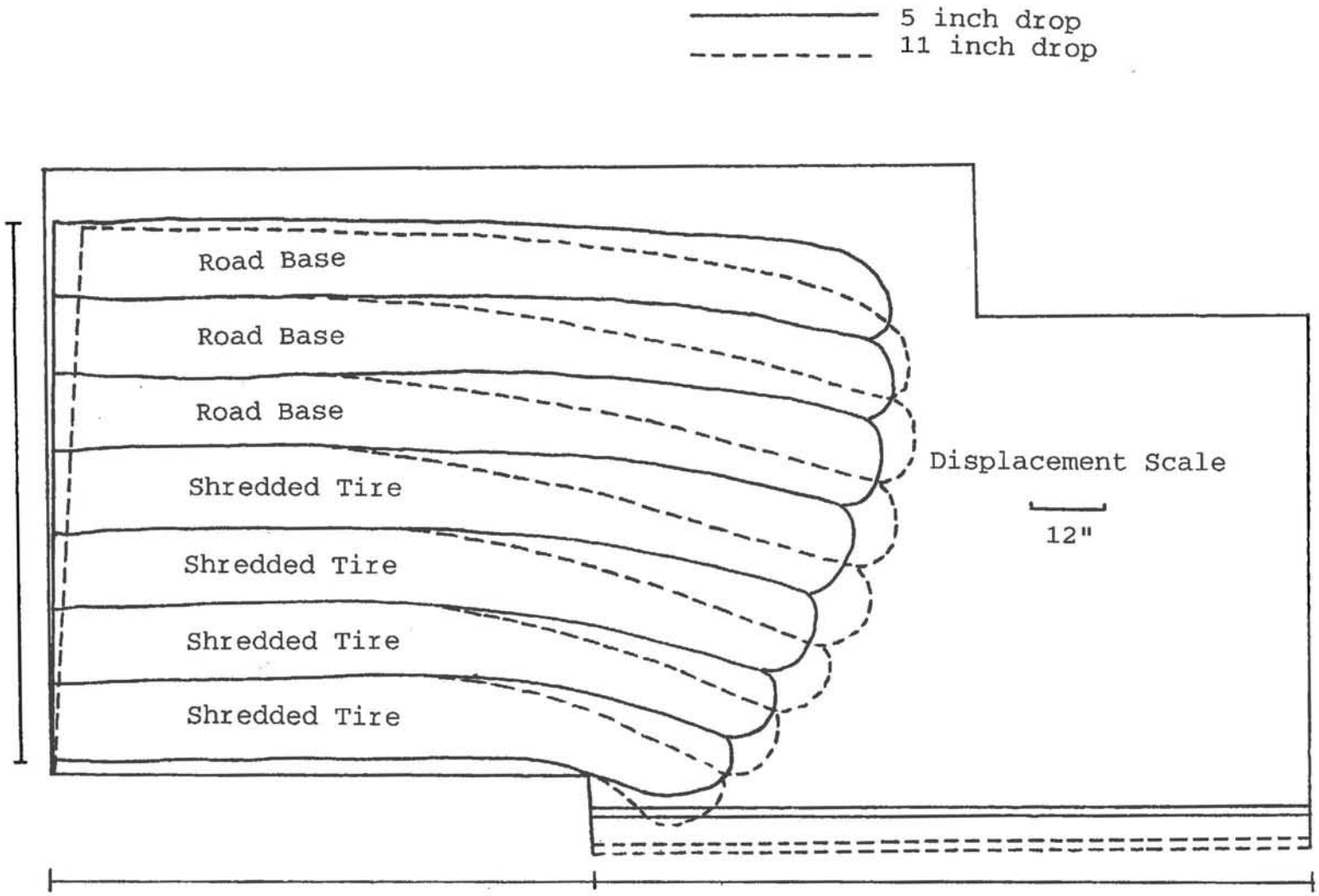

Figure 4.6 Displacement Field of the CTI Deep Patch Test with Shredded Tire Backfill